SANDIA REPORT
SAND2021-xxxx
Printed September 2021

Sandia National Laboratories

Final report of activities for the LDRD-express project #223796 titled: "Fluid models of charged species transport: numerical methods with mathematically guaranteed properties", PI: Ignacio Tomas, Co-PI: John Shadid.

Ignacio Tomas, John Shadid, Michael Crockatt, Matthias Maier, Jean-Luc Guermond, Roger Pawlowski

Prepared by
Sandia National Laboratories
Albuquerque, New Mexico 87185
Livermore, California 94550

Issued by Sandia National Laboratories, operated for the United States Department of Energy by National Technology & Engineering Solutions of Sandia, LLC.

Available to DOE and DOE contractors from

U.S. Department of Energy
Office of Scientific and Technical Information
P.O. Box 62
Oak Ridge, TN 37831

Telephone: (865) 576-8401
Facsimile: (865) 576-5728
E-Mail: reports@osti.gov
Online ordering: http://www.osti.gov/scitech

Available to the public from

U.S. Department of Commerce
National Technical Information Service
5301 Shawnee Road
Alexandria, VA 22312

Telephone: (800) 553-6847
Facsimile: (703) 605-6900
E-Mail: orders@ntis.gov
Online order: https://classic.ntis.gov/help/order-methods

Final report of activities for the LDRD-express project #223796 titled: "Fluid models of charged species transport: numerical methods with mathematically guaranteed properties", PI: Ignacio Tomas, Co-PI: John Shadid.

Ignacio Tomas
Computational Mathematics, MS-1320
Sandia National Laboratories
Albuquerque, NM 87185-1320
itomas@sandia.gov

John Shadid
Center for Computing Research, MS-1320
Sandia National Laboratories
Albuquerque, NM 87185-1320
jnshadi@sandia.gov

Michael Crockatt
Center for Computing Research, MS-1320
Sandia National Laboratories
Albuquerque, NM 87185-1320
mmcrock@sandia.gov

Matthias Maier
Department of Mathematics, MS-3368
Texas A&M University
College Station, TX 77843-3368
maier@math.tamu.edu

Jean-Luc Guermond
Department of Mathematics, MS-3368
Texas A&M University
College Station, TX 77843-3368
guermond@math.tamu.edu

Roger Pawlowski
Center for Computing Research, MS-1320
Sandia National Laboratories
Albuquerque, NM 87185-1320
rppawlo@sandia.gov

SAND2021-xxxx

ABSTRACT

This report summarizes the findings and outcomes of the LDRD-express project with title “Fluid models of charged species transport: numerical methods with mathematically guaranteed properties”. The primary motivation of this project was the computational/mathematical exploration of the ideas advanced in [61], aiming to improve the state-of-the-art on numerical methods for the one-fluid Euler-Poisson models and gain some understanding on the Euler-Maxwell model.

Euler-Poisson and Euler-Maxwell, by themselves are not the most technically relevant PDE plasma-models. However, both of them are elementary building blocks of PDE-models used in actual technical applications and include most (if not all) of their mathematical difficulties. Outside the classical ideal MHD models, rigorous mathematical and numerical understanding of one-fluid models is still a quite undeveloped research area, and the treatment/understanding of boundary conditions is minimal (borderline non-existent) at this point in time. This report focuses primarily on bulk-behaviour of Euler-Poisson’s model, touching boundary conditions only tangentially. Primary focus is on the development of methods that:

- Are mathematically guaranteed to preserve positivity of density and internal energy.
- Are capable of preserving the electro-kinetic energy in the source-dominated regime.
- Either electrostaic plasma period does not have to be time-resolved and/or plasma oscillation does not represent a source of numerical instabilities, in particular, in the context of very large densities.
- Either the coupled problem or the source-system encoding the electrostatic plasma oscillation is asymptotically well-posed. By “asymptotically well-posed” we mean that the resulting linear algebra systems are guaranteed to be invertible regardless of of the electron density.

The authors believe that they have succeeded in the achievement of such goals with ample margin of confidence. In order to understand, in a much broader sense, the contents of this report we suggest the reader that is well-seasoned in plasma physics modeling and numerical analysis of partial differential equations to jump immediately to the conclusion section at the end of this report. That will help the reader further motivate the reading process, better navigate this document and understand its scientific and technical merits.

ACKNOWLEDGMENTS

This material is based upon work supported by the LDRD-express program of Sandia National Laboratories, project #223796 titled: “Fluid models of charged species transport: numerical methods with mathematically guaranteed properties. Their encouragement and financial and support throughout the development of this project is greatly acknowledged. Without their financial support prototype code-development and algorithmic evaluation would have not been possible.

CONTENTS

LIST OF FIGURES

LIST OF TABLES

NOMENCLATURE

In this manuscript:

- Here $d : 1,2,3$ is the space dimension. In this manuscript we focus primarily on the case $d = 2$.
- $\mathbf{U} = [\rho, \mathbf{p}, \mathcal{E}, \varphi]^\top \in \mathbb{R}^{d+3}$ will denote the whole state of Euler-Poisson's model.
- $\mathbf{u} = [\rho, \mathbf{p}, \mathcal{E}]^\top \in \mathbb{R}^{d+2}$ will denote the state of Euler's subsystem.
- $\mathbf{v} = \rho^{-1}\mathbf{p} \in \mathbb{R}^d$ will be used to denote the velocity.
- $|\cdot|_{\ell^2}$ and $|\cdot|$ denote the Euclidean norm of a vector. For instance $|\mathbf{p}| = (\sum_{i=1}^d \mathbf{p}_i^2)^{\frac{1}{2}}$.
- $\varepsilon = \mathcal{E} - \frac{1}{2\rho}|\mathbf{p}|^2$ is the internal energy of Euler's subsystem.
- $e = \rho^{-1}\varepsilon = \frac{\mathcal{E}}{\rho} - \frac{1}{2\rho^2}|\mathbf{p}|^2$ is the specific internal energy of Euler's subsystem.
- $v = \rho^{-1}$ is the specific volume.
- $s(v,e)$ denotes the specific entropy of Euler's subsystem. The specific entropy describes the entire thermodynamic behaviour of the electron gas (pressure, sound speed, etc).
- $\eta = -\rho s(v,e)$ denotes the mathematical entropy of Euler subsystem.
- $\mathbf{q} = -\mathbf{p}s$ is the entropy-flux associated to the mathematical entropy η.
- μ and ε are the magnetic permeability and electric permittivity of the conducting medium: either vacuum, a low-pressure gas, a metal, a semiconductor, etc.
- $m_e > 0$ the specific particle mass of the electron with units $[m_e] =$ mass (mass per unit particle).
- $\mathscr{T}$ a characteristic collision/relaxation time with units $[\mathscr{T}] =$ time. Also called "mean free time" between collision (e.g. Drude's model).
- $q_e < 0$ is the specific electric charge of the electron $[q_e] =$ charge (charge per unit particle).
- $q_i > 0$ is the specific electric charge of the ions.
- $n_e := \frac{\rho}{m_e} \geq 0$ is the electron number density with units $[n_e] = \frac{1}{\text{volume}}$.
- $n_i \geq 0$ is the ion number density.
- $\rho_e := n_e q_e$ is the negative or electron charge density.
- $\rho_i := n_i q_i$ is the positive or ion electric charge density.
- $\omega_p = \left(\rho(\frac{q_e}{m_e})^2 \frac{1}{\varepsilon}\right)^{\frac{1}{2}} = \left(\frac{n_e q_e^2}{\varepsilon m_e}\right)^{\frac{1}{2}}$ is the plasma angular frequency.
- $\omega_c = \frac{|B|q_e}{m_e}$, with $|B|$ being the magnitude of the magnetic field, is the cyclotron angular frequency.

- both $\frac{\partial}{\partial t}$ and ∂_t will be indistinctively used to denote partial derivative in time.
- $\mathbb{V}$: scalar-valued nodal finite element space used to discretize the each component of Euler's subsystem.
- $\mathbf{V} = [\mathbb{V}]^{d+2}$: vector-valued nodal finite element space used to discretize the Euler's subsystem.
- $\mathcal{V}$: set of integers identifying each spatial node $\boldsymbol{x}_i$ of the scalar-valued finite element space $\mathbb{V}$.
- $\{\phi_i\}_{i\in\mathcal{V}}$: finite element basis of the nodal space $\mathbb{V}$.
- $\mathbb{H}$: scalar-valued nodal finite element space used to discretize electric potential.
- $\mathcal{H}$: set of integers identifying each spatial node $\boldsymbol{x}_i$ of the scalar-valued finite element space $\mathbb{H}$.
- $\{\chi_i\}_{i\in\mathcal{H}}$: finite element basis of the nodal space $\mathbb{H}$.

1. INTRODUCTION

The one-fluid Euler-Maxwell model is frequently used to describe the dynamics of electrons inside a low-pressure gas (gaseous plasma), a semiconductor (solid state plasma), and conductors subject to very high-voltage gradients (e.g. magnetically insulated transmission lines). The Euler-Maxwell model consists in the following set of equations:

$$\partial_t \rho + \operatorname{div} \mathbf{p} = 0\,, \tag{1a}$$
$$\partial_t \mathbf{p} + \operatorname{div}\left(\rho^{-1}\mathbf{p}\mathbf{p}^\top + \mathbb{I} p\right) = \tfrac{q_e}{m_e}\rho \mathrm{E} + \tfrac{q_e}{m_e}\mathbf{p}\times \mathrm{B} - \tfrac{1}{\mathscr{T}}\mathbf{p}\,, \tag{1b}$$
$$\partial_t \mathcal{E} + \operatorname{div}\left(\tfrac{\mathbf{p}}{\rho}(\mathcal{E}+p)\right) = \tfrac{q_e}{m_e}\mathrm{E}\cdot\mathbf{p} - \tfrac{1}{\rho\mathscr{T}}|\mathbf{p}|^2\,, \tag{1c}$$
$$\partial_t \mathrm{B} + \operatorname{curl}\mathrm{E} = 0\,, \tag{1d}$$
$$\varepsilon\mu\partial_t \mathrm{E} - \operatorname{curl}\mathrm{B} = -\tfrac{\mu q_e}{m_e}\mathbf{p}\,, \tag{1e}$$

where $\rho \in \mathbb{R}$, $\mathbf{p} \in \mathbb{R}^3$ and $\mathcal{E} \in \mathbb{R}$ are the density, linear momentum, and total mechanical energy per unit volume respectively, $\mathrm{B} \in \mathbb{R}^3$ is the magnetic induction field, and $\mathrm{E} \in \mathbb{R}^3$ is the electric field.

The model of primary interest in this manuscript is the electrostatic limit of system (1a)-(1e), the Euler-Poisson system, defined by the following set of equations [64, 73]:

$$\partial_t \rho + \operatorname{div} \mathbf{p} = 0\,, \tag{2a}$$
$$\partial_t \mathbf{p} + \operatorname{div}\left(\rho^{-1}\mathbf{p}\mathbf{p}^\top + \mathbb{I} p\right) = -\tfrac{q_e}{m_e}\rho\nabla\varphi - \tfrac{1}{\mathscr{T}}\mathbf{p}\,, \tag{2b}$$
$$\partial_t \mathcal{E} + \operatorname{div}\left(\tfrac{\mathbf{p}}{\rho}(\mathcal{E}+p)\right) = -\tfrac{q_e}{m_e}\nabla\varphi\cdot\mathbf{p} - \tfrac{1}{\rho\mathscr{T}}|\mathbf{p}|^2\,, \tag{2c}$$
$$-\varepsilon\Delta\partial_t\varphi = -\tfrac{q_e}{m_e}\operatorname{div}\mathbf{p}\,, \tag{2d}$$

System, (2a)-(2d) is algebraically equivalent to setting $\mathrm{B} \equiv \mathbf{0}$ and $\mathrm{E} := -\nabla\varphi$ in (1a)-(1e) and taking the divergence to both sides of (1e).

Applicability of the Euler-Poisson model goes beyond the physics plasmas, semiconductors, and vacuum electronics [107]. Flipping the sign of the forces in Euler-Poisson's model the nature of the forces shifts from repulsive to attractive. In fact, after such change of sign it becomes a well-established model for non-relativistic self-gravitation [97]. More precisely, we have that the self-gravitational Euler-Poisson model is given by:

$$\partial_t \rho + \operatorname{div} \mathbf{p} = 0\,, \tag{3a}$$
$$\partial_t \mathbf{p} + \operatorname{div}\left(\rho^{-1}\mathbf{p}\mathbf{p}^\top + \mathbb{I} p\right) = -\rho\nabla\varphi\,, \tag{3b}$$
$$\partial_t \mathcal{E} + \operatorname{div}\left(\tfrac{\mathbf{p}}{\rho}(\mathcal{E}+p)\right) = -\nabla\varphi\cdot\mathbf{p}\,, \tag{3c}$$
$$-\tfrac{1}{\alpha(d)}\Delta\partial_t\varphi = \operatorname{div}\mathbf{p}\,. \tag{3d}$$

For $d = 2$ we have that $\alpha(d) = 2\pi G$ and for $d = 3$ we have that $\alpha(d) = 4\pi G$, where G is the universal gravitational constant. More generally for $d \geq 3$ we have that $\alpha(d) = d(d-2)\omega(d)G$, where $\omega(d)$ is the measure of the ball of radius $r = 1$ in d-space dimensions. We also note in passing that Euler-Poisson model has important relations with quantum mechanical descriptions [63] which are gradually gaining attention in the context of mathematical modeling of very

dense/degenerate electron-plasmas and warm dense matter [79, 18]. This further emphasizes the importance of centering a research program starting with the repulsive Euler-Poisson's model as primary object of concern.

The term $-\frac{1}{\mathscr{T}}\mathbf{p}$ in the right-hand side of (1b) and (2b) models collisions/friction with the background. Losely speaking, we expect $\frac{1}{\mathscr{T}}$ to be negligible for gaseous plasmas where electric charges travel through a rarefied gas, and non-negligible for electrons traveling inside semiconductors and/or metals and high-density plasmas. In this manuscript emphasis is placed in the case $\frac{1}{\mathscr{T}} \equiv 0$. Occasionally, we will present some simple results that do not make this assumption.

The one-fluid Euler-Maxwell and Euler-Poisson models are the simplest within a large family of multi-fluid PDE systems used to model electric charge transport in semiconductors and plasmas (see early works [22, 101, 106] and more recent references [76, 41, 95, 77]). Some of the most relevant members of this large family are the one-fluid relativistic Euler-Maxwell model (see [102, 103, 80, 8]), the two-fluid Euler-Maxwell (ions and electrons) of fully ionized (non-reactive) plasmas with and without collision-momentum transfer (see [59, 1, 81]), and three-fluid models of reactive plasmas (ions, electrons, and neutrals undergoing ionization and/or recombination) see for instance [77, 10, 69]. In spite of their apparent simplicity, one-fluid models share some of the numerical difficulties that appear in much more sophisticated multi-fluid models, in particular its multiscale nature.

Linear stability analysis (see [98]) reveals that fluid-models contain the usual elementary non-smooth waves associated to hyperbolic systems of conservation laws (shocks, expansions and contacts) but also a rich family of high-frequency (in general smooth) purely *dispersive* waves. In this manuscript, we use the terminology *dispersive* as an equivalent of *Hamiltonian*: prototypical behaviour is harmonic-like oscillation phenomena describing the transformation of one form of energy into another (e.g. kinetic into potential and converse) while preserving the sum of both invariant in time. If both regimes (low-frequency non-smooth and high-frequency smooth) were clearly separated the choices of numerical scheme are very clear:

- Non-smooth low-frequency regime is representative of what is usually called shock hydrodynamics: possibly discontinuous, having arbitrary levels of vacuum, with pressure and density jumps ratios in well past 10^6. At present, the most well-established and most robust numerical methodologies for such regime are either time-explicit nodal-like schemes (finite difference, finite volumes, continuous finite elements, discontinuous finite elements, etc) allowing for control of pointwise properties such as pointwise positivity of density and internal energy.

- Smooth, very high-frequency, almost linear, highly oscillatory regimes: time-implicit p-adaptive spectral-like methods of very high polynomial order (e.g. [27, 67]) are the most efficient choice.

However, even in the simplest numerical tests (see for instance [68, 1]), it is evident that separation of regimes does not occur: both non-smooth low-frequency and smooth high-frequency phenomena coexist making the one-fluid Euler-Maxwell and Euler-Poisson systems genuine multiscale problems. The dispersive phenomena manifests graphically as

high-frequency oscillations in space (usually misjudged as Gibbs phenomena by the non-initiated) "superposed" on top of the shock-hydrodynamics discontinuous behaviour. This makes models such as (1a)-(1e) drastically more difficult to solve than usual compressible MHD model (e.g.[23]) which, at its core, is a low-frequency fluid-dynamics model with reasonable clustering of its space and time scales.

To major extent, the main computational bottlenecks (in equal order of relevance) are:

- Robustness in the context of non-smooth highly shocked phenomena and/or near vacuum conditions (very small densities and/or internal energies). A good reference in this regard is [1].
- Robustness when approximating solution with high spatial-frequency (large wavenumbers in space) using coarse meshes. Numerical methods that either do not preserve Hamiltonian invariants or do not introduce some form of damping (to dissipate the energy from unresolved modes) are not robust or require tens of thousands of elements on the real line. A good reference in this regard are the IMEX schemes considered in [81] where computational simulations (with merely a few hundreds of elements in the real line) are able to deal with space and time scales well beyond the resolution of spatial mesh and time-step size.

At present, there is no universally acceptable scheme that can deal efficiently and robustly with both regimes. Such statements holds true for the for simplest one-fluid models too. Schemes such as those in [68, 1] can require tens of thousands of cells in the real line, but schemes such as those in [81] would require further development in order to deal with the highly-shocked regime. To make the problem even more complicated, numerical solution of Maxwell's equations require the preservation of non-local constraints and/or involutions.

In this manuscript we try to describe the core PDE-structure of the one-fluid systems and find a basic constructions (schemes) that preserve these properties. The core targets are: preservation of robustness in the shock-hydrodynamics regime, preservation of the internal energy, preservation of the minimum principle of the hydrodynamic entropy, preservation and/or dissipation of Hamiltonian invariants, asymptotic well-posedness (i.e. linear algebra systems that are always invertible), and preservation of energy-stability properties.

The outline of this brief report is the following one: in Section 2 we review the core properties of the Euler-Maxwell and Euler-Poisson systems. In Section 3 we propose a simple approach to develop first and second-order accurate time-integration schemes assuming a collocated (or nodal) equal-order discretization in space for Euler-Maxwell system. Perhaps, the most important outcome of Section 3 is Lemma 3.3 which proves that energy-stability is perfectly achievable in the context of splitting schemes. To the best of our knowledge this Lemma is the first of its kind. The core ideas of that Lemma have already been exploited in the context of compressible Navier-Stokes system [54]. Section 3 is mostly an incomplete (but somewhat pedagogical) template of ideas which require significant intellectual development in order to work properly for the electrostatic limit (Euler-Poisson). In Section 4 we effectively bridge that gap by considering two precise choices of source-update schemes. One of these schemes is a fully-coupled numerical scheme for the source terms that preserves positivity of the internal energy and electro-kinetic energy, but it might run into ill-conditioning in the context of high-densities, see Section §(4.2)

for more details. The second source-update scheme avoids completely the method of lines leading to a fully-decoupled scheme. In this second scheme the linear algebra systems are guaranteed to be invertible provided the density remains strictly positive. However, preservation of the electro-kinetic energy requires very special choices of space discretization. Both schemes preserve positivity of the internal energy without any major difficulty. The fully-decoupled scheme is inspired in some early ideas from [32].

2. BASIC MATHEMATICAL/PHYSICAL PROPERTIES OF THE MODELS

We briefly develop and/or present the core structural properties of the one-fluid Euler-Maxwell and Euler-Poisson systems. Some of these properties are properly developed (and proved). However, for some properties we will not provide a proof, instead we will provide bibliographic references for the interested reader.

2.1. Euler system with and without forces

The following proposition requires invoking the notion of *complete equation of state* which we briefly describe in Appendix §A.1 for the sake of completeness. To avoid getting distracted from the main ideas, the reader may ignore such notion in its entirety and focus on the main statements of this proposition.

Proposition 2.1 (Natural invariants Euler's equations)**.** *Let* $\mathbf{u} = [\rho, \mathbf{p}, \mathcal{E}]^\top \in \mathbb{R}^{d+2}$ *denote the hydrodynamic state. Let* $s = \sigma(v,e)$ *be the specific entropy describing the thermodynamic behaviour of the gas. With slight abuse of notation we will use* $s = s(\mathbf{u})$ *to actually mean* $s = \sigma(v(\mathbf{u}), e(\mathbf{u}))$*. We assume that hydrodynamic state is subject to the evolution law* $\partial_t \mathbf{u} + div\, \mathbb{f}(\mathbf{u}) = \mathbf{0}$ *where*

$$\mathbb{f}(\mathbf{u}) = \begin{bmatrix} \mathbf{p}^\top \\ \rho^{-1}\mathbf{p}\mathbf{p}^\top + \mathbb{I}p \\ \rho^{-1}\mathbf{p}^\top(\mathcal{E}+p) \end{bmatrix} \tag{4}$$

and the pressure p *follows from a complete equations of state (see* (107)*). Assume that the initial data* $\mathbf{u}_0 = \mathbf{u}_0(\boldsymbol{x}) \in \mathbb{R}^{d+2}$ *has positive density and specific internal energy for all* $\boldsymbol{x}$*. Then, the solution* $\mathbf{u}(\boldsymbol{x},t)$ *of Euler's equations belongs to the set* $\mathcal{A}$ *for all* $\boldsymbol{x}$ *and time* $t > 0$ *where*

$$\mathcal{A} = \left\{ \mathbf{u} = [\rho, \mathbf{p}, \mathcal{E}]^\top \in \mathbb{R}^{d+2} \,\middle|\, \rho > 0,\, \rho e(\mathbf{u}) > 0,\, s(\mathbf{u}) \geq \min_x s(\mathbf{u}_0(\boldsymbol{x})) \right\} \subset \mathbb{R}^{d+2}. \tag{5}$$

The proof of this proposition is far from trivial and it is not (to the best of the authors' knowledge) a standard result that can be found in the thermodynamics or physics literature. With different levels of completeness and generality, the proof of proposition 2.1 can be found in [100, 60, 96, 47, 56]. We note that the statement about the minimum principle can be local (as in [100, 56]). The choice of equation of state and viscous regularization that is compatible with these properties can be made more general (see [56]).

The practical importance of this proposition lies (primarily) in the minimum principle of the specific entropy, which together with positivity of density, are the only mathematically solid guidelines we have at our disposal to design flux/slope limiters. In particular, discrete satisfaction of the minimum principle of the specific entropy and positivity of density are enough to guarantee positivity of the internal energy, which in turn is enough to guarantee that a scheme does not crash catastrophically.

The set $\mathcal{A}$, defined in (5), is a convex subset of $\mathbb{R}^{d+2}$. We will refer to it as the invariant-set of Euler's equations. To simplify the discussion, in this presentation we will refer (informally) to the preservation of positivity of density and internal energy (which are our main targets) as invariant-set properties.

Regarding the interaction of Euler's equations (more generally: conservation of mass, momentum and total mechanical energy) with force fields of any type we have the following result.

Lemma 2.1 (Tangent in-time invariance of the density and internal energy)**.** *Consider the Euler's equations of gas dynamics subject to the effects of an external force* $\frac{\partial}{\partial t}\mathbf{u} + div\,\mathbb{f}(\mathbf{u}) = \mathbf{s}(\mathbf{f})$*, that is*

$$\mathbf{u} = \begin{bmatrix} \rho \\ \mathbf{p} \\ \mathcal{E} \end{bmatrix}, \ \mathbb{f}(\mathbf{u}) = \begin{bmatrix} \mathbf{p}^\top \\ \rho^{-1}\mathbf{p}\mathbf{p}^\top + \mathbb{I}p \\ \rho^{-1}\mathbf{p}^\top(\mathcal{E}+p) \end{bmatrix}, \ \mathbf{s}(\mathbf{f}) = \begin{bmatrix} 0 \\ \mathbf{f} \\ \rho^{-1}\mathbf{p}\cdot\mathbf{f} \end{bmatrix}, \tag{6}$$

here $\mathbf{f} := \mathbf{f}(\boldsymbol{x},t) : \mathbb{R}^d \times \mathbb{R} \to \mathbb{R}^d$ *is an arbitrary vector field (a force per unit volume) possibly depending on the state* $\mathbf{u}$*, the space* $\boldsymbol{x}$ *and time* t*. Note that* $\rho^{-1}\mathbf{p}\cdot\mathbf{f}$*, acting on the energy equation, is the power of the force* $\mathbf{f}$*. Define* $\Psi(\mathbf{u}) := \rho^\lambda \varepsilon$ *where* λ *is an arbitrary real number and* $\varepsilon = \mathcal{E} - \frac{|\mathbf{p}|^2}{2\rho}$ *is the internal energy per unit volume. Then we have that*

$$\nabla_{\mathbf{u}}\Psi(\mathbf{u}) \cdot \mathbf{s}(\mathbf{f}) \equiv 0. \tag{7}$$

The proof is omitted since (7) can be easily checked by direct computation.

Remark 2.1 (Colloquial interpretation)**.** Lemma 2.1 basically says that the time evolution of the internal energy is independent of arbitrary exterior forces (whether they are aligned with the velocity field or not, whether they depend on $\mathbf{u}$ or not). This follows by taking the dot-product of Euler's subsystem $\partial_t\mathbf{u} + \operatorname{div}\mathbb{f}(\mathbf{u}) = \mathbf{s}(\mathbf{f})$ with $\nabla_{\mathbf{u}}\Psi(\mathbf{u})$ to get

$$\tfrac{\partial}{\partial t}\Psi(\mathbf{u}) = -\nabla_{\mathbf{u}}\Psi(\mathbf{u}) \cdot \operatorname{div}\mathbb{f}(\mathbf{u}) + \underbrace{\nabla_{\mathbf{u}}\Psi(\mathbf{u}) \cdot \mathbf{s}(\mathbf{f})}_{\equiv 0}.$$

This is, with greatest likelyhood, a trivial statement in the context of rational continuum mechanics. In other words, sources of the form described in (6) preserve the internal energy $\varepsilon := \mathcal{E} - \frac{|\mathbf{p}|^2}{2\rho}$ of Euler's system.

Lemma (2.1) has the following immediate consequence.

Corollary 2.1. *Using the same notation described in Proposition 2.1, define* $\eta(\mathbf{u}) := -\rho\sigma(v(\mathbf{u}), e(\mathbf{u}))$ *as the mathematical entropy. Then we have that*

$$\nabla_{\mathbf{u}}\sigma(v,e)\cdot\mathbf{s}(\mathbf{f}) \equiv 0 \;\; \textit{therefore} \;\; \nabla_{\mathbf{u}}\eta(\mathbf{u})\cdot\mathbf{s}(\mathbf{f}) \equiv 0\,,$$

which follows using the chain rule and identity (7) *respectively. This implies that exterior forces acting on the momentum equation (ergo in the total energy equation too: through the power of the forces) cannot modify the specific and/or mathematical entropy. In other words: entropy dissipative/productive forces do not exist.*

2.2. Euler-Maxwell model: formal balance and source-dominated regime.

In order to understand the nature of the coupling within system Euler-Maxwell system (1a)-(1e) we will consider two drastically different asymptotic regimes. First, we will consider the regime where the dynamics is dominated by hyperbolic terms while the right hand side (the source terms) are vanishingly small, that is

$$\partial_t\rho + \operatorname{div}\mathbf{p} = 0\,, \tag{8a}$$
$$\partial_t\mathbf{p} + \operatorname{div}\left(\rho^{-1}\mathbf{p}\mathbf{p}^{\top} + \mathbb{I}p\right) = \mathbf{0}\,, \tag{8b}$$
$$\partial_t\mathcal{E} + \operatorname{div}\left(\tfrac{\mathbf{p}}{\rho}(\mathcal{E}+p)\right) = 0\,, \tag{8c}$$
$$\partial_t\mathrm{B} + \operatorname{curl}\mathrm{E} = \mathbf{0}\,, \tag{8d}$$
$$\varepsilon\mu\partial_t\mathrm{E} - \operatorname{curl}\mathrm{B} = \mathbf{0}\,. \tag{8e}$$

Similarly, we will consider the asymptotic regime for (1a)-(1e) where source terms dominate the dynamics (i.e. hyperbolic wave phenomena is assumed to be negligible or vanishingly small):

$$\partial_t\rho = 0\,, \tag{9a}$$
$$\partial_t\mathbf{p} = \tfrac{q_e}{m_e}\rho\mathrm{E} + \tfrac{q_e}{m_e}\mathbf{p}\times\mathrm{B}\,, \tag{9b}$$
$$\partial_t\mathcal{E} = \tfrac{q_e}{m_e}\mathrm{E}\cdot\mathbf{p}\,, \tag{9c}$$
$$\partial_t\mathrm{B} = \mathbf{0}\,, \tag{9d}$$
$$\varepsilon\mu\partial_t\mathrm{E} = -\mu\tfrac{q_e}{m_e}\mathbf{p}\,. \tag{9e}$$

Note that only (9b) and (9e) are actually coupled.
We could think of (8a)-(8e) as the hyperbolic-dominated regime. Similarly, we could think of (9a)-(9e) as the source-dominated regime. The invariants associated to the ODE system (9a)-(9e) are described by the following Lemma which follows from similar arguments to those found in [1].

Lemma 2.2 (Natural invariants of the source terms)**.** *In addition to* ρ *and* B *being invariants of* (9a)-(9e) *we also have that:*

$$\partial_t\left(\mathcal{E} - \tfrac{|\mathbf{p}|^2}{2\rho}\right) \equiv 0\,, \tag{10}$$
$$\partial_t\left(\tfrac{|\mathbf{p}|^2}{2\rho} + \tfrac{\varepsilon}{2}|\mathrm{E}|^2\right) \equiv 0\,. \tag{11}$$

The proof is omitted since it follows from standard energy arguments. Invariance (10) follows from lemma 2.1.

Some comments and notes:

- Invariance (11) is directly related to the so-called plasma oscillation: harmonic-like oscillation phenomena that transforms electric energy into kinetic energy and conversely.
- Naming convention: we will call the functional $\frac{|\mathbf{p}|^2}{2\rho} + \frac{\varepsilon}{2}|\mathrm{E}|^2$ the electro-kinetic energy.
- If we were to consider collision terms (i.e. $\mathscr{T}^{-1} \not\equiv 0$) in the ODE system (9a)-(9e) invariance (10) holds too, but (11) does not hold anymore. More precisely, we have that the evolution of such ODE would dissipate the electro-kinetic energy:

$$\partial_t\big(\tfrac{|\mathbf{p}|^2}{2\rho} + \tfrac{\varepsilon}{2}|\mathrm{E}|^2\big) = -\tfrac{1}{\mathscr{T}\rho}|\mathbf{p}|^2\,.$$

Using corollary 2.1, we can establish that system (1a)-(1e) satisfies two strikingly decoupled a priori bounds: one of them for the mathematical entropy of the Euler subsystem (1a)-(1c) and another one for the sum of the mechanical and electromagnetic energy of (1a)-(1e).

Lemma 2.3 (Formal balance)**.** *Multiplying* (1a)-(1c) *by* $\nabla_{\mathbf{u}}\eta(\mathbf{u})$*, where* $\mathbf{u} := [\rho, \mathbf{p}, \mathcal{E}]^\top$ *is the state of Euler's subsystem, we get*

$$\tfrac{\partial}{\partial t}\eta(\mathbf{u}) + div\,\mathbf{q}(\mathbf{u}) = 0 \;\; where \;\; \mathbf{q}(\mathbf{u}) := -\mathbf{p}s(\mathbf{u}) \tag{12}$$

Similarly, taking the dot-product of $[1, \mu^{-1}\mathrm{B}, \mu^{-1}\mathrm{E}]^\top$ *with* $[\partial_t\mathcal{E}, \partial_t\mathrm{B}, \partial_t\mathrm{E}]^\top$ *as defined in* (1c)-(1e) *we can obtain an energy energy-flux balance*

$$\tfrac{\partial}{\partial t}\big(\mathcal{E} + \tfrac{1}{2\mu}|\mathrm{B}|^2 + \tfrac{\varepsilon}{2}|\mathrm{E}|^2\big) + div\,\big(\tfrac{\mathbf{p}}{\rho}(\mathcal{E}+p) + \tfrac{1}{\mu}\mathrm{E}\times\mathrm{B}\big) = -\tfrac{\alpha}{\rho\mathscr{T}}|\mathbf{p}|^2\,. \tag{13}$$

We note that the proof of (12) requires using the identity $\nabla_{\mathbf{u}}\eta(\mathbf{u})^\top\nabla_{\mathbf{u}}\mathbb{f}(\mathbf{u}) = \nabla_{\mathbf{u}}\mathbf{q}^\top$. This is a standard result which can be found for instance in [50, Chapter 1].

Remark 2.2 (Physically admissible)**.** We will assume that Euler-Maxwell system is the zero-viscosity limit (or vanishing-viscosity limit) in the sense described for instance in [56] in the context of Euler's equations. Therefore, we are only interested in approximating solution satisfying

$$\begin{aligned} \tfrac{\partial}{\partial t}\eta(\mathbf{u}) + \operatorname{div}\mathbf{q}(\mathbf{u}) &\leq 0\,, \\ \tfrac{\partial}{\partial t}\big(\mathcal{E} + \tfrac{1}{2\mu}|\mathrm{B}|^2 + \tfrac{\varepsilon}{2}|\mathrm{E}|^2\big) + \operatorname{div}\,\big(\tfrac{\mathbf{p}}{\rho}(\mathcal{E}+p) + \tfrac{1}{\mu}\mathrm{E}\times\mathrm{B}\big) &\leq -\tfrac{\alpha}{\rho\mathscr{T}}|\mathbf{p}|^2\,, \end{aligned} \tag{14}$$

with equalities holding for smooth solutions and strict inequality once $\mathcal{C}^1$ regularity is lost. Establishing the structure of a viscous regularization that could lead to a formally meaningful family of solutions is an question that is beyond the scope of this manuscript.

Whichever scheme we devise to update the effects of the sources: we would like it to be compatible with the invariance (10) and (11), and either a weak or integral version of stability properties described in (14). In Section §3 we present the simplest time-discretization technique (ignoring entirely space-discretization and boundary conditions) that we could use in order to preserve such stability properties.

2.3. Euler-Poisson repulsive case: formal balance and source-dominated regime

Lemma 2.4 (Formal balance: repulsive case)**.** *The repulsive Euler-Poisson system* (2a)-(2d) *satisfies the following integral energy/energy-flux balance*

$$\frac{\partial}{\partial t}\int_\Omega \mathcal{E}+\tfrac{\varepsilon}{2}|\nabla\varphi|^2\,\mathrm{d}\boldsymbol{x}=-\int_{\partial\Omega}\big(\tfrac{\mathbf{p}}{\rho}(\mathcal{E}+p)\big)\cdot\mathrm{n}+\varphi\big(\tfrac{q}{m}\mathbf{p}-\varepsilon\nabla\partial_t\varphi\big)\cdot\mathrm{n}\,\mathrm{d}\boldsymbol{s}-\int_\Omega \tfrac{1}{\rho\mathscr{T}}|\mathbf{p}|^2\,, \tag{15}$$

or pointwise

$$\frac{\partial}{\partial t}\big(\mathcal{E}+\tfrac{\varepsilon}{2}|\nabla\varphi|^2\big)+div\,\big(\tfrac{\mathbf{p}}{\rho}(\mathcal{E}+p)+\varphi\big(\tfrac{q}{m}\mathbf{p}-\varepsilon\nabla\partial_t\varphi\big)\big)=-\tfrac{1}{\rho\mathscr{T}}|\mathbf{p}|^2\,. \tag{16}$$

Proof. In order to get (15): we multiply (2d) by φ and integrate by parts (both sides of the equality) and add it to the integral (in space) of line of (2c). □

Remark 2.3 (Physically admissible solutions)**.** We will assume that Euler-Poisson system is the zero-viscosity limit (or vanishing-viscosity limit) in the sense described for instance in [56] in the context of Euler's equations. Therefore, we are only interested in approximating solution satisfying

$$\begin{aligned}\frac{\partial}{\partial t}\eta(\mathbf{u})+\operatorname{div}\mathbf{q}(\mathbf{u})&\leq 0\,,\\ \frac{\partial}{\partial t}\big(\mathcal{E}+\tfrac{\varepsilon}{2}|\nabla\varphi|^2\big)+\operatorname{div}\big(\tfrac{\mathbf{p}}{\rho}(\mathcal{E}+p)+\tfrac{q}{m}\varphi\mathbf{p}-\varepsilon\varphi\nabla\partial_t\varphi\big)+\tfrac{\alpha}{\rho\mathscr{T}}|\mathbf{p}|^2&\leq 0\,,\end{aligned}$$

with equality holding for smooth solutions and strict inequality holding once $\mathcal{C}^1$ regularity is lost.

We define the source-dominated regime for the repulsive Euler-Poisson system (2a)-(2d) as

$$\partial_t\rho=0\,, \tag{17a}$$
$$\partial_t\mathbf{p}=-\tfrac{q_e}{m_e}\rho\nabla\varphi-\tfrac{\alpha}{\mathscr{T}}\mathbf{p}\,, \tag{17b}$$
$$-\varepsilon\Delta\partial_t\varphi=-\tfrac{q_e}{m_e}\operatorname{div}\mathbf{p}\,, \tag{17c}$$
$$\partial_t\mathcal{E}=-\tfrac{q_e}{m_e}\nabla\varphi\cdot\mathbf{p}-\tfrac{\alpha}{\rho\mathscr{T}}|\mathbf{p}|^2\,. \tag{17d}$$

Note that only (17b) and (17c) are actually coupled.

Remark 2.4 (Repulsive source-system: formal balance)**.** From Lemma 2.1 we know that system (17a)-(17d) satisfies the identity $\partial_t\big(\mathcal{E}-\frac{|\mathbf{p}|^2}{2\rho}\big)\equiv 0$. In addition, subsystem (17b)-(17c) satisfies the following integral energy/energy-flux balance

$$\frac{\partial}{\partial t}\int_\Omega \tfrac{1}{2\rho}|\mathbf{p}|^2+\tfrac{\varepsilon}{2}|\nabla\varphi|^2\,\mathrm{d}\boldsymbol{x}=-\int_{\partial\Omega}\varphi\big(\tfrac{q_e}{m_e}\mathbf{p}-\varepsilon\nabla\partial_t\varphi\big)\cdot\mathrm{n}\,\mathrm{d}\boldsymbol{s}-\int_\Omega \tfrac{1}{\rho\mathscr{T}}|\mathbf{p}|^2\,, \tag{18}$$

or pointwise

$$\frac{\partial}{\partial t}\big(\tfrac{1}{2\rho}|\mathbf{p}|^2+\tfrac{\varepsilon}{2}|\nabla\varphi|^2\big)+\operatorname{div}\big(\varphi\big(\tfrac{q_e}{m_e}\mathbf{p}-\varepsilon\nabla\partial_t\varphi\big)\big)=-\tfrac{1}{\rho\mathscr{T}}|\mathbf{p}|^2\,. \tag{19}$$

Remark 2.5 (Nonlocal nature of the electrostatic source-dominated regime)**.** Since $\partial_t \rho$ in the source-dominated regime, see (17a), density can be factored-out from (17b). In the absence of collision/friction terms (i.e. $\mathscr{T}^{-1} \equiv 0$) expression (17b) can be rewritten as

$$\partial_t \mathbf{v} = -\tfrac{q_e}{m_e} \nabla \varphi \tag{20}$$

Expression (20) implies that in the source-dominated regime, in the absence of background collisions, only the curl-free component of $\mathbf{v}$ can evolve, while its div-free component remains unchanged. In other words, the coupled system (17b)-(17c) has an intrinsic non-local nature. Regardless of the choice of space discretization (e.g. discontinuous or discontinuous finite elements), the numerical solution of source system (17b)-(17c) will necessarily involve some form of global-matrix inversion in order to deal with the nonlocality of the problem.

Remark 2.6 (Elimination of variables and plasma frequency)**.** Neglecting collision terms (i.e. $\mathscr{T}^{-1} \equiv 0$) and taking the divergence to both sides of (17b) and a second time-derivative of (17c) we get:

$$\begin{aligned} \operatorname{div} \partial_t \mathbf{p} &= -\tfrac{q_e}{m_e} \operatorname{div} (\rho \nabla \varphi) \,, \\ -\varepsilon \Delta \partial_{tt} \varphi &= -\tfrac{q_e}{m_e} \operatorname{div} \partial_t \mathbf{p} \,. \end{aligned}$$

Combining both we can eliminate $\operatorname{div} \partial_t \mathbf{p}$ to get

$$-\Delta \partial_{tt} \varphi - \tfrac{1}{\varepsilon} \left(\tfrac{q_e}{m_e} \right)^2 \operatorname{div} (\rho \nabla \varphi) = 0 \,. \tag{21}$$

Here we note that $\frac{\rho}{\varepsilon} \left(\frac{q_e}{m_e} \right)^2 >> 1$ for most technical applications in the context of high-energy-density sciences. We also note that if $\rho = \rho_0 = \text{const}$ in space, with proper boundary conditions, then (21) describes a harmonic oscillator with angular frequency $\omega_p = \left(\frac{\rho_0}{\varepsilon} \left(\frac{q_e}{m_e} \right)^2 \right)^{1/2}$. Here ω_p is the so-called plasma frequency. Directly and/or indirectly expression (21) is at the core of this manuscript: the goal is to design schemes that can use time-step sizes larger than $\frac{2\pi}{\omega_p}$ or, at the very least, stability is not severely affected by this high-frequency oscillatory phenomena.

2.4. Euler-Poisson attractive case: formal balance and source-dominated regime

Lemma 2.5 (Formal balance: attractive case)**.** *The Euler-Poisson system with attractive force* (3a)-(3d) *satisfies the following integral balance*

$$\tfrac{\partial}{\partial t} \int_\Omega \left(\mathcal{E} - \tfrac{\lambda}{2} |\nabla \varphi|^2 \right) \mathrm{d}\boldsymbol{x} + \int_{\partial \Omega} \left(\tfrac{\mathbf{p}}{\rho} (\mathcal{E} + p) + \lambda \varphi \nabla \partial_t \varphi + \varphi \mathbf{p} \right) \cdot \mathrm{n} \, \mathrm{d}\boldsymbol{s} = 0$$

or pointwise

$$\tfrac{\partial}{\partial t} \left(\mathcal{E} - \tfrac{\lambda}{2} |\nabla \varphi|^2 \right) + div \left(\tfrac{\mathbf{p}}{\rho} (\mathcal{E} + p) + \lambda \varphi \nabla \partial_t \varphi + \varphi \mathbf{p} \right) = 0 \,.$$

Note that $\mathcal{E} - \frac{\lambda}{2} |\nabla \varphi|^2$ is not an energy.

The source-dominated system for the attractive Euler-Poisson system is:

$$\partial_t \rho = 0\,, \tag{22a}$$
$$\partial_t \mathbf{p} = -\rho \nabla \varphi\,, \tag{22b}$$
$$-\lambda \Delta \partial_t \varphi = \operatorname{div} \mathbf{p}\,, \tag{22c}$$
$$\partial_t \mathcal{E} = -\nabla \varphi \cdot \mathbf{p}\,. \tag{22d}$$

Note that only (22b) and (22c) are actually coupled.

Lemma 2.6 (Attractive source-system: invariance and formal balance)**.** *The source-system* (22a)-(22d) *satisfies the invariance* $\partial_t\big(\mathcal{E} - \frac{|\mathbf{p}|^2}{2\rho}\big) \equiv 0$ *(see Lemma 2.1). In addition, the subsystem* (22b)-(22c) *satisfies the following integral balance*

$$\tfrac{\partial}{\partial t}\Big(\int_\Omega \tfrac{|\mathbf{p}|^2}{2\rho} - \tfrac{\lambda}{2}|\nabla\varphi|^2 \,\mathrm{d}\boldsymbol{x}\Big) + \int_{\partial\Omega} \varphi(\lambda \nabla \partial_t \varphi + \mathbf{p}) \cdot \mathbf{n}\,\mathrm{d}\boldsymbol{s} = 0\,, \tag{23}$$

or pointwise

$$\tfrac{\partial}{\partial t}\big(\tfrac{|\mathbf{p}|^2}{2\rho} - \tfrac{\lambda}{2}|\nabla\varphi|^2\big) + div\,(\lambda\varphi\nabla\partial_t\varphi + \varphi\mathbf{p}) = 0\,. \tag{24}$$

Remark 2.7. Note that $\frac{|\mathbf{p}|^2}{2\rho} - \frac{\lambda}{2}|\nabla\varphi|^2$ is not an energy, a norm, a positive-definite quadratic-like functional, or a generalization of such concept. More precisely, $\frac{|\mathbf{p}|^2}{2\rho} - \frac{\lambda}{2}|\nabla\varphi|^2$ is a Lagrangian: the difference between kinetic and potential energy. In other words, the source system (22a)-(22d) preserves the internal thermal energy $\mathcal{E} - \frac{|\mathbf{p}|^2}{2\rho}$ while the Lagrangian $\frac{|\mathbf{p}|^2}{2\rho} - \frac{\lambda}{2}|\nabla\varphi|^2$ satisfies a flux-balance as described in (24). The integral of the Lagrangian may or may not be a conserved quantity depending on the boundary conditions used.

3. BASELINE NUMERICAL ARGUMENTS USING COLLOCATED DISCRETIZATIONS

In this section we construct a simple two-stage scheme assuming collocated/nodal discretization for all variables. This assumption is equivalent to considering a spatial discretization of either cell-centered finite volumes or nodal continuous finite elements (algebraically equivalent to vertex-centered finite volumes, cf.[93, 94, 58]) for all fields. Collocated-like discretizations are a good choice for Eulerian shock-hydrodynamics and optimal from the approximation point of view: every field is approximated with the same polynomial degree in space, therefore the same convergence rate should be expected for all fields. In fact, some of most mathematically mature and computationally robust schemes for Eulerian shock-hydrodynamics require a purely nodal space discretization (see for instance [55, 58] and references therein).

However, the choice of a purely collocated/nodal discretization does not play well with Maxwell's equations and it may be entirely inapplicable for the Euler-Poisson model. For the time being, we will ignore these very important issues, develop the basic mathematics in relationship to time-integration and reconcile these problems later in Section §4. This entire section intends to be

primarily of pedagogical nature. However most these lemmas/propositions carry over important consequences that we indeed apply in the context of Euler-Poisson in Section §4.

The presentation is gradual, in the sense that each concern/constraint (e.g. positivity of the internal energy) is separated from each other in order to minimize intellectual difficulties. Primary results of this section are: Proposition 3.1 which establishes minimal requirements for preservation of internal energy when considering any arbitrary force, Lemma 3.2 which establishes minimal requirements for the preservation of the electro-kinetic energy, and finally Lemma (3.4) integrates all previous results establishing minimal requirements for the preservation of positivity of internal energy and total energy in the context of Euler-Maxwell when using operator Splitting.

Here we adopt the notation in [58]. We will assume the existence of nodes $\mathcal{V} = \{1, ..., \text{card}\{\mathcal{V}\}\}$ (a list of integers) identifying space coordinates $\{\boldsymbol{x}_i\}_{i\in\mathcal{V}}$. These space coordinates could be, for instance, interpolation points of a finite element space or barycenters of a finite volumes representation. We will also assume that the nodes exchange mass with a small number of neighboring nodes, more precisely we will assume that for each node $i \in \mathcal{V}$ there is a list of integers $I(i) \subset \mathcal{V}$ called the stencil at the node i such that:

$$i \in I(j) \;\Leftrightarrow\; j \in I(i)\,. \tag{25}$$

With this notation we will assume that all components of the system ρ, $\mathbf{p}$, $\mathcal{E}$, E and B are approximated using a basis $\{\phi_i\}_{i\in\mathcal{V}}$. That is, we will consider the expansions

$$\rho_h = \sum_{i\in\mathcal{V}} \rho_i\phi_i\ ,\ \ \mathbf{p}_h = \sum_{i\in\mathcal{V}} \mathbf{p}_i\phi_i\ ,\ \ \mathcal{E}_h = \sum_{i\in\mathcal{V}} \mathcal{E}_i\phi_i\ ,\ \ \mathrm{E}_h = \sum_{i\in\mathcal{V}} \mathrm{E}_i\phi_i\ ,\ \ \mathrm{B}_h = \sum_{i\in\mathcal{V}} \mathrm{B}_i\phi_i\ ,$$

in order to build finite dimensional approximations of ρ, $\mathbf{p}$, $\mathcal{E}$, E and B.

3.1. Euler's equations with forces.

Assume that we want to solve Euler's balance law $\frac{\partial}{\partial t}\mathbf{u} + \operatorname{div}\mathbb{f}(\mathbf{u}) = \mathbf{s}(\mathbf{f})$ with $\mathbf{u}$, $\mathbb{f}(\mathbf{u})$ and $\mathbf{s}(\mathbf{f})$ as described in (6). The simplest first-order operator splitting scheme for such a problem would look as

$$m_i\frac{\mathbf{u}_i^{n+1}-\mathbf{u}_i^n}{\tau} + \sum_{j\in I(i)} \mathbf{F}_{ij} = m_i\mathbf{S}_i\ \ \forall i \in \mathcal{V}, \tag{26}$$

where $m_i = \int_\Omega \phi_i\,\mathrm{d}\boldsymbol{x}$, $\mathbf{u}_i^n = [\rho_i^n, \mathbf{p}_i^n, \mathcal{E}_i^n]^\top$ represents the state at time t^n at the node $\boldsymbol{x}_i$, τ is the time-step size, $\{\mathbf{F}_{ij}\}_{j\in I(i)}$ is the set of algebraic fluxes with $\mathbf{F}_{ij} \in \mathbb{R}^{d+2}$ and $\mathbf{F}_{ij} = -\mathbf{F}_{ji}$ for all $j \in I(i)$. Scheme (26) can also be rewritten as a two-stage method:

$$\textbf{Stage \#1: } \widetilde{\mathbf{u}}_i^{n+1} := \mathbf{u}_i^n - \tfrac{\tau}{m_i}\sum_{j\in I(i)} \mathbf{F}_{ij} \tag{27}$$

$$\textbf{Stage \#2: } \mathbf{u}_i^{n+1} := \widetilde{\mathbf{u}}_i^{n+1} + \tau\mathbf{S}_i\,. \tag{28}$$

usually known as Yanenko splitting. Here $\widetilde{\mathbf{u}}_i^n = [\widetilde{\rho}_i^n, \widetilde{\mathbf{p}}_i^n, \widetilde{\mathcal{E}}_i^n]^\top$ will be the so-called "hyperbolic-update". From now on quantities with a tilde (such as $\widetilde{\rho}_i^{n+1}$, $\widetilde{\mathbf{p}}_i^{n+1}$, and $\widetilde{\mathcal{E}}_i^{n+1}$) refer to quantities obtained as a result of the hyperbolic update. So far we have not defined $\mathbf{S}_i$: we want to keep our choices open as to whether $\mathbf{S}_i$ should be fully explicit, fully implicit, or something in between. Therefore we consider:

$$\mathbf{S}_i := \begin{bmatrix} 0 \\ \mathbf{f}_i^{n+\theta} \\ \frac{1}{\widetilde{\rho}_i^{n+1}} \mathbf{f}_i^{n+\theta} \cdot \mathbf{p}^{\beta} \end{bmatrix}, \tag{29}$$

here $\mathbf{f}_i^{n+\theta}$ represents an approximation of the force at time $t^{n+\theta} := \theta t^{n+1} + (1-\theta)t^n$ for some $\theta \in [0,1]$, similarly $\mathbf{p}^{n+\beta}$ represents an approximation of the force for some intermediate time $t^{n+\beta} := \beta t^{n+1} + (1-\beta)t^n$ for some $\beta \in [0,1]$. As it's shown in the following proposition, the choice of θ has no consequence in the preservation of internal energy: the force could be fully explicit (i.e. $\theta = 0$, Forward-Euler), fully implicit (i.e. $\theta = 1$, Backward-Euler), or anything in between. However, it seems to be that we don't have much wiggle room for the choice of β.

Proposition 3.1 (Source update scheme for Euler's system: basic scheme)**.** *Let* $\widetilde{\mathbf{u}}_i^{n+1} = [\widetilde{\rho}_i^{n+1}, \widetilde{\mathbf{p}}_i^{n+1}, \widetilde{\mathcal{E}}_i^{n+1}]^\top$ *be the output produced by the hyperbolic-update* (27)*. If the final state* $\mathbf{u}_i^{n+1} = [\rho_i^{n+1}, \mathbf{p}_i^{n+1}, \mathcal{E}_i^{n+1}]^\top$ *follow from the following sequence of computations/definitions*

$$\rho_i^{n+1} := \widetilde{\rho}_i^{n+1}, \tag{30}$$

$$\mathbf{p}_i^{n+1} := \widetilde{\mathbf{p}}_i^{n+1} + \tau \mathbf{f}_i^{n+\theta}, \tag{31}$$

$$\mathbf{v}^{n+\frac{1}{2}} := \frac{(\mathbf{p}_i^{n+1} + \widetilde{\mathbf{p}}_i^{n+1})}{2\rho_i^{n+1}}, \tag{32}$$

$$\mathcal{E}_i^{n+1} := \widetilde{\mathcal{E}}_i^{n+1} + \tau \mathbf{f}_i^{n+\theta} \cdot \mathbf{v}^{n+\frac{1}{2}}, \tag{33}$$

then we have that

$$\mathcal{E}_i^{n+1} - \tfrac{1}{2}\frac{|\mathbf{p}_i^{n+1}|^2}{\rho_i^{n+1}} = \widetilde{\mathcal{E}}_i^{n+1} - \tfrac{1}{2}\frac{|\widetilde{\mathbf{p}}_i^{n+1}|^2}{\widetilde{\rho}_i^{n+1}}. \tag{34}$$

Proof. The proof follows by taking the dot-product of (31) with $\mathbf{v}^{n+\frac{1}{2}}$ and adding it to (33). □

Remark 3.1. Proposition 3.1 is nothing else than the discrete counterpart of Lemma 2.1.

Remark 3.2. Note that $\widetilde{\mathbf{u}}_i^{n+1} = [\widetilde{\rho}_i^{n+1}, \widetilde{\mathbf{p}}_i^{n+1}, \widetilde{\mathcal{E}}_i^{n+1}]^\top$ defined in (27) is the hyperbolic update (no contribution from the sources). We will assume that $\widetilde{\mathbf{u}}_i^{n+1}$ has positive density and internal energy. At the time of this writing there are numerical techniques can achieve such targets with ample margin of confidence (see [85, 110, 55, 58]). In particular, the techniques developed in [57, 55, 58] preserve not only the positivity of the density and internal energy but more generally the invariant set of Euler's equation as described in proposition 2.1 well-beyond the context of the simplistic ideal-gas law. We also mention that the notation used in (25)-(26) was taken from [55, 58] since the vast majority of space discretization techniques (finite volumes, continuous finite elements and discontinuous finite elements, etc) can be rewritten using such notation.

3.2. Euler-Maxwell: preservation of the internal energy

For the case of Euler-Maxwell's system we have that the source term on the right hand side of Euler's system is

$$\mathbf{S}_i = \begin{bmatrix} 0 \\ \frac{q_e}{m_e}\rho_1 \mathrm{E}_1 + \frac{q_e}{m_e}\mathbf{p}_1 \times \mathrm{B}_1 \\ \frac{q_e}{m_e}\mathrm{E}_2 \cdot \mathbf{p}_2 \end{bmatrix}, \tag{35}$$

where the optimal values of ρ_1, E_1, $\mathbf{p}_1$, B_1, E_2, $\mathbf{p}_2$ have to be determined. In principle $\mathbf{S}_i$ could be explicit, semi-implicit, fully-implicit, or something else entirely (e.g. "given data" coming from another piece of legacy code). As usual, we want to keep our options open and postpone these decisions for as long as it could be possible: we want understand what is the minimal amount of time-implicitness we can afford and still preserve the properties that we want to preserve. For instance, we have already learned from Proposition (3.1) that if our sole target is preservation of the internal energy we don't need to consider time-implicit forces (at all). For the time being we want to determine which variables can be lagged and which ones have to left implicit in order to preserve a discrete counterpart of constraint (10). The following lemma makes more specific the minimal constraints on ρ_1, E_1, $\mathbf{p}_1$, B_1, E_2, $\mathbf{p}_2$ that we have to satisfy in order to guarantee preservation of the internal energy.

Lemma 3.1. *The choice*

$$\rho_1 := \widetilde{\rho}_i^{n+1}\ ,\ \ \mathbf{p}_1 = \mathbf{p}_2 = \mathbf{p}^{n+\frac{1}{2}} := \tfrac{1}{2}(\mathbf{p}^{n+1} + \widetilde{\mathbf{p}}^{n+1})\ ,\ \ \mathrm{E}_2 = \mathrm{E}_1 := \mathrm{E}_i \text{ and } \mathrm{B}_1 := \mathrm{B}_i \tag{36}$$

with E_i *and* B_i *being* arbitrary *for* (35) *is such that identity* (34) *is preserved.*

Proof. The proof follows either by re-use of Proposition 3.1 or direct computation of the internal energy of $\mathbf{u}_i^{n+1} = [\rho_i^{n+1}, \mathbf{p}_i^{n+1}, \mathcal{E}_i^{n+1}]^\top$ and $\widetilde{\mathbf{u}}_i^{n+1} = [\widetilde{\rho}_i^{n+1}, \widetilde{\mathbf{p}}_i^{n+1}, \widetilde{\mathcal{E}}_i^{n+1}]^\top$ and verification that they take the same symbolic vale. □

Summarizing what we have learned so far: the source update scheme for the hydrodynamics part would look as follows

$$\begin{aligned} \mathbf{p}_i^{n+1} &= \widetilde{\mathbf{p}}_i^{n+1} + \tfrac{\tau q_e}{m_e}\rho_i^{n+1}\mathrm{E}_i + \tfrac{\tau q_e}{2m_e}(\mathbf{p}_i^{n+1} + \widetilde{\mathbf{p}}_i^{n+1}) \times \mathrm{B}_i\,, \\ \mathcal{E}_i^{n+1} &= \widetilde{\mathcal{E}}_i^{n+1} + \tfrac{\tau q_e}{2m_e}\mathrm{E}_i \cdot (\mathbf{p}_i^{n+1} + \widetilde{\mathbf{p}}_i^{n+1})\,, \end{aligned} \tag{37}$$

Note that: in (37) first we have to solve for $\mathbf{p}_i^{n+1}$ by inverting a $\mathbb{R}^{3\times 3}$ matrix, once we have the value of $\mathbf{p}_i^{n+1}$ we just plug it into the second line of (37). Note that the $\mathbb{R}^{3\times 3}$ matrix is always invertible for every time step size: this stems from the fact that the matrix is the identity with a skew-symmetric perturbation (guaranteed to be positive definite).

The local update (37) does not describe a "complete scheme" that we can readily implement. It leaves a few questions open such as the proper choices for E_i and B_i (fully explicit? fully implicit?). Local update (37) solves only one problem: it preserves the positivity of the internal energy by coupling the effects of the sources in the momentum and the mechanical energy. It does not take care of the invariant property (11). That's that topic of next section, which will allow us to define a scheme involving all fields of the Euler-Maxwell system.

3.3. Euler-Maxwell: preservation of the electro-kinetic energy and global energy-stability

Essentially, we want to guarantee that the coupling introduced by the sources is such that the following constraint is satisfied

$$\frac{|\mathbf{p}_i^{n+1}|^2}{2\rho_i^{n+1}} + \frac{\varepsilon}{2}|\mathrm{E}_i^{n+1}|^2 \leq \frac{|\widetilde{\mathbf{p}}_i^{n+1}|^2}{2\rho_i^{n+1}} + \frac{\varepsilon}{2}|\widetilde{\mathrm{E}}_i^{n+1}|^2 \quad \forall i \in \mathcal{V}, \tag{38}$$

which is the discrete counterpart of (11) in the case of equality. If (38) happens to be a strict inequality then, the coupling introduced by the sources will be energy-dissipative rather than energy-preserving. Some amount of dissipation might be desirable. Here we will only present the energy conservative case, the energy dissipative case is very similar.

We propose the following source-update of the momentum and the electric field :

$$\begin{aligned} \mathbf{p}_i^{n+1} - \widetilde{\mathbf{p}}_i^{n+1} &= \tfrac{\tau q_e}{m_e}\rho_i^{n+1}\mathrm{E}_i + \tfrac{\tau q_e}{m_e}\tfrac{(\mathbf{p}_i^{n+1}+\widetilde{\mathbf{p}}_i^{n+1})}{2} \times \mathrm{B}_i\,, \\ \varepsilon(\mathrm{E}_i^{n+1} - \widetilde{\mathrm{E}}_i^{n+1}) &= -\tfrac{\tau q_e}{m_e}\mathbf{p}_i \end{aligned} \tag{39}$$

where the values for E_i, B_i, $\mathbf{p}_i$ have to be determined. Note that in (39) we have committed to the choice $\frac{(\mathbf{p}_i^{n+1}+\widetilde{\mathbf{p}}_i^{n+1})}{2}$ in the cross product which is consistent with expression (37) if our goal is to preserve internal energy too. The following lemma settles the choices for E_i and $\mathbf{p}_i$.

Lemma 3.2. *If we choose*

$$\mathrm{E}_i := \mathrm{E}_i^{n+\frac{1}{2}} = \tfrac{1}{2}(\mathrm{E}_i^{n+1} + \widetilde{\mathrm{E}}_i^{n+1}) \;\; \textit{and} \;\; \mathbf{p}_i := \mathbf{p}_i^{n+\frac{1}{2}} = \tfrac{1}{2}(\mathbf{p}_i^{n+1} + \widetilde{\mathbf{p}}_i^{n+1})$$

and B_i *arbitrary in* (39)*, then we have that the electro-kinetic energy is preserved, i.e.*

$$\frac{|\mathbf{p}_i^{n+1}|^2}{2\rho_i^{n+1}} + \frac{\varepsilon}{2}|\mathrm{E}_i^{n+1}|^2 = \frac{|\widetilde{\mathbf{p}}_i^{n+1}|^2}{2\rho_i^{n+1}} + \frac{\varepsilon}{2}|\widetilde{\mathrm{E}}_i^{n+1}|^2\,. \tag{40}$$

Proof. The proof follows by using the elementary algebraic identity $(a-b)(a+b) = a^2 - b^2$. Multiplying the first line of (39) by $\frac{1}{2}(\mathbf{p}_i^{n+1} + \widetilde{\mathbf{p}}_i^{n+1})$ and the second line by $\frac{1}{2}(\mathrm{E}_i^{n+1} + \widetilde{\mathrm{E}}_i^{n+1})$ we get

$$\tfrac{1}{2}(|\mathbf{p}_i^{n+1}|^2 - |\widetilde{\mathbf{p}}_i^{n+1}|^2) = \tfrac{\tau q_e}{m_e}\rho_i^{n+1}\mathrm{E}_i \cdot \tfrac{1}{2}(\mathbf{p}_i^{n+1} + \widetilde{\mathbf{p}}_i^{n+1}) \tag{41}$$

$$\tfrac{\varepsilon}{2}(|\mathrm{E}_i^{n+1}|^2 - |\widetilde{\mathrm{E}}_i^{n+1}|^2) = -\tfrac{\tau q_e}{m_e}\mathbf{p}_i \cdot \tfrac{1}{2}(\mathrm{E}_i^{n+1} + \widetilde{\mathrm{E}}_i^{n+1}) \tag{42}$$

The results follows dividing (41) by ρ_i^{n+1} and adding both lines. □

3.4. Euler-Maxwell: complete source-update scheme.

Combining the lessons learned in Lemmas 3.1 and 3.2 we are now in position of defining a first-order time-update scheme in the spirit of Yanenko-splitting. Generalization to second-order accuracy is straightforward using Strang-Marchuk splitting.

Remark 3.3 (A first-order scheme)**.** Given $[\rho^n, \mathbf{p}^n, \mathrm{B}^n, \mathrm{E}^n, \mathcal{E}^n]$ we consider the following two-stage scheme:

- **Stage #1 (hyperbolic update).** Compute the pure-hyperbolic update using a full time-step size τ:
  - Euler's subsystem: $[\rho^{n+1}, \widetilde{\mathbf{p}}^{n+1}, \widetilde{\mathcal{E}}^{n+1}]^\top$ can be computed using Forward-Euler or a convex combination of Forward-Euler steps preserving convex constraints (e.g. SSP2 or SSP3 schemes [53]).
  - Maxwell's subsystem: we could use, for instance, the implicit midpoint rule (i.e. Crank-Nicolson) in order to compute $[\widetilde{\mathrm{B}}^{n+1}, \widetilde{\mathrm{E}}^{n+1}]^\top$ which is second-order accurate and preserves the Hamiltonian of Maxwell's equation $\int_\Omega \frac{\varepsilon}{2}|\mathrm{E}|^2 + \frac{1}{2\mu}|\mathrm{B}|^2$.
- **Stage #2 (source update).** Define $\rho_i^{n+1} := \widetilde{\rho}_i^{n+1}$ and $\mathrm{B}_i^{n+1} := \widetilde{\mathrm{B}}_i^{n+1}$, then
  - **Stage #2.1:** find $\mathbf{p}_i^{n+1}$ and E_i^{n+1} solving

$$\mathbf{p}_i^{n+1} - \widetilde{\mathbf{p}}_i^{n+1} = \tfrac{\tau q_e}{2m_e}\rho_i^{n+1}(\mathrm{E}_i^{n+1} + \widetilde{\mathrm{E}}_i^{n+1}) + \tfrac{\tau q_e}{2m_e}(\mathbf{p}_i^{n+1} + \widetilde{\mathbf{p}}_i^{n+1}) \times \mathrm{B}_i^{n+1}\,, \tag{43}$$

$$\varepsilon(\mathrm{E}_i^{n+1} - \widetilde{\mathrm{E}}_i^{n+1}) = -\tfrac{\tau q_e}{2m_e}(\mathbf{p}_i^{n+1} + \widetilde{\mathbf{p}}_i^{n+1})\,.\mathrm{E}_i^{n+1} + \widetilde{\mathrm{E}}_i^{n+1}) \tag{44}$$

    Note that this requires inverting an $\mathbb{R}^{6\times 6}$ matrix at every cell/node.

  - **Stage #2.2:** with the values of $\mathbf{p}_i^{n+1}$ and E_i^{n+1} found the Stage 2.1, compute $\mathcal{E}_i^{n+1}$ as

$$\mathcal{E}_i^{n+1} - \widetilde{\mathcal{E}}_i^{n+1} = \tfrac{\tau q_e}{4m_e}(\mathrm{E}_i^{n+1} + \widetilde{\mathrm{E}}_i^{n+1}) \cdot (\mathbf{p}_i^{n+1} + \widetilde{\mathbf{p}}_i^{n+1})\,. \tag{45}$$

The scheme described by 43-(45) naturally preserves the convex invariants (see proposition 3.1 and 3.2) of the hyperbolic subsystem: catastrophic failure because of negative density or internal energy is not possible. We also have the following energy-stability lemma which establishes conditions for stability on the whole scheme consisting of Stages #1 and #2 described above.

Lemma 3.3 (Minimal conditions for energy-stability)**.** *For the scheme described in Remark 3.3. In the Stage #1, assume that the scheme used to solve Euler's equation is conservative in the sense that*

$$\sum_{i\in\mathcal{V}} m_i \widetilde{\mathcal{E}}_i^{n+1} = \sum_{i\in\mathcal{V}} m_i \mathcal{E}_i^n\,, \tag{46}$$

where $\mathcal{V}$ represents the set of all cells (or nodes) and m_i is the measure of the cells (or lumped mass entry) in the cases of cell-centered finite volumes (or continuous nodal finite elements respectively). Similarly, assume that the hyperbolic update of Maxwell's equation (in Stage #1) is either energy-conservative or energy-dissipative in the sense that

$$\sum_{i\in\mathcal{V}} m_i\Big(\tfrac{\varepsilon}{2}|\widetilde{\mathrm{E}}_i^{n+1}|^2 + \tfrac{1}{2\mu}|\widetilde{\mathrm{B}}_i^{n+1}|^2\Big) \le \sum_{i\in\mathcal{V}} m_i\Big(\tfrac{\varepsilon}{2}|\mathrm{E}_i^n|^2 + \tfrac{1}{2\mu}|\mathrm{B}_i^n|^2\Big)\,. \tag{47}$$

If Stage #2 is such that

$$\sum_{i\in\mathcal{V}} m_i\Big(\mathcal{E}_i^{n+1} - \tfrac{|\mathbf{p}_i^{n+1}|^2}{2\rho_i^{n+1}}\Big) \le \sum_{i\in\mathcal{V}} m_i\Big(\widetilde{\mathcal{E}}_i^{n+1} - \tfrac{|\widetilde{\mathbf{p}}_i^{n+1}|^2}{2\rho_i^{n+1}}\Big), \tag{48}$$

$$\sum_{i\in\mathcal{V}} m_i\Big(\tfrac{|\mathbf{p}_i^{n+1}|^2}{2\rho_i^{n+1}} + \tfrac{\varepsilon}{2}|\mathrm{E}_i^{n+1}|^2\Big) \le \sum_{i\in\mathcal{V}} m_i\Big(\tfrac{|\widetilde{\mathbf{p}}_i^{n+1}|^2}{2\rho_i^{n+1}} + \tfrac{\varepsilon}{2}|\widetilde{\mathrm{E}}_i^{n+1}|^2\Big), \tag{49}$$

then we have

$$\sum_{i\in\mathcal{V}} m_i\Big(\mathcal{E}_i^{n+1} + \tfrac{\varepsilon}{2}|\mathrm{E}_i^{n+1}|^2 + \tfrac{1}{2\mu}|\mathrm{B}_i^{n+1}|^2\Big) \le \sum_{i\in\mathcal{V}} m_i\Big(\mathcal{E}_i^{n} + \tfrac{\varepsilon}{2}|\mathrm{E}_i^{n}|^2 + \tfrac{1}{2\mu}|\mathrm{B}_i^{n}|^2\Big), \tag{50}$$

which is a discrete counterpart of the energy estimate (13) *in the case of* $\mathscr{T}^{-1} \equiv 0$.

Proof. Adding (48) and (49) we get

$$\sum_{i\in\mathcal{V}} m_i\Big(\mathcal{E}_i^{n+1} + \tfrac{\varepsilon}{2}|\mathrm{E}_i^{n+1}|^2\Big) \le \sum_{i\in\mathcal{V}} m_i\Big(\widetilde{\mathcal{E}}_i^{n+1} + \tfrac{\varepsilon}{2}|\widetilde{\mathrm{E}}_i^{n+1}|^2\Big). \tag{51}$$

Now we add $\sum_{i\in\mathcal{V}} \frac{m_i}{2\mu}|\mathrm{B}_i^{n+1}|^2$ to both sides of (51) and exploit the fact that $\mathrm{B}_i^{n+1} = \widetilde{\mathrm{B}}_i^{n+1}$ to get

$$\begin{aligned}\sum_{i\in\mathcal{V}} m_i\Big(\mathcal{E}_i^{n+1} + \tfrac{\varepsilon}{2}|\mathrm{E}_i^{n+1}|^2 + \tfrac{1}{2\mu}|\mathrm{B}_i^{n+1}|^2\Big) &\le \sum_{i\in\mathcal{V}} m_i\Big(\widetilde{\mathcal{E}}_i^{n+1} + \tfrac{\varepsilon}{2}|\widetilde{\mathrm{E}}_i^{n+1}|^2 + \tfrac{1}{2\mu}|\widetilde{\mathrm{B}}_i^{n+1}|^2\Big)\\ &\le \sum_{i\in\mathcal{V}} m_i\Big(\mathcal{E}_i^{n} + \tfrac{\varepsilon}{2}|\mathrm{E}_i^{n}|^2 + \tfrac{1}{2\mu}|\mathrm{B}_i^{n}|^2\Big)\end{aligned} \tag{52}$$

where the last inequality was obtained using (46) and (47). □

Some comments and notes:

- In particular, the constructions/schemes proposed in Remark 3.3 comply with the requirements and assumptions of Lemma 3.3.
- We note that artificial heating appears to be incompatible with energy stablity. In other words, if instead of (48) we had the reverse inequality, i.e.

  $$\sum_{i\in\mathcal{V}} m_i\Big(\mathcal{E}_i^{n+1} - \tfrac{|\mathbf{p}_i^{n+1}|^2}{2\rho_i^{n+1}}\Big) \ge \sum_{i\in\mathcal{V}} m_i\Big(\widetilde{\mathcal{E}}_i^{n+1} - \tfrac{|\widetilde{\mathbf{p}}_i^{n+1}|^2}{2\rho_i^{n+1}}\Big),$$

  implying an increase of the internal energy/temperature, then it does not seem possible to establish energy-stability property (50).
- Extension of the ideas described in 3.3 to second-order accuracy (in time) is straightforward using operator-splitting and related ideas [99, 89]. Essentially, let $\mathcal{S}_E(\tau)$, $\mathcal{S}_M(\tau)$ and $\mathcal{S}_S(\tau)$ be the exact solution operators for the Euler's subsystem, Maxwell's subsystem, and ODE-source problem (9a)-(9e) respectively. If we replace these exact solution operators by

second-order accurate counterparts $\mathcal{S}_{E,h}(\tau)$, $\mathcal{S}_{M,h}(\tau)$ and $\mathcal{S}_{S,h}(\tau)$ we can define an approximate solution operator $S_h(\tau)$ as the composition

$$\mathcal{S}_h(\tau) := \mathcal{S}_{H,h}(\tfrac{\tau}{2}) \circ \mathcal{S}_{S,h}(\tau) \circ \mathcal{S}_{H,h}(\tfrac{\tau}{2}) \text{ or } S_h(\tau) := \mathcal{S}_{S,h}(\tfrac{\tau}{2}) \circ \mathcal{S}_{H,h}(\tau) \circ \mathcal{S}_{S,h}(\tfrac{\tau}{2}), \quad (53)$$
$$\text{where } S_{H,h}(\tau) = \begin{bmatrix} \mathcal{S}_{E,h}(\tau) \\ \mathcal{S}_{M,h}(\tau) \end{bmatrix},$$

leading to the time-update scheme $\mathbf{U}^{n+1} = \mathcal{S}_h(\tau)\mathbf{U}^n$. Formula (53) is the well-known symmetric second-order Marchuk-Strang splitting. Preservation of the convex invariants of Euler's subsystem is guaranteed for each stage (equivalently by each discrete solution operator), therefore it's guaranteed for the final solution too. Extension to third-order accuracy using the operator splitting approach of Goldman and Kaper (see [52]) is certainly possible provided each stage is the discretization of a time-reversible PDE-problem.

The best of the author's knowledge Lemma 3.3 is possibly the first nonlinear stability statement for Euler's system with sources using operator Splitting. We are not aware of any similar or comparable result in the context of Runge-Kutta IMEX schemes or comparable time-integrators.

We highlight that some of the ideas presented in this section have been used in the context of compressible Navier-Stokes equation (quite recently) leading to new schemes with mathematically and computationally guaranteed robustness [54]. The novelty is not in the use of operator splitting. The novelty is in the choices of space and time-integration techniques used for each stage, the choice of semi-implicit lagging of specific variables, all of which which allow to establish the natural nonlinear stability properties of the PDE.

4. NUMERICAL SCHEMES FOR EULER-POISSON

In this section we describe numerical schemes for Euler-Poisson model using operator splitting approach in (53) and key ideas outlined in Section §(3). At its core, this section is primarily about the source update-scheme (i.e. Stage #2 in the context of Strang-splitting, see for instance Remark 3.3), the choices of space-discretization, asymptotic well-posedness of the linear algebra problem, and the preservation of the electro-kinetic energy. In section §4.4 we describe a complete source-update scheme involving the total mechanical energy and the preservation of internal energy.

4.1. Notation: space discretization

We will assume that the hydrodynamics subsystem is discretized with nodal-finite finite element space $\mathbb{V} = [\mathbb{V}]^{d+2}$ where $\mathbb{V}$ is either a $\mathbb{P}^1$ (in the context of simplices) or $\mathbb{Q}^1$ (in the context of quadrilateras/hexahedrons) scalar-valued finite element space [55]. We define local-to-physical geometrical map $\boldsymbol{T}_K(\widehat{\boldsymbol{x}}) : \widehat{K} \to K$, where $\widehat{K}$ is the reference element, K is an element in physical space, the gradient of the local-to-physical geometrical map is denoted as $\mathbb{J}_K(\widehat{\boldsymbol{x}}) := \nabla_{\widehat{\boldsymbol{x}}} \boldsymbol{T}_K(\widehat{\boldsymbol{x}})$ i.e. $\mathbb{J}_K(\widehat{\boldsymbol{x}}) : \widehat{K} \to \mathbb{R}^{d\times d}$ which we will call the Jacobian. We note that the Jacobian is just a constant

matrix in the context of affinely mapped elements, but it's function of space for general mappings such as the general bilinear maps used for quadrilaterals. We will use $(v,w)_{L^2(\Omega)}$ to denote the traditional L^2-inner product

$$(v,w)_{L^2(\Omega)} = \int_\Omega vw \,\mathrm{d}\boldsymbol{x}\,.$$

In the computational context $(v_h,w_h)_{L^2(\Omega)}$ will denote computation of the inner-product to either machine accuracy or overkill quadrature. On the other hand, we define the discrete or lumped inner-product by $\langle\cdot,\cdot\rangle_h$

$$\langle \mathbf{v}_h, \mathbf{w}_h\rangle_h = \sum_{K\subset\mathcal{T}_h}\sum_{q\in\mathcal{N}(\widehat{K})} \mathbf{v}_h(\boldsymbol{T}_K(\widehat{\boldsymbol{x}}_q))\cdot\mathbf{w}_h(\boldsymbol{T}_K(\widehat{\boldsymbol{x}}_q))\,\det\mathbb{J}(\boldsymbol{T}_K(\widehat{\boldsymbol{x}}_q))\,\widehat{\boldsymbol{\omega}}_q \tag{54}$$

where $\mathcal{T}_h$ represents the set of all elements, $\mathcal{N}(\widehat{K})$ is the set of indexes of the interpolation/quadrature points and weights in the reference element $\widehat{K}$, $\widehat{\boldsymbol{x}}_q\in\widehat{K}$ represents the coordinate of the q-th interpolation/quadrature point, and $\widehat{\boldsymbol{\omega}}_q$ is q-th the quadrature weight.

We note that:

- As written, (54) is only valid if both $\mathbf{v}_h$ and $\mathbf{w}_h$ are nodal vector-valued finite element functions. Div-conforming and curl-conforming finite element spaces require much more sophisticated Piola transformations. Such transformations are particularly well reported in Section §3.9 of [82] and for the sake of brevity will not be part of this report. We will however invoke the discrete inner product $\langle\mathbf{v}_h,\mathbf{w}_h\rangle_h$ far beyond the context of purely nodal finite element spaces. We will tacitly assume that the reader is aware that definition (54) has to be modified accordingly for each possible case.
- If $\mathbf{v}_h\in\mathbb{V}$, a continuous nodal space, then $\mathbf{v}_h(\boldsymbol{T}_K(\widehat{\boldsymbol{x}}_q))\equiv\mathbf{v}_h(\boldsymbol{x}_q)$ the unique nodal value. However, let K and K' be two elements containing the node/vertex with physical coordinates $\boldsymbol{x}_i$ such that: $\boldsymbol{T}_K(\widehat{\boldsymbol{x}}_q)=\boldsymbol{T}_{K'}(\widehat{\boldsymbol{x}}_p)=\boldsymbol{x}_i$ and $\mathbf{v}_h$ belongs to a curl-conforming or div-conforming finite element space then we have that: in general, $\mathbf{v}_h(\boldsymbol{T}_K(\widehat{\boldsymbol{x}}_q))\not\equiv\mathbf{v}_h(\boldsymbol{T}_{K'}(\widehat{\boldsymbol{x}}_p))$ since edge or face elements are not guaranteed to have uniquely defined nodal values. The same situation holds true, more generally, with completely discontinuous finite element spaces.

4.2. Method of lines and its shortcomings.

In this section we focus on the coupled subsystem (17b)-(17c) and the preservation of the electro-kinetic energy. In order to avoid discussions on boundary conditions and remove additional difficulties we assume that $\mathbf{p}\cdot\mathrm{n}\equiv 0$ and either $\nabla\varphi\cdot\mathrm{n}\equiv 0$ or $\varphi\equiv 0$ on the entirety of the boundary $\partial\Omega$. This makes the source system an electro-mechanically isolated system. We may start by considering the following scheme: Find $\mathbf{v}_h^{n+1}\in\mathbb{V}$ and $\varphi_h^{n+1}\in\mathbb{H}$ solution of

$$\varepsilon\big(\nabla\varphi_h^{n+1}-\nabla\widetilde{\varphi}_h^{n+1},\nabla\omega_h\big)_{\mathbf{L}^2(\Omega)} = -\tfrac{\tau\nu}{2}\big(\mathbf{p}_h^{n+1}+\widetilde{\mathbf{p}}_h^{n+1},\nabla\omega_h\big)_{\mathbf{L}^2(\Omega)}\,, \tag{55}$$

$$\langle\mathbf{v}_h^{n+1}-\widetilde{\mathbf{v}}_h^{n+1},\mathbf{z}_h\rangle_h = \tfrac{\tau\nu}{2}(\nabla\varphi_h^{n+1}+\nabla\widetilde{\varphi}_h^{n+1},\mathbf{z}_h)_{\mathbf{L}^2(\Omega)}\,, \tag{56}$$

for all $\omega\in\mathbb{H}$ and $\mathbf{z}_h\in\mathbb{V}$, where $\nu:=\frac{q_e}{m_e}$.

Lemma 4.1. *Scheme* (55)-(56) *is such that*

$$\tfrac{\varepsilon}{2}\|\nabla\varphi_h^{n+1}\|^2_{\mathbf{L}^2(\Omega)} + \sum_{i\in\mathcal{V}} \tfrac{m_i}{2\rho_i^{n+1}}|\mathbf{p}_i^{n+1}|^2_{\ell^2} = \tfrac{\varepsilon}{2}\|\nabla\widetilde{\varphi}_h^{n+1}\|^2_{\mathbf{L}^2(\Omega)} + \sum_{i\in\mathcal{V}} \tfrac{m_i}{2\rho_i^{n+1}}|\widetilde{\mathbf{p}}_i^{n+1}|^2_{\ell^2}\,.$$

Proof. The proof follows by taking $\nabla\omega_h = \frac{1}{2}(\nabla\varphi_h^{n+1} + \nabla\widetilde{\varphi}_h^{n+1})$ in (55) and taking $\mathbf{z}_h = \frac{1}{2}(\mathbf{p}_h^{n+1} + \widetilde{\mathbf{p}}_h^{n+1})$ in (56), and adding both lines. □

However, this good news bought by Lemma (4.1) have to be confronted with the algebraic difficulties that might be encountered in order to actually solve the linear system associated to (55)-(56).

Remark 4.1 (Algebraic/matrix representation)**.** The coupled linear system (55)-(56) leads to the following block-matrix system:

$$\begin{aligned}\varepsilon\mathcal{K}_{\Phi\Phi}(\Phi^{n+1} - \widetilde{\Phi}^{n+1}) &= -\tfrac{\tau\nu}{2}\mathcal{M}_{\Phi\mathbf{v}}\mathcal{D}^{n+1}(\mathbf{V}^{n+1} + \widetilde{\mathbf{V}}^{n+1})\,,\\ \mathcal{M}^{\mathrm{L}}_{\mathbf{vv}}(\mathbf{V}^{n+1} - \widetilde{\mathbf{V}}^{n+1}) &= \tfrac{\tau\nu}{2}\mathcal{M}_{\mathbf{v}\Phi}(\Phi^{n+1} + \widetilde{\Phi}^{n+1})\,,\end{aligned} \tag{57}$$

where Φ is vector containing the degrees of freedom of the potential, $\mathbf{V}^{n+1}$ is vector containing the degrees of freedom of the velocity, and the matrices $\mathcal{M}^{\mathrm{L}}_{\mathbf{vv}}$, $\mathcal{M}_{\Phi\mathbf{v}}$, $\mathcal{M}_{\mathbf{v}\Phi}$, $\mathcal{K}_{\Phi\Phi}$, and $\mathcal{D}^{n+1}$ are defined as

$$\begin{aligned}[\mathcal{M}^{\mathrm{L}}_{\mathbf{vv}}]_{ij} = \delta_{ij}\int_\Omega \phi_i\,\mathrm{d}\boldsymbol{x}\,,\ \ [\mathcal{K}_{\Phi\Phi}]_{ij} = \int_\Omega \nabla\chi_i\nabla\chi_j\,\mathrm{d}\boldsymbol{x}\,,\\ [\mathcal{M}_{\mathbf{v}\Phi}]_{ij} = \int_\Omega \phi_i\nabla\chi_j\,\mathrm{d}\boldsymbol{x}\,,\ \ [\mathcal{M}_{\Phi\mathbf{v}}]_{ij} = \int_\Omega \nabla\chi_i\phi_j\,\mathrm{d}\boldsymbol{x}\,,\ \ [\mathcal{D}^{n+1}]_{ij} = \delta_{ij}\rho_i^{n+1}.\end{aligned}$$

Note that $\mathcal{M}_{\Phi\mathbf{v}} = \mathcal{M}_{\mathbf{v}\Phi}^\top$ and that $\mathcal{M}^{\mathrm{L}}_{\mathbf{vv}}$ and $\mathcal{D}^{n+1}$ are diagonal matrices. In particular, note that the momentum vector can be computed as the diagonal scaling $\mathbf{P}^{n+1} = \mathcal{D}^{n+1}\mathbf{V}^{n+1}$. Blockwise solution of the linear algebra system (57) leads to

$$\begin{aligned}\big(\varepsilon\mathcal{K}_{\Phi\Phi} + (\tfrac{\tau\nu}{2})^2\mathcal{M}_{\Phi\mathbf{v}}\mathcal{D}^{n+1}\mathcal{M}^{\mathrm{L}\,-1}_{\mathbf{vv}}\mathcal{M}_{\mathbf{v}\Phi}\big)\Phi^{n+1} = \big(\varepsilon\mathcal{K}_{\Phi\Phi} - (\tfrac{\tau\nu}{2})^2\mathcal{M}_{\Phi\mathbf{v}}\mathcal{D}^{n+1}\mathcal{M}^{\mathrm{L}\,-1}_{\mathbf{pp}}\mathcal{M}_{\mathbf{v}\Phi}\big)\widetilde{\Phi}^{n+1}\\ - \tau\nu\mathcal{M}_{\Phi\mathbf{v}}\widetilde{\mathbf{P}}^{n+1}\,.\end{aligned} \tag{58}$$

Regarding the structure of the matrices in (58) we note the following:

- The Schur complement $\varepsilon\mathcal{K}_{\Phi\Phi} + (\frac{\tau\nu}{2})^2\mathcal{M}_{\Phi\mathbf{v}}\mathcal{D}^{n+1}\mathcal{M}^{\mathrm{L}\,-1}_{\mathbf{vv}}\mathcal{M}_{\mathbf{v}\Phi}$ is symmetric and invertible. For the case of Dirichlet and mixed (Dirichlet-Neumann) data, upon algebraic elimination of the non-DOFs, invertibility holds trivially true since the matrix is positive definite. For the case of pure Neumann data, the matrix will have a one-dimensional kernel (the subspace of constants) which presents no difficulty for Krylov space methods provided the right-hand side of the linear algebra system is on the column space of the matrix.
- However, the fact that "invertibility" holds true, as mentioned in the previous bullet, may or may not have much computational implications. If the finite element space $\mathbb{V}$ used to discretize each component of the momentum/velocity is, for instance, a continuous $[\mathbb{Q}^1]^d$ (or $[\mathbb{P}^1]^d$) finite element space and a continuous $\mathbb{Q}^1$ (or $\mathbb{P}^1$ respectively) is used for the

scalar finite element space $\mathbb{H}$ (used to discretize the electric potential) then the block $\mathcal{M}_{\Phi\mathbf{v}}(\mathcal{D}^{n+1}\mathcal{M}^{\mathrm{L}}_{\mathbf{vv}})^{-1}\mathcal{M}_{\mathbf{v}\Phi}$ is necessarily rank-deficient (non-invertible). This is a well-documented fact that can be found in standard literature for Darcy and Stokes mixed formulations [49, 45]. This rank-deficiency is usually manifested graphically as checker-board modes. Similar spurious defects also appear in ad-hoc finite-difference, finite-volume, or discontinuous discontinuous finite element constructions.

- In the context of high-energy-density physics applications, the number $\frac{\nu^2}{\varepsilon}\max_{i\in\mathcal{V}}\rho_i^{n+1}$ is disproportionately larger than one. This means that the Schur complement matrix in (58) is entirely dominated by the second block (with the exception of the low-density regimes). We can speculate that the modes contained in the kernel of the block $\mathcal{M}_{\Phi\mathbf{v}}(\mathcal{D}^{n+1}\mathcal{M}^{\mathrm{L}}_{\mathbf{vv}})^{-1}\mathcal{M}_{\mathbf{v}\Phi}$ will manifest visually far beyond what could have any physical meaning in practice and cause severe deterioration of iterative solvers.

In other words, the source-update scheme (56)-(55) is stable (it preserves the electro-kinetic energy) but leads to an ill-conditioned system, where spurious modes can grow unboundedly in the context of high-density regimes. This is an interesting example of a scheme that is stable, but not "asymptotically stable" or "asymptotically well-posed".

Remark 4.2 (An unsatisfactory solution)**.** The asymptotic ill-conditioning of the Schur complement in (58) is a problem that we can solve quite straightforwardly if we are open to using alternative choices of finite elements spaces. For instance, using curl-conforming finite element space for the velocity or momentum this rank-deficiency can be solved almost immediately. To be more precise, consider the following thought experiment: let's make a series of simplifying assumptions. If we replace the lumped matrix $\mathcal{M}^{\mathrm{L}}_{\mathbf{pp}}$ in (56) by a consistent mass matrix, and assume a constant density $\rho\equiv 1$ for the entirety of the domain, then we would end-up with the following Schur complement matrix:

$$\varepsilon\mathcal{K}_{\Phi\Phi}+(\tfrac{\tau\nu}{2})^2\mathcal{M}_{\Phi\mathbf{v}}\mathcal{M}^{-1}_{\mathbf{vv}}\mathcal{M}_{\mathbf{v}\Phi}.$$

Let's further assume that the space of gradients of potentials $\nabla\mathbb{H}$ is a subspace of the finite element space use to represent the momentum/velocity, i.e. $\nabla\mathbb{H}\subset\mathbb{V}$. Then we would have that

$$\mathcal{M}_{\Phi\mathbf{v}}\mathcal{M}^{-1}_{\mathbf{vv}}\mathcal{M}_{\mathbf{v}\Phi}=\mathcal{K}_{\Phi\Phi}$$

which is a perfectly well-conditioned full-rank matrix. Similar statement will hold true with an non-homogeneous density using a perturbation argument. In short: representing the momentum/velocity with a curl-conforming finite element space $\mathbb{V}$ satisfying the assumption $\nabla\mathbb{H}\subset\mathbb{V}$ (where $\mathbb{H}$ is the finite element space of the scalar potential) will lead to a well-conditioned system.

However, the fact that well-conditioning of the linear algebra system can be easily achieved using curl-conforming elements for the velocity is somewhat at odds with the current state of affairs for numerical shock-hydrodynamics. At the time of this writing, we are not aware of any mathematically solid theory of numerical methods for shock-hydrodynamics using curl-conforming and/or div-conforming finite elements. Pretty much all the mathematically mature choices available in the literature for the hydrodynamics subsystem are either nodal in nature or require some notion of pointwise state/value [85, 110, 54] which cannot be easily

accommodated by either curl-conforming or div-conforming elements. In particular, our intention is using the methods advanced in [58] which offer significant mathematical assurances. For the time being, using curl-conforming elements to represent the velocity does not seem to be a technically meaningful solution.

4.3. Avoiding the method of lines and Rothe's method.

The scheme proposed in (55)-(56)-(58) is a consequence of the standard workflow that we know as "method of lines":

$$\begin{gathered} \textit{PDE} \rightarrow \textit{Discretize in space} \rightarrow \textit{Discretize in time} \rightarrow \textit{Algebraic block-system} \rightarrow \\ \textit{Eliminate variables} \rightarrow \textit{Algebraic Schur complement}\,, \end{gathered}$$

which transforms a PDE into a coupled algebraic block-system, leading to an upper or lower triangular Matrix system during the process of variable elimination (also known as factorization). This approach works for the vast majority of problems while also achieving separation of concerns in the context of software development.

An alternative to the method of lines, is Rothe's method, which is just a permutation of the discretization order, more precisely it consists of

$$\begin{gathered} \textit{PDE} \rightarrow \textit{Discretize in time} \rightarrow \textit{Discretize in space} \rightarrow \textit{Algebraic block-system} \rightarrow \\ \textit{Eliminate variables} \rightarrow \textit{Algebraic Schur-complement}\,. \end{gathered}$$

In this section we propose using neither the method of lines nor Rothe's method. More precisely we will use the following workflow

$$\begin{gathered} \textit{PDE} \rightarrow \textit{Discretize in time} \rightarrow \textit{Eliminate variables} \rightarrow \textit{Lower-triangular PDE system} \\ \rightarrow \textit{Discretize in space} \rightarrow \textit{PDE Schur-complement} \end{gathered} \tag{59}$$

in order to derive a scheme for the coupled system (17b)-(17c). We start by considering the following Crank-Nicolson semi-discretization of the coupled system (17b)-(17c):

$$\mathbf{p}^{n+1} - \widetilde{\mathbf{p}}^{n+1} = -\tfrac{\tau\nu}{2}\rho^{n+1}(\nabla\varphi^{n+1} + \nabla\widetilde{\varphi}^{n+1})\,, \tag{60}$$

$$-\varepsilon(\Delta\varphi^{n+1} - \Delta\widetilde{\varphi}^{n+1}) = -\tfrac{\tau\nu}{2}(\operatorname{div}\mathbf{p}^{n+1} + \operatorname{div}\widetilde{\mathbf{p}}^{n+1})\,. \tag{61}$$

We eliminate $\mathbf{p}^{n+1}$ from (60) and take the divergence to both sides of the equality

$$\operatorname{div}\mathbf{p}^{n+1} = \operatorname{div}\widetilde{\mathbf{p}}^{n+1} - \tfrac{\tau\nu}{2}\operatorname{div}(\rho^{n+1}(\nabla\varphi^{n+1} + \nabla\widetilde{\varphi}^{n+1}))\,.$$

Finally, we substitute this identity into the right hand side of (61) to finally get

$$-\varepsilon\Delta\varphi^{n+1} - (\tfrac{\tau\nu}{2})^2\operatorname{div}(\rho^{n+1}\nabla\varphi^{n+1})) = -\varepsilon\Delta\widetilde{\varphi}^{n+1} + (\tfrac{\tau\nu}{2})^2\operatorname{div}(\rho^{n+1}\nabla\widetilde{\varphi}^{n+1}) - \tau\nu\operatorname{div}\widetilde{\mathbf{p}}^{n+1} \tag{62}$$

$$\mathbf{p}^{n+1} - \widetilde{\mathbf{p}}^{n+1} = -\tfrac{\tau\nu}{2}\rho^{n+1}(\nabla\varphi^{n+1} + \nabla\widetilde{\varphi}^{n+1}) \tag{63}$$

Remark 4.3. We highlight that (62)-(63) is a lower-triangular PDE-system which can be solved by forward-substitution. In other words, the solution workflow is: we solve (62) in order to find φ^{n+1}, then we insert this result into the right hand side of (63) and compute $\mathbf{p}^{n+1}$. There is no matrix Schur-complement: the differential operator on the left-hand side of (62) is a PDE Schur-complement which admits the following symmetric bilinear form

$$a(\varphi,\omega)=\int_\Omega \nabla\varphi^{n+1}\cdot\nabla\omega+(\tfrac{\tau\nu}{2})^2\rho^{n+1}\nabla\varphi^{n+1}\cdot\nabla\omega\,\mathrm{d}\boldsymbol{x}+\text{B.C.} \tag{64}$$

which is always positive provided the density ρ^{n+1} is strictly positive. In addition, its always invertible (when using Dirichlet or Mixed data) or invertible in some quotient-space when using pure-Neumann data. We mention in the passing that the robust iterative solution and preconditioning of matrices arising from the discretization of discontinuous heterogenous diffussion problems, such as (64) with large contrast ratios (e.g. $\frac{\max_{\boldsymbol{x}}\rho^{n+1}(\boldsymbol{x})}{\min_{\boldsymbol{x}}\rho^{n+1}(\boldsymbol{x})}\geq 10^6$) is an open problem. That's a topic is well-beyond the scope of the current manuscript.

So far, (62)-(63) is a semi-discrete system, we want to consider a discretization in space too. In order to simplify matters we assume boundary conditions $\mathbf{p}\cdot\mathrm{n}\equiv 0$ and $\varphi\equiv 0$ (or $\nabla\varphi\cdot\mathrm{n}\equiv 0$) on the entirety of the boundary $\partial\Omega$ and consider the following variational formulation:

$$\varepsilon\big(\nabla\varphi_h^{n+1}-\nabla\widetilde{\varphi}_h^{n+1},\nabla\omega_h\big)_{\mathbf{L}^2(\Omega)}+(\tfrac{\tau\nu}{2})^2\big(\rho_h^{n+1}(\nabla\varphi_h^{n+1}+\nabla\widetilde{\varphi}_h^{n+1}),\nabla\omega_h\big)_{\mathbf{L}^2(\Omega)}=-\tau\nu\big(\rho_h^{n+1}\mathbf{v}_h^n,\nabla\omega_h\big)_{\mathbf{L}^2(\Omega)}, \tag{65}$$

$$\big(\rho_h^{n+1}(\mathbf{v}_h^{n+1}-\widetilde{\mathbf{v}}_h^{n+1}),\mathbf{z}_h\big)_{\mathbf{L}^2(\Omega)}=-\tfrac{\tau\nu}{2}\big(\rho_h^{n+1}(\nabla\varphi_h^{n+1}+\nabla\widetilde{\varphi}_h^{n+1}),\mathbf{z}_h\big)_{\mathbf{L}^2(\Omega)}, \tag{66}$$

for all $\omega_h\in\mathbb{H}$ and $\mathbf{z}_h\in\mathbb{V}$. At this point in time $\mathbb{H}$ and $\mathbb{V}$ represent open-ended choices of finite element spaces. Scheme (65)-(66) is just a decoupled version Crank-Nicolson scheme. It would be somewhat comforting to know that it enjoys the same stability properties as the usual coupled Crank-Nicolson scheme (e.g. scheme (55)-(56)) at least for some choice of spaces $\mathbb{H}$ and $\mathbb{V}$. The following proposition provides part of the answer to such question.

Proposition 4.1. *Scheme* (65)-(66) *satisfies the following identity*

$$\begin{aligned}&\varepsilon\|\nabla\varphi_h^{n+1}\|^2-\varepsilon\|\nabla\widetilde{\varphi}_h^{n+1}\|^2+\int\rho_h^{n+1}|\mathbf{v}_h^{n+1}|-\rho_h^{n+1}|\widetilde{\mathbf{v}}_h^{n+1}|^2\,\mathrm{d}\boldsymbol{x}=\\&\quad=\tfrac{\tau\nu}{2}\big(\rho_h^{n+1}(\mathbf{v}_h^{n+1}-\widetilde{\mathbf{v}}_h^{n+1}+\tfrac{\tau\nu}{2}(\nabla\varphi_h^{n+1}+\nabla\widetilde{\varphi}_h^{n+1})),\nabla\varphi_h^{n+1}+\nabla\widetilde{\varphi}_h^{n+1}\big)_{\mathbf{L}^2(\Omega)},\end{aligned} \tag{67}$$

for any choice of finite element spaces $\mathbb{H}$ *and* $\mathbb{V}$*. This proposition follows simply by taking* $\omega_h=\varphi_h^{n+1}+\widetilde{\varphi}_h^{n+1}$ *in* (65) *and* $\mathbf{z}_h=\mathbf{v}_h^{n+1}+\widetilde{\mathbf{v}}_h^{n+1}$ *in* (66) *and adding both lines.*

In the following lemma we establish more precisely the core requirement for energy-stability.

Lemma 4.2 (Conditions for energy-stability)**.** *Let the inclusion of spaces* $\nabla\mathbb{H}\subseteq\mathbb{V}$ *hold true, then the right hand side of* (67) *is zero.*

Proof. Rewriting (66) in residual form

$$\big(\rho_h^{n+1}\big(\mathbf{v}_h^{n+1}-\widetilde{\mathbf{v}}_h^{n+1}+\tfrac{\tau\nu}{2}(\nabla\varphi_h^{n+1}+\nabla\widetilde{\varphi}_h^{n+1})\big),\mathbf{z}_h\big)_{\mathbf{L}^2(\Omega)}=0\ \ \forall\mathbf{z}_h\in\mathbb{V} \tag{68}$$

we note that if $\nabla\mathbb{H}\subseteq\mathbb{V}$ then $\mathbf{z}_h:=\nabla\varphi_h^{n+1}+\nabla\widetilde{\varphi}_h^{n+1}$ is a valid test function for (68). □

Proposition 4.1 and Lemma (4.2) still do not provide a specific choice of space discretization. The following remark provides one example of a specific construction that can be materialized as computer code.

Remark 4.4 (An energy-compatible example)**.** Consider a mesh of affinely mapped simplices and

- Continuous nodal $\mathbb{P}^1$ elements for the potential φ_h

$$\mathbb{H}=\{\omega_h\in\mathcal{C}^0(\Omega)\,|\,\omega_h(\boldsymbol{T}_K(\widehat{\boldsymbol{x}}))\in\mathbb{P}^1(\widehat{K})\ \forall K\in\mathcal{T}_h\}\,.$$

- Fully discontinuous nodal $[\mathbb{P}^1]^d$ elements for the velocity $\mathbf{v}_h$ (equivalently for the momentum $\mathbf{p}_h$).

$$\mathbb{V}=[\mathbb{V}]^d\ \text{ where }\ \mathbb{V}=\{z_h\in L^2(\Omega)\,|\,z_h(\boldsymbol{T}_K(\widehat{\boldsymbol{x}}))\in\mathbb{P}^1(\widehat{K})\ \forall K\in\mathcal{T}_h\}\,.$$

Assuming that the simplices are affinely-mapped guarantees the preservation of the polynomial space: the space $\nabla\mathbb{H}$ will be piecewise polynomial in physical space (the jacobian of the transformation is a constant matrix in each element) more precisely it will be a subspace of the vector-valued space $\mathbb{V}$. Note that the choice of nodal velocity for the momentum implies a commitment to using nodal $\mathbb{P}^1$ elements for each component of the hydrodynamics subsystem if our goal is using the hyperbolic framework of [58].

We also note that in this context $\nabla\varphi_h$ is piecewise constant. Therefore most of the bilinear forms in (65)-(66) can be computed exactly using nodal-quadrature. We therefore propose the scheme:

$$\varepsilon\big(\nabla\varphi_h^{n+1}-\nabla\widetilde{\varphi}_h^{n+1},\nabla\omega_h\big)_{\mathbf{L}^2(\Omega)}+(\tfrac{\tau\nu}{2})^2\langle\rho_h^{n+1}(\nabla\varphi_h^{n+1}+\nabla\widetilde{\varphi}_h^{n+1}),\nabla\omega_h\rangle=-\tau\nu\langle\rho_h^{n+1}\mathbf{v}_h^n,\nabla\omega_h\rangle\,, \tag{69}$$

$$\langle\rho_h^{n+1}(\mathbf{v}_h^{n+1}-\widetilde{\mathbf{v}}_h^{n+1}),\mathbf{z}_h\rangle=-\tfrac{\tau\nu}{2}\langle\rho_h^{n+1}(\nabla\varphi_h^{n+1}+\nabla\widetilde{\varphi}_h^{n+1}),\mathbf{z}_h\rangle\,, \tag{70}$$

satisfying the a piori bound

$$\tfrac{\varepsilon}{2}\|\nabla\varphi_h^{n+1}\|^2_{L^2(\Omega)}+\sum_{i\in\mathcal{V}}\tfrac{m_i}{2\rho_i^{n+1}}|\mathbf{p}_i^{n+1}|^2_{\ell^2}=\tfrac{\varepsilon}{2}\|\nabla\widetilde{\varphi}_h^{n+1}\|^2_{L^2(\Omega)}+\sum_{i\in\mathcal{V}}\tfrac{m_i}{2\widetilde{\rho}_i^{n+1}}|\widetilde{\mathbf{p}}_i^{n+1}|^2_{\ell^2} \tag{71}$$

The proof of this last fact is omitted since the ideas required for such a proof have already been repeated a few times in this manuscript.

The indirect implication behind this remark is that: nodal-like space discretizations which are compatible with energy-principles can only use affinely mapped elements. In practice, this means that if we want to have assurances of energy stability we have to use affinely mapped simplices in the context of technical application. For instance, the use of quadrilaterals is not optimal, since general bilinear maps are rarely ever affine in the context of unstructured meshes.

4.4. A complete source-update scheme.

Subsections §4.2 and §4.3 explain us what to do with the coupling between the momentum $\mathbf{p}$ and the potential φ, but they don't tell us what are our choices regarding the update of the total mechanical energy $\mathcal{E}$. We consider the following complete source-update scheme (i.e. Stage #2 in the context of a Strang-Splitting scheme):

- **Stage #2.1 (update of momentum-potential coupling):** given $\widetilde{\mathbf{p}}_h^{n+1}$ and $\widetilde{\varphi}_h^{n+1}$ the outputs of the Stage #1 (the hyperbolic-update) we compute $\mathbf{p}_h^{n+1}$ and φ_h^{n+1} using your scheme of choice, that is either scheme (55)-(56) or (69)-(70).

- **Stage #2.2 (update of total mechanical energy):** define $\tau\mathbf{f}_i^{n+\frac{1}{2}}$ and $\mathbf{v}^{n+\frac{1}{2}}$ as

$$\tau\mathbf{f}_i^{n+\frac{1}{2}} := \mathbf{p}_i^{n+1} - \widetilde{\mathbf{p}}_i^{n+1}, \tag{72}$$

$$\mathbf{v}^{n+\frac{1}{2}} := \frac{(\mathbf{p}_i^{n+1} + \widetilde{\mathbf{p}}_i^{n+1})}{2\rho_i^{n+1}}, \tag{73}$$

  and compute the total mechanical energy as

$$\mathcal{E}_i^{n+1} := \widetilde{\mathcal{E}}_i^{n+1} + \tau\mathbf{f}_i^{n+\frac{1}{2}} \cdot \mathbf{v}^{n+\frac{1}{2}} \tag{74}$$

This two-stage source-update scheme preserves the internal energy (pointwise) and the Electro-Kinetic. The proof of these facts follows from Proposition 3.1, Lemma 4.1, Proposition 4.1 and Lemma 4.2.

Remark 4.5 (Keeping our choices open)**.** Note that we do not strictly advocate for the use of asymptotic preserving scheme (69)-(70) and want to discard (55)-(56) in its entirety. Scheme (69)-(70) is particularly advantageous since it's asymptotically well-posed, it's fully decoupled, and does not require the assembly of an matrix Schur-complement. The use of algebraic Schur complements quite frequently require the explicit computation of a matrix-matrix products. This operation is not just expensive in itself but also leads wider sparsity patterns and a major increase of the cost of each matrix-vector product in the context of Krylov methods. Last but not least we mention that traditional enforcement of Dirichlet boundary conditions requires direct access to the resulting sparsity pattern (replacement of diagonal with ones, elimination or row/columns, etc) all of which becomes expensive due larger sparsity pattern. None of these operations is either trivial nor cheap to implement. With all that being said about the potential disadvantages of scheme (55)-(56) it is worth mentioning that:

- It's hard to predict what is the easiest thing to implement: that is heavily dictated by the choice of finite element software framework/library. In some software frameworks (55)-(56) might turn-up to be the easiest to implement, in particular those with heavy support of linear algebra.

- Scheme (55)-(56) is not asymptotically well-posed for the most naive choice of finite element spaces (equal-order). That is not equivalent to saying that scheme (55)-(56) represents a dead-end. With greatest likelyhoood there is a purely nodal choice of finite element spaces that is inf-sup compatible (i.e. leading to a full-rank matrix $\mathcal{M}_{\Phi\mathbf{v}}$). Finding the proper choice of finite element spaces will be investigated elsewhere or a future report.

■ Scheme (55)-(56) preserves the total mechanical energy when compounded with the Stage #22 defined by (72)-(74).

4.5. Inclusion of static background of ions.

Let's also assume that there is a time-dependent electron-gas charge density $\rho_e < 0$. Let's also assume that there is a background of positively charged ions with charge density $\rho_i > 0$. The electrostatic problem can be understood as a time-independent elliptic PDE-problem

$$-\varepsilon\Delta\varphi = \rho_i + \rho_e \tag{75}$$

usually known as the electric Gauss-law. Alternatively, the electrostatic problem can also be understood as an evolutionary problem by taking time-derivatives to both sides of (75):

$$-\varepsilon\Delta\partial_t\varphi = \partial_t\rho_i + \partial_t\rho_e\,. \tag{76}$$

If the ions are static, and the dynamics of the electrons is described by Euler-Poisson system (2a)-(2d), then in such particular case we have that: $\frac{\partial}{\partial t}\rho_i \equiv 0$, $\rho_e = \frac{q_e}{m_e}\rho$, $\partial_t\rho_e = -\frac{q_e}{m_e}\mathrm{div}\,\mathbf{p}$ and (76) becomes

$$-\varepsilon\Delta\partial_t\varphi = -\tfrac{q_e}{m_e}\mathrm{div}\,\mathbf{p}\,. \tag{77}$$

which exactly the same as (2d).

The approach used in the entirety of this manuscript is strongly aligned with the second view presented by (76): the electrostatic problem understood as an evolutionary problem. This greatly simplifies the derivation of fundamental stability properties of Euler-Poisson's system (see for instance Lemmas 2.4, 2.4, 2.5, 2.6, 4.1 and identity (71) for a special case) that translates into concrete stability properties, such as energy-stability.

The question remains: How to incorporate the effect of the static-background of ions into the time-dependent formulation (76)? Let's consider the hypothetical situation where a portion of the boundary has prescribed voltage (Dirichlet data) and the complementary portion of the boundary has prescribed normal component of the gradient, that is

$$\varphi = \varphi_D \text{ on } \partial\Omega_D \;\text{ and }\; \nabla\varphi\cdot\mathrm{n} = g \text{ on } \partial\Omega_N \tag{78}$$

where φ_D is the Dirichlet data, g is the Neumann data, $\partial\Omega_D$ is the portion of the boundary with prescribed Dirichlet data, and $\partial\Omega_N$ is the portion of the boundary with prescribed Neumann data. The strategy used to incorporate a static background of ions consists in decomposing the elliptic problem (75) into two fictitious problems. More precisely consider:

$$\begin{cases} -\varepsilon\Delta\varphi_e = \rho_e & \text{in } \Omega \\ \varphi_e = 0 & \text{in } \partial\Omega_D \\ \nabla\varphi_e\cdot\mathrm{n} = 0 & \text{on } \partial\Omega_N \end{cases} \quad\text{and}\quad \begin{cases} -\varepsilon\Delta\varphi_i = \rho_i & \text{in } \Omega \\ \varphi_i = \varphi_D & \text{in } \partial\Omega_D \\ \nabla\varphi_i\cdot\mathrm{n} = g & \text{on } \partial\Omega_N \end{cases}$$

Note that we have decided to assign homogeneous Dirichlet and Neumann boundary conditions to the "electron-potential" φ_e while the actual non-homogeneous Dirichlet and Neumann data has

been assigned to the "ion-potential" φ_i. This choice is completely arbitrary: it is perfectly possible reverse roles assign non-homogeneous boundary conditions to the potential φ_e and homogeneous boundary conditions to φ_i if that turns out to be advantageous in some mathematical or computational sense. We note that neither φ_e nor φ_i have any physical meaning by themselves. However, the total electric potential $\varphi := \varphi_e + \varphi_i$ is physically meaningful, it is the physical electric potential and has the right boundary conditions. Note that if ρ_i represents a time-independent charge, then φ_i has to be computed only once.

The bottom line is that we can exploit linearity in order to decompose the electrostatic problem into two fictitious problems regardless of the choice of boundary conditions. Considering each possible case (Dirichlet, Neumann, Mixed, Robin, etc) of boundary conditions will add more obscurity than clarity to the presentation. Therefore, in order to clean-up the presentation, without loss of generality, let's assume that the total electrical potential φ satisfies homogeneous Dirichlet boundary conditions on the entirety of the boundary. Assuming that we have already computed the fictitious ion-potential φ_h^i, then scheme (55)-(56) becomes

$$\varepsilon\big(\nabla\varphi_h^{e,n+1} - \nabla\widetilde{\varphi}_h^{e,n+1}, \nabla\omega\big)_{\mathbf{L}^2(\Omega)} = -\tfrac{\tau\nu}{2}\big(\mathbf{p}_h^{n+1} + \widetilde{\mathbf{p}}_h^{n+1}, \nabla\omega\big)_{\mathbf{L}^2(\Omega)}, \tag{79}$$

$$\langle \mathbf{v}_h^{n+1} - \widetilde{\mathbf{v}}_h^{n+1}, \mathbf{z}_h\rangle_h = \tau\nu\big(\tfrac{1}{2}(\nabla\varphi_h^{e,n+1} + \nabla\widetilde{\varphi}_h^{e,n+1}) + \nabla\varphi_h^i, \mathbf{z}_h\big)_{\mathbf{L}^2(\Omega)} \tag{80}$$

Note that (79) is perfectly consistent with (77) (the ion-potential plays no role), while (80) should include the forces due to the ion-potential. Similarly, following the derivation of scheme (62)-(63) we can deduce that scheme (69)-(70) becomes

$$\begin{aligned}
&\varepsilon\big(\nabla\varphi_h^{e,n+1} - \nabla\widetilde{\varphi}_h^{e,n+1}, \nabla\omega_h\big)_{\mathbf{L}^2(\Omega)} + (\tfrac{\tau\nu}{2})^2\langle\rho_h^{n+1}(\nabla\varphi_h^{e,n+1} + \nabla\widetilde{\varphi}_h^{e,n+1}), \nabla\omega_h\rangle = \\
&\qquad -\tau\nu\langle\rho_h^{n+1}\mathbf{v}_h^n, \nabla\omega_h\rangle - \tfrac{(\tau\nu)^2}{2}\langle\rho_h^{n+1}\nabla\varphi_h^i, \nabla\omega_h\rangle \\
&\langle\rho_h^{n+1}(\mathbf{v}_h^{n+1} - \widetilde{\mathbf{v}}_h^{n+1}), \mathbf{z}_h\rangle = -\tau\nu\langle\rho_h^{n+1}\big(\tfrac{1}{2}(\nabla\varphi_h^{e,n+1} + \nabla\widetilde{\varphi}_h^{e,n+1}) + \nabla\varphi_h^i\big), \mathbf{z}_h\rangle,
\end{aligned}$$

when a static background of ions is present.

Remark 4.6 (Generalization to time-dependent positive charges)**.** If the background ions are not static, i.e. $\frac{\partial}{\partial t}\rho_i \not\equiv 0$ then we have that scheme (55)-(56) becomes

$$\begin{aligned}
\varepsilon\big(\nabla\varphi_h^{e,n+1} - \nabla\widetilde{\varphi}_h^{e,n+1}, \nabla\omega\big)_{\mathbf{L}^2(\Omega)} &= -\tfrac{\tau\nu}{2}\big(\mathbf{p}_h^{n+1} + \widetilde{\mathbf{p}}_h^{n+1}, \nabla\omega\big)_{\mathbf{L}^2(\Omega)} - \varepsilon\big(\nabla\varphi_h^{i,n+1} - \nabla\varphi_h^{i,n}, \nabla\omega\big)_{\mathbf{L}^2(\Omega)}, \\
\langle\mathbf{v}_h^{n+1} - \widetilde{\mathbf{v}}_h^{n+1}, \mathbf{z}_h\rangle_h &= \tau\nu\big(\tfrac{1}{2}(\nabla\varphi_h^{e,n+1} + \nabla\widetilde{\varphi}_h^{e,n+1}) + \nabla\varphi_h^{i,n+\frac{1}{2}}, \mathbf{z}_h\big)_{\mathbf{L}^2(\Omega)}
\end{aligned}$$

where $\varphi_h^{i,n+1}$ is the approximate numerical solution of $-\varepsilon\Delta\varphi^i = \rho_i^{n+1}$ with ρ_i^{n+1} being (known) given data, and $\varphi_h^{i,n+\frac{1}{2}} := \frac{1}{2}(\varphi_i^n + \varphi_i^{n+1})$.

Similarly, the scheme (69)-(70) becomes

$$\begin{aligned}
&\varepsilon\big(\nabla\varphi_h^{e,n+1} - \nabla\widetilde{\varphi}_h^{e,n+1}, \nabla\omega_h\big)_{\mathbf{L}^2(\Omega)} + (\tfrac{\tau\nu}{2})^2\langle\rho_h^{n+1}(\nabla\varphi_h^{e,n+1} + \nabla\widetilde{\varphi}_h^{e,n+1}), \nabla\omega_h\rangle = \\
&\qquad -\tau\nu\langle\rho_h^{n+1}\mathbf{v}_h^n, \nabla\omega_h\rangle - \tfrac{(\tau\nu)^2}{2}\langle\rho_h^{n+1}\nabla\varphi_h^i, \nabla\omega_h\rangle - \varepsilon\big(\nabla\varphi_h^{i,n+1} - \nabla\widetilde{\varphi}_h^{i,n+1}, \nabla\omega_h\big)_{\mathbf{L}^2(\Omega)} \\
&\langle\rho_h^{n+1}(\mathbf{v}_h^{n+1} - \widetilde{\mathbf{v}}_h^{n+1}), \mathbf{z}_h\rangle = -\tau\nu\langle\rho_h^{n+1}\big(\tfrac{1}{2}(\nabla\varphi_h^{n+1} + \nabla\widetilde{\varphi}_h^{n+1}) + \nabla\varphi_h^i\big), \mathbf{z}_h\rangle,
\end{aligned}$$

when time-dependent positive charges are present. Note that these implementations require one additional Poisson solve per-time step in order to find the ion-potential corresponding to a given positive charge density ρ_i. More computational efficient implementations that do not require this additional Poisson solve are possible can be easily conceived too.

4.6. Source-scheme for the attractive case (self-gravitation).

The semi-discretization of the attractive source system (22a)-(22d) using Crank-Nicolson is

$$\mathbf{p}^{n+1} - \widetilde{\mathbf{p}}^{n+1} = -\tfrac{\tau}{2}\rho(\nabla\varphi^{n+1} + \nabla\widetilde{\varphi}^{n}) \tag{81}$$

$$-\lambda(\Delta\varphi^{n+1} - \Delta\widetilde{\varphi}^{n+1}) = \tfrac{\tau}{2}(\operatorname{div}\mathbf{p}^{n+1} + \operatorname{div}\widetilde{\mathbf{p}}^{n+1}) \tag{82}$$

This semi-discretization satisfies the following discrete balance.

Proposition 4.2. *The semi-discrete scheme* (81)-(82) *satisfies the balance identity*

$$\begin{aligned}\int_\Omega \tfrac{1}{2\rho^{n+1}}|\mathbf{p}^{n+1}|^2_{\ell^2} - \tfrac{\lambda}{2}|\nabla\varphi^{n+1}|^2_{\ell^2}\,\mathrm{d}\boldsymbol{x} = \int_\Omega \tfrac{1}{2\widetilde{\rho}^{n+1}}|\widetilde{\mathbf{p}}^{n+1}|^2_{\ell^2} - \tfrac{\lambda}{2}|\nabla\widetilde{\varphi}^{n+1}|^2_{\ell^2}\,\mathrm{d}\boldsymbol{x}\\ + \int_{\partial\Omega}\tfrac{\lambda}{2}(\varphi^{n+1}+\widetilde{\varphi}^{n+1})(\nabla\varphi^{n+1} - \nabla\widetilde{\varphi}^{n+1})\cdot\mathrm{n}\,\mathrm{d}\boldsymbol{s}\\ + \tfrac{\tau}{4}\int_{\partial\Omega}(\varphi^{n+1}+\widetilde{\varphi}^{n+1})(\mathbf{p}^{n+1}+\widetilde{\mathbf{p}}^{n+1})\cdot\mathrm{n}\,\mathrm{d}\boldsymbol{s}\end{aligned}$$

Note that if the last two boundary integrals vanish (e.g. $(\mathbf{p}^{n+1}+\widetilde{\mathbf{p}}^{n+1})\cdot\mathrm{n} = 0$ *and/or* $\varphi^{n+1}+\widetilde{\varphi}^{n+1} \equiv 0$ *and/or* $(\nabla\varphi^{n+1} - \nabla\widetilde{\varphi}^{n})\cdot\mathrm{n} = 0$ *in the entirety of the boundary), then the semi-discrete Crank-Nicolson scheme preserves the integral of the Hamiltonian* $\int_\Omega \frac{1}{2\rho}|\mathbf{p}|^2_{\ell^2} - \frac{\lambda}{2}|\nabla\varphi|^2_{\ell^2}\,\mathrm{d}\boldsymbol{x}$.

Just like we did in Section §4.3, we use the workflow described in (59) in order to derive a decoupled scheme. From (81) we get:

$$\operatorname{div}\mathbf{p}^{n+1} = \operatorname{div}\widetilde{\mathbf{p}}^{n+1} - \tfrac{\tau}{2}\operatorname{div}\left(\rho^{n+1}(\nabla\varphi^{n+1} + \nabla\widetilde{\varphi}^{n+1})\right).$$

Inserting this identity into the right hand side of (82) and reorganizing the terms the decoupled semi-discrete scheme for the attractive Euler-Poisson's source system is:

$$-\lambda\Delta\varphi^{n+1} + (\tfrac{\tau}{2})^2\operatorname{div}(\rho^{n+1}\nabla\varphi^{n+1}) = -\lambda\Delta\widetilde{\varphi}^{n+1} - (\tfrac{\tau}{2})^2\operatorname{div}(\rho^{n+1}\nabla\widetilde{\varphi}^{n+1}) + \tau\operatorname{div}\widetilde{\mathbf{p}}^{n+1}, \tag{83}$$

$$\mathbf{p}^{n+1} - \widetilde{\mathbf{p}}^{n+1} = -\tfrac{1}{2}\tau\rho^{n+1}(\nabla\varphi^{n+1} + \nabla\widetilde{\varphi}^{n+1}). \tag{84}$$

Inclusion of static background of dark-matter can be accommodated following a similar approach to that one described for the repulsive case in Section §4.5.

Remark 4.7 (CFL constraints)**.** We note that differential operator on the left-hand side (83) is not unconditionally positive. More precisely, the finite dimensional bilinear form associated to problem (83) is of the form

$$a(\chi_j,\chi_i) = \int_\Omega \lambda\nabla\chi_j\cdot\nabla\chi_i - (\tfrac{\tau}{2})^2\rho_h^{n+1}\nabla\chi_j\cdot\nabla\chi_i\,\mathrm{d}\boldsymbol{x} + \text{B.C.} \tag{85}$$

In practical terms, this means that the time-step size should satisfy a CFL-like constraint

$$\tau \leq 2\,\mathrm{cfl}\left(\frac{\lambda}{\max_{i\in\mathcal{V}}\rho_i^{n+1}}\right)^{1/2} \tag{86}$$

in order to guarantee the coercivity of the resulting bilinear form. Here $\mathrm{cfl}\in(0,1)$ is a user defined constant. We note however that in practice, λ is usually a monstrously large constant while densities are only large in the interior of solar objects. It's very unlikely the constraint (86) would become active in practice. However, its still good practice to curb the time-step size in order to guarantee that the bilinear form (85) is dominated by the positive-part in order to mitigate degradation of iterative solvers and the efficacy of preconditioners.

Finally, the choice of space discretization for (83)-(84) that is compatible with preservation of an integral balance of the Hamiltonian has to follow similar constraints to those outlined in Lemma 4.2, which boils down to the inclusion $\nabla\mathbb{H}\subset\mathbb{V}$.

5. ALGORITHMIC/COMPUTATIONAL DETAILS

5.1. Unified notation for both attractive and repulsive cases

The source-update scheme for the repulsive (electrostatic) or attractive (self-gravitation) are very much the same up-to a minor change of constants. More precisely, actual computer code uses the following notation:

$$-\lambda\Delta\varphi_e^{n+\frac{1}{2}} - \tfrac{\xi\tau^2}{4}\,\mathrm{div}\,(\rho\nabla\varphi_e^{n+\frac{1}{2}}) = -\lambda\Delta\varphi_e^{n} + \tfrac{\xi\tau^2}{4}\mathrm{div}\,(\rho\nabla\varphi_i^{0}) - \tfrac{\tau\nu}{2}\,\mathrm{div}\,\mathbf{p}^n \tag{87}$$

$$\varphi^{n+1} = 2\varphi^{n+\frac{1}{2}} - \varphi^n \tag{88}$$

$$\mathbf{p}^{n+1} - \mathbf{p}^n = -\tfrac{\mu\tau}{2}\rho(\nabla\varphi^{n+1} + \nabla\varphi^n)$$

where

$$\{\lambda,\xi,\nu,\mu\} = \begin{cases} \{\varepsilon, \left(\frac{q}{m}\right)^2, \frac{q_e}{m_e}, \frac{q_e}{m_e}\} & \text{for the electrostatic case} \\ \{\frac{1}{\alpha(d)}, -1, -1, 1\} & \text{for the gravitational case}\,. \end{cases}$$

We note that the choice of an update scheme (87) in terms of the pseudo-time step $t^{n+\frac{1}{2}}$ followed by the extrapolation step (88) is strictly necessary. Second-order accuracy in the context of Strang-Splitting requires enforcement of boundary conditions at the pseudo-time step $t^{n+\frac{1}{2}}$ in order to achieve its full second-order accuracy. This is in principle not much of an issue for time-independent boundary conditions but it will definitely be important in the context of code-validation with time-dependent boundary conditions, see for instance [54].

5.2. Initialization of the scheme and mean-value charge-neutrality

Our intention is using the splitting approach (53) with the source-update scheme described in Section §4.4. As such, the scheme will not be self-starting. More precisely, we need to supply a value for the initial electric potential φ_0. As described in §4.5, the computation of the electric potential can be divided in two fictitious potentials φ_e and φ_i, and only one of them needs to satisfy the boundary conditions of the actual total potential $\varphi = \varphi_e + \varphi_i$.

In principle, the initialization of the data is as simple as solving one Poisson problem with homogeneous boundary conditions for φ_e and another Poisson problem with non-homogeneous boundary conditions for φ_e. However, there is more than meets the eye here. We cannot discuss all possible boundary conditions, but we can focus on two important cases: the mixed problem (Dirichlet-Neumann) and the pure-Neumann problem:

- Mixed boundary conditions: if we assume boundary condition as described in (78), then the bilinear forms associated to the elliptic problem $-\varepsilon\Delta\varphi = \rho_i + \rho_e$ are guaranteed be uniformly coercive and the linear system is invertible, for any right-hand side [89]. This is true even if the right hand side does not satisfy $\int_\Omega \rho_i + \rho_e \, d\boldsymbol{x} \neq 0$. In other words, the mixed problem is automatically data-compatible with the electrically non-neutral case.
- Pure-Neumann case: in such case we have that the total initial potential has to satisfy the variational formulation

$$\int_\Omega \nabla\varphi \cdot \nabla\omega \, d\boldsymbol{x} = \int_\Omega (\rho_i + \rho_e)\omega \, d\boldsymbol{x} + \int_{\partial\Omega} \omega g \, d\boldsymbol{s} \quad \forall \omega \in H^1(\Omega)\backslash\mathbb{R} \tag{89}$$

  where g is the Neumann data. In particular, (89) should hold true when $\omega \equiv 1$, leading to the well-known data-compatibility constraint

$$\int_\Omega (\rho_i + \rho_e) \, d\boldsymbol{x} + \int_{\partial\Omega} g \, d\boldsymbol{s} = 0 \, .$$

  This implies, in particular, that homogeneous pure-Neumann boundary conditions (i.e. $g \equiv 0$ on the entirety of the boundary) can only combined with initial data satisfying mean-value charge-neutrality $\int_\Omega (\rho_i + \rho_e) \, d\boldsymbol{x} = 0$. In practice we can deal with this constraints at the purely algebraic level without ever introducing a positive background charge into the variational formulation, see numerical experiments in subsection §7.1 for more details.

6. EULER-POISSON REPULSIVE CASE: DISCUSSION ON BOUNDARY CONDITIONS

6.1. Background and pre-existing literature

Boundary conditions (BCs) are a very delicate issue both in terms of the PDE-stability and physical correctness. With rare few exceptions most of the leading plasma physics books

[13, 46, 28] (among others) neither cover, develop or even mention boundary conditions. Boundary conditions are an essential part of a computationally/technically useful PDE model. On the other hand, a large body of the numerical/computational literature of fluid models for plasma physics and semiconductors uses periodic BCs. The PDE literature focusing on plasma-sheath and boundary layer phenomena appears to fill part of the gap, see for instance [48] and the list of references in [83]. It fair to say that very little, if not nothing, is rigorously understood in relationship to boundary conditions for Euler-Maxwell and Euler-Poisson models.

To illustrate how easy it is to formulate an unstable boundary condition consider the following situation: taking a look at (15) it is very tempting to choose the boundary condition $(\frac{q_e}{m_e}\mathbf{p} - \varepsilon\nabla(\partial_t\varphi))\cdot \mathrm{n} = 0$ either in whole or in part of the boundary. After all such BCs are nothing else than Ampere's law $\varepsilon_0\partial_t \mathrm{E} = -\mathbf{j}$ (in the absense of magnetic fields) dotted with the normal and its reasonable to think that it should hold true as a trace or restriction to the boundary (it expresses a fundamental conservation). In addition, such choice of BC is perfectly compatible with the energy stability estimate (15)-(16). However, the above rationalization is very much flawed: for instance, if the solution is a strong solution (at least for a short time), and the current is constant in-time prescribed inflow data then such BC implies

$$\partial_t(\nabla\varphi\cdot \mathrm{n}) = \tfrac{q_e}{\varepsilon m_e}\mathbf{p}\cdot \mathrm{n} = \text{const}$$

leading to unbounded growth of the normal component of the electric field at the boundary (i.e. unbounded steepness of the electric field near the boundary). We could conjecture/speculate that such unbounded growth will lead to an spectacular blow-up of the boundary layers near the electrodes. Boundary layers by themselves are not nonphysical, but their unbounded growth in time most likely is. This pathological boundary condition was brought to the attention of the authors by the reference [83] which provides both additional mathematical and physical insight.

A practical approach is to take a quick look at (15) and make a few simple questions: What boundary conditions make the repulsive Euler-Poisson system stable/dissipative? What boundary conditions make the Euler-Poisson system an electro-mechanically isolated system? What boundary conditions for the potential are mathematically compatible with what boundary conditions for Euler's system? A overly optimistic expectation is that boundary conditions should satisfy the constraint:

$$-\big(\tfrac{\mathbf{p}}{\rho}(\mathcal{E}+p)\big)\cdot \mathrm{n} + \varphi\big(\tfrac{q}{m}\mathbf{p} - \varepsilon\nabla\partial_t\varphi\big)\cdot \mathrm{n} \leq 0 \ \text{ on } \partial\Omega \tag{90}$$

in some distributional/trace sense, or at the very least a mean value version of it

$$-\int_{\partial\Omega}\big(\tfrac{\mathbf{p}}{\rho}(\mathcal{E}+p)\big)\cdot \mathrm{n} + \varphi\big(\tfrac{q}{m}\mathbf{p} - \varepsilon\nabla\partial_t\varphi\big)\cdot \mathrm{n}\,\mathrm{d}\boldsymbol{s} \leq 0\,. \tag{91}$$

For the time being, neither (90) nor (91) seem to be reasonable expectations in the context of any realistic technical application: we should not expect the repulsive Euler-Poisson to be a dissipative system. If Euler-Poisson's system cannot be a dissipative system the second best expectation is that it is an electrically and thermo-mechanically isolated system (i.e. mechanical energy + potential energy = constant in time). Among the boundary conditions that would make the repulsive Euler-Poisson system an isolated system the most natural candidate seems to be $\mathbf{p}\cdot \mathrm{n}$ for Euler's system and $\varphi \equiv 0$ (or alternatively $\nabla\varphi\cdot \mathrm{n} \equiv 0$) for the potential on the entirety of the

boundary. But then again, such boundary conditions would be of minimal technical interest since it would describe an electron-gas trapped in a cavity. Most technical application involve portions of the boundary with an inflow and outflows and are driven by an external source of energy.

In the next subsection we consider some simple cases that shed some light into boundary conditions that are compatible with the nature of the PDE. Quoting manuscript [38], the idea is to

> *"propose some boundary conditions which are operational and, in particular, which avoid the appearance of boundary layers"*

In this context "operational" may not necessarily imply physically or technically valid, but rather that such boundary conditions lead to a predictable or stable behavior of the PDE and its numerical scheme.

6.2. Sketch of a technical problem: compatibility of boundary conditions.

In order to fix ideas we will consider a simple bounded domain and physical device (a gas-filled tube), see Figure 6-1. We will call the boundaries boundaries $\partial\Omega^+$ and $\partial\Omega^-$ the electrodes, and $\partial\Omega^0$ the insulating wall.

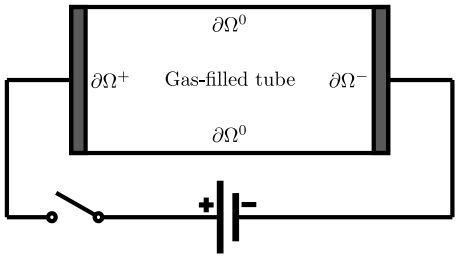

Figure 6-1 Gas-filled tube

In this context we will assume piecewise-constant Dirichlet data for the electrodes (prescribed voltage): that is $\varphi \equiv \varphi^+$ on $\partial\Omega^+$ and $\varphi \equiv \varphi^-$ on $\partial\Omega^-$. The assumption of the Dirichlet data being piecewise constant implies $\nabla\varphi \times \mathrm{n} = 0$ on $\partial\Omega^+$ and $\partial\Omega^-$. We assume homogeneous Neumann-data $\nabla\varphi \cdot \mathrm{n} \equiv 0$ on $\partial\Omega_N = \partial\Omega^0$ which consists on the bottom and top walls of the gas-filled tube.

Establishing data-compatibility of boundary conditions for the whole Euler-Poisson system is not a trivial task and we do not have a complete understanding at this point in time. However, direct inspection into the source-dominated regime reveals basic insight that we can use for numerical purposes. Assuming that we can interpret (17b) in some trace sense (or formal restriction to the boundary), and considering no resistive effects ($\frac{1}{\mathscr{T}} \equiv 0$) we take dot and cross product of (17b) with the normal n to get

$$\partial_t \mathbf{p} \cdot \mathrm{n} = -\tfrac{q_e}{m_e} \rho \nabla\varphi \cdot \mathrm{n} \ \text{ on } \ \partial\Omega_N \tag{92}$$

$$\partial_t \mathbf{p} \times \mathrm{n} = -\tfrac{q_e}{m_e} \rho \nabla\varphi \times \mathrm{n} \ \text{ on } \ \partial\Omega_D \tag{93}$$

We can deduce the following:

- **Prescription of homogeneous Neumann-data is formally compatible with reflecting boundary conditions.** From (92) we deduce that if we enforce normal condition $\mathbf{p}\cdot \mathrm{n} = 0$ on $\partial\Omega_N$ on the initial hydrodynamics state and the hyperbolic solver (Stages #1 and #3 of Strang-Splitting), then the source-update scheme with $\nabla\varphi\cdot \mathrm{n} = g = 0$ on $\partial\Omega_N$ should respect such constraint.

- **Prescription of time-independent piecewise constant Dirichlet data is compatible with the preservation of the tangent component.** From (93) we note that if the initial data is such that there is no electric current tangent to the surface of the electrodes (i.e. $\mathbf{p}\times \mathrm{n}$ on $\partial\Omega_D$) the source-update scheme should preserve such zero tangent-current. However, the source update-scheme will not preserve the normal component of the current and either an inflow ($\frac{q_e}{m_e}\mathbf{p}\cdot \mathrm{n}\leq 0$) or outflow ($\frac{q_e}{m_e}\mathbf{p}\cdot \mathrm{n}\geq 0$) condition will might develop in the hydrodynamic subsystem.

We also note that:

- In the absence of resistive effects ($\mathscr{T}^{-1}\equiv 0$): time-independent nonzero Neumann data implies unbounded growth ofinflow/outflow currents. For instance, if we consider $\partial_t\mathbf{p}\cdot \mathrm{n} = -\frac{q_e}{m_e}\rho\nabla\varphi\cdot \mathrm{n} = g$ with $g<0$ and constant in time, this implies that $\mathbf{p}\cdot \mathrm{n}$ can grow unboundedly (unbounded growth of an inflow current). In other words, without resistive source terms the only mathematically and physically meaningul Neumann boundary conditions are necessarily homogeneous.

- If we need to consider non-zero Neumann data $g\not\equiv 0$ into the model we will necessarily have to incorporate $\frac{1}{\mathscr{T}}$ strictly positive on $\partial\Omega_N$ in order to preserve boundedness of the inflow/outflow currents. More precisely, assuming that we can interpret (17b) in some trace sense taking the dot product with the normal and assuming that $\nabla\varphi\cdot \mathrm{n} = g$ on $\partial\Omega_N$ we get

$$\partial_t\mathbf{p}\cdot \mathrm{n} = -\frac{\rho q_e}{m_e}g - \frac{1}{\mathscr{T}}\mathbf{p}\cdot \mathrm{n} \ \text{ on } \ \partial\Omega_N$$

  which is formally an ODE that can be solved using integrating factors. The solution of such ODE will decay exponentially to the stationary condition

$$\frac{q_e}{m_e}\mathbf{p}\cdot \mathrm{n} = -\mathscr{T}\rho\left(\frac{q_e}{m_e}\right)^2 g\,.$$

  This last expression is just Ohm's law with normal current $\mathbf{j}_e = \frac{q_e}{m_e}\mathbf{p}\cdot \mathrm{n}$, conductivity $\sigma = \mathscr{T}\rho\left(\frac{q_e}{m_e}\right)^2$ (also known as Drude's model), and normal electric field $\mathrm{E}\cdot \mathrm{n} = -\nabla\varphi\cdot \mathrm{n} = -g$.

7. NUMERICAL EXPERIMENTS

7.1. Perturbed electron-gas column: pure plasma-oscillation

We consider a the simplest example possible in order to capture plasma oscillation in its purest form. We consider the setup of physical parameters and physical domain

$$\varepsilon = 10^{-4}\,,\ \tfrac{q_e}{m_e} = -1\,,\ \Omega = [0,1]\times[0,h]\ \text{ with }\ h = 400^{-1}\,. \tag{94}$$

The initial conditions given in primitive state (density/velocity/pressure) are

$$\rho_0 = \begin{cases} \overline{\rho} - \delta & \text{if } x \in [0, 0.5) \\ \overline{\rho} + \delta & \text{if } x \in [0.5, 0] \end{cases} \text{ with } \overline{\rho} = 10.0 \text{ and } \delta = 0.001\ ,\ \ \mathbf{v}_0 = 0\ ,\ \ p_0 = 0.01 \tag{95}$$

In other words, the initial setup consists of a quasi-1d column of plasma with discontinuous density, no velocity and low pressure (equivalently: low temperature). The goal of such low pressure is to make pressure forces $-\nabla p$ negligible in comparison the electric-force $\frac{q_e}{m_e}\rho\nabla\varphi$. The pressure follows the ideal gas law (i.e. $p = (\gamma-1)(\mathcal{E} - \frac{1}{2}\rho^{-1}|\mathbf{p}|^2_{\ell^2})$) with $\gamma = 5/3$ as it is expected from statistical mechanics considerations for a single-species with three degrees of freedom per particle. With this setup the approximate value of the plasma frequency $\omega_p \approx \sqrt{10^5}$, therefore the plasma period is $T_p \approx 0.01986$. We consider a final simulation time of $t_F = 5T_p$.

We use Neumann boundary conditions $\nabla\varphi\cdot\mathrm{n} = 0$ on the entirety of the boundary $\partial\Omega$ for the potential. This is a quite technical issue that requires a few explanations. For starters, note that the scheme actually never computes φ but rather φ_e, see Section 4.5. The initial potential $\varphi_h^{e,0}$ satisfying the mean-value constraint $\int_\Omega \varphi_h^{e,0}\,\mathrm{d}\boldsymbol{x} = 0$ is computed by solving the problem

$$(\nabla\varphi_h^{e,0}, \nabla\chi_i)_{L^2(\Omega)} = \sum_j \mathcal{P}_{ij}(\rho_0, \chi_i)_{L^2(\Omega)}\ \ \forall i \in \mathcal{H}\,.$$

where $\mathcal{H}$ is the set of indices identifying the nodes/DOFs from the spatial discretization of the potential, the linear operator $\mathcal{P} \in \mathbb{R}^{M\times M}$ applied to some vector $\Phi \in \mathbb{R}^M$, with $M = \mathrm{card}\{\mathcal{H}\}$ is defined as

$$(\mathcal{P}\Phi)_i = \Phi_i - \tfrac{\mu(\Phi)}{\mu(\Omega)}\ \text{ where }\ \mu(\Phi) = \sum_{j\in\mathcal{H}} m_j\Phi_j\ ,\ \mu(\Omega) := \sum_{j\in\mathcal{H}} m_j\ \text{ and }\ m_i := \int_\Omega \chi_i\,\mathrm{d}\boldsymbol{x}\,.$$

The purpose of the algebraic operator $\mathcal{P}$ is to recover the data-compatibility [15]: without this modification the right hand-side $(\rho_0,\chi_i)_{L^2(\Omega)}$ might not belong to the column-space of the matrix. This is particularly true in the context of distorted meshes. This allows direct use of conjugate gradient method even though the matrix is actually singular. From a physical standpoint, the operator $\mathcal{P}$ is equivalent to setting a constant background of positively charged ions that create mean-value charge neutrality.

We used the algebraic scheme described in [58] with nodal discontinuous affinely-mapped $\mathbb{Q}^1$ elements with SSP3 time-integration for the Stage #1 and Stage #3 of Strang-Splitting. Positivity

of the density and internal energy are safeguarded by convex-limiting: catastrophic failure is not possible. The Stage #2 of Strang-splitting (i.e. source-update) uses the scheme (69)-(70).

We note that the source-update scheme does not have any intrinsic time-stability constraint. More precisely we have that: the scheme is such that the only time-step size constraints are those determined by the purely hyperbolic Stage #1 which have to be carried over Stages #2 and Stage #3. With the current setup of physical parameters and initial data (94)-(95), material velocities and sound speed lead to very mild cfl constraints. In fact, the scheme can cover the entire simulation time $[0,t_F]$ in just 4 time steps or less if we use a large cfl such as cfl $= 0.75$. By this we mean, that the only time-step size bottleneck is that one dictated by the hyperbolic system. This is an ideal situation, in the sense that the plasma period is not the primary time-scale of concern. In order to fully resolve the plasma oscillation, and produce a time-resolved simulation we had to use cfl $= 0.005$, see Figure 7-1. Figure 7-1 shows a half plasma-period of simulation extracted from the total of five periods of simulation time. One of the noticeable features of these snapshots is the preservation of a stationary contact in the middle of the domain.

7.2. Electrostatic Implosion

In this section we describe a numerical setup that puts some stress into the scheme. More precisely, the goal of this setup is to test the performance of the scheme in the context of strong expansions/rarefactions, vacuum-like conditions, strong shocks, and strong electrostatic forces. We consider the following setup of physical parameters and physical domain

$$\varepsilon = 10^{-3}\,,\ \tfrac{q_e}{m_e} = -1\,,\ \Omega = \left\{ \boldsymbol{x} \in \mathbb{R}^2 \mid |\boldsymbol{x}-\boldsymbol{x}_0|_{\ell^2} \leq 16 \right\} \tag{96}$$

The initial conditions given in primitive state are

$$\rho_0 = 1\,,\ \mathbf{v}_0 = 0\,,\ p_0 = 10^{-4} \tag{97}$$

for the electrons. The ions number density n_i satisfies the following distribution for all time:

$$n_i = \begin{cases} 10^4 & \text{if } \boldsymbol{x} \in \Omega_A \\ 0 & \text{if } \boldsymbol{x} \in \Omega \backslash \Omega_A \end{cases} \quad \text{where } \ \Omega_A = \left\{ \boldsymbol{x} \in \mathbb{R}^2 \mid 4 \leq |\boldsymbol{x}-\boldsymbol{x}_0|_{\ell^2} \leq 6 \right\}$$

with $\boldsymbol{x}_0 = (0,0)$. The specific ion charge is set to $q_i = 1$. In other words: there is positive charge-density of magnitude $\rho_i = q_i n_i = 10^4$ on the annulus Ω_A that will pull the electrons into the center of the circular domain Ω. The electrons will try to stick to the annulus but because of their inertia they will miss the target and implode. The pulling process will necessary create vacuum-like conditions in the outskirts of the circle, close to the boundary. Long term behaviour is that one of electrons oscillating around the annulus Ω_A. We notice that the initial conditions are such that mean-value charge-neutrality $\int_\Omega \rho_i + \rho_e \, \mathrm{d}\boldsymbol{x} = 0$ is not satisfied. We therefore use homogeneous Dirichlet boundary conditions $\varphi \equiv 0$ on the entirety of the boundary $\partial\Omega$.

With this setup, the initial plasma frequency is $\omega_p = \sqrt{\rho_0} = \sqrt{10^3}$. The total simulation time is set to be one plasma period $t_F = T_p = \frac{2\pi}{\omega_p}$. Note that the plasma period is a function of the density, therefore as the simulation evolves, and the electron-plasma gets compressed, the actual value of

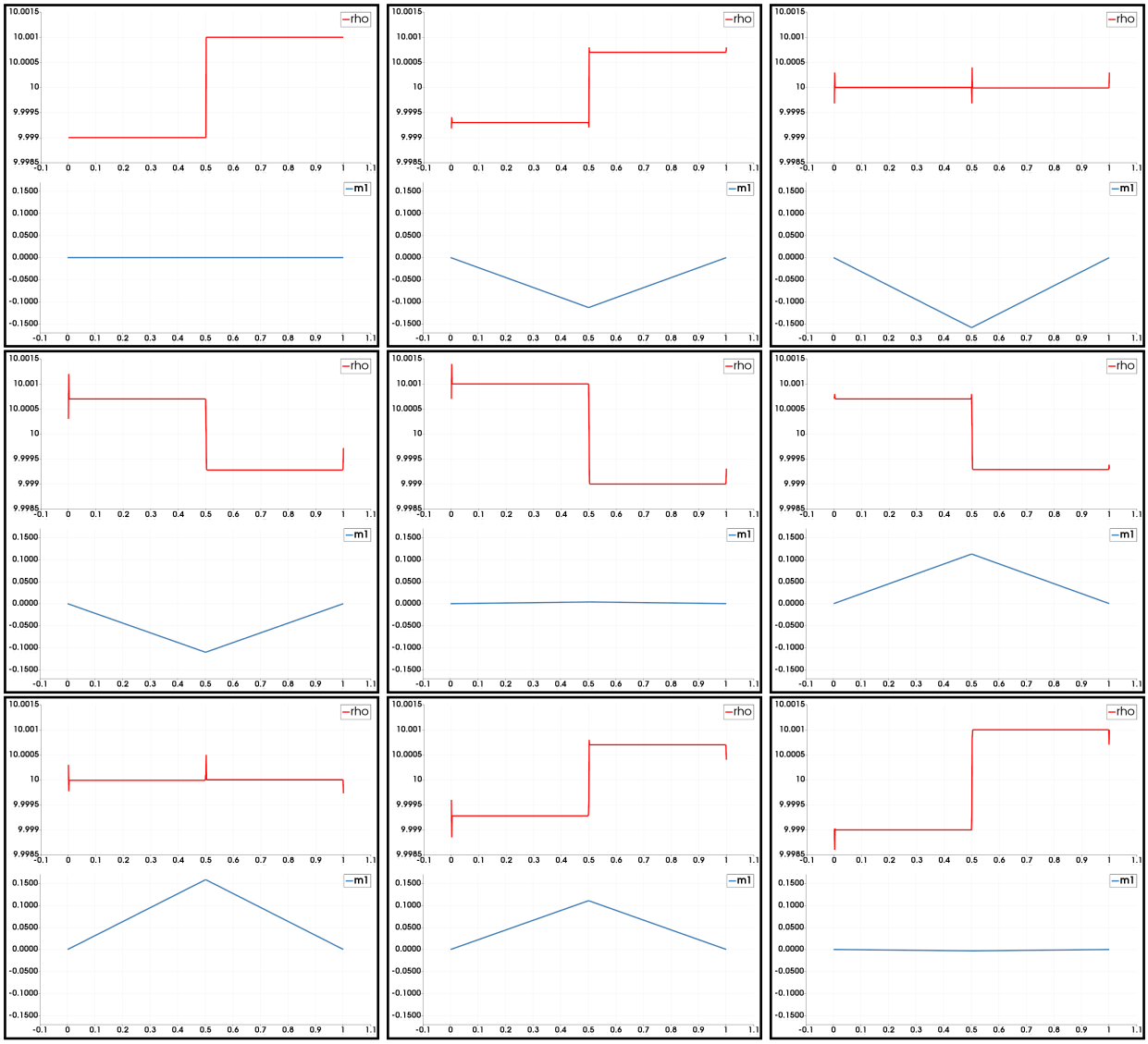

Figure 7-1 Pure plasma oscillation: evolution screenshots.

This figure illustrates evolution of the density (red) and momentum (blue) for half plasma period T_p. The sample times are, approximately $t = 0$, $\frac{1}{16}T_p$, $\frac{2}{16}T_p$, $\frac{3}{16}T_p$, $\frac{4}{16}T_p$, $\frac{5}{16}T_p$, $\frac{6}{16}T_p$, $\frac{7}{16}T_p$, $\frac{8}{16}T_p$. The dynamics is almost purely Hamiltonian given that the plasma pressure/temperature is quite low. It is worth noting the stationary contact in the density profile, and the sticky nature of the electrons near the walls at $x = 0$ and $x = 1$. This last feature is most possibly a defect of the current implementation of reflecting boundary conditions.

the smallest plasma-period in the domain will shrink by a few orders of magnitude. See Figure 7-2 for preliminary 2d-results displaying the evolution of the electron density. See also Figure 7-3 with a plot-overline of the density across the horizontal lines passing through the origin. This plot overline illustrates part the dynamic range in density of this simulation (at least six-orders of magnitude on the whole simulation).
We have experimented with this problem with a large range of parameters, some of which lead to much more severe conditions/shocks/expansions etc. Overall we have a very high degree of confidence in the capabilities of this scheme for this kind of problems. We have not yet found the limits of breakdown of these schemes in the context of implosion-like tests. It is worth mentioning that actual mesh used for this problem is not affinely mapped. The mesh actually uses quadrilaterals with general bilinear maps. In this context there is no mathematical guarantee that we can preserve the electro-kinetic energy during Stage #2. Still, the scheme provides significant robustness, even though we are operating past the point of validity of any mathematical certificate of quality.

8. OUTLOOK: PROBLEMS BEYOND THE SCOPE OF CURRENT WORK

The goal of this section is discussing open problems and related lines of research that were not part of the originally proposed plan of work. Among them, a very important topic is asymptotic preservation in relationship to magnetic drift-limits. This is both an area where where important developments in the literature already exist but further investment is needed in order to achieve a higher degree of generality and applicability.

8.1. Magnetic drift-limits

Consider the two-dimensional Euler-Poisson model with a given magnetic field $\mathbf{B}$

$$\begin{aligned} \partial_t \rho + \operatorname{div} \mathbf{p} &= 0\,, \\ \partial_t \mathbf{p} + \operatorname{div}\left(\rho^{-1}\mathbf{p}\mathbf{p}^\top + \mathbb{I} p\right) &= -\tfrac{q_e}{m_e}\rho\nabla\varphi + \tfrac{q_e}{m_e}\mathbf{p}\times\mathbf{B}\,, \\ -\varepsilon\Delta\partial_t\varphi &= -\tfrac{q_e}{m_e}\operatorname{div}\mathbf{p}\,, \end{aligned} \tag{98}$$

Here $\mathbf{B} = B\widehat{k}$ is given, perpendicular to the xy-plane (i.e. $\mathbf{p}\cdot\mathbf{B} = 0$), constant in space and constant in time. The pressure is given by $p = \theta_0\rho$ with θ_0 being a given constant temperature (this is called an isothermal closure). Model (98) can still be understood as a purely electrostatic problem. In the naked eye (98) appears to be simpler than the full Euler-Poisson equation system that includes a total mechanical energy equation. However, the additional term $\frac{q_e}{m_e}\mathbf{p}\times\mathbf{B}$ is far from being an ancillary appendage. It changes the dynamics of the problem quite significantly as it brings in a new time-scale into play (the cyclotron frequency) and new asymptotic limits that are not as simple to digest as the source dominated-regime of the purely electrostatic problem.

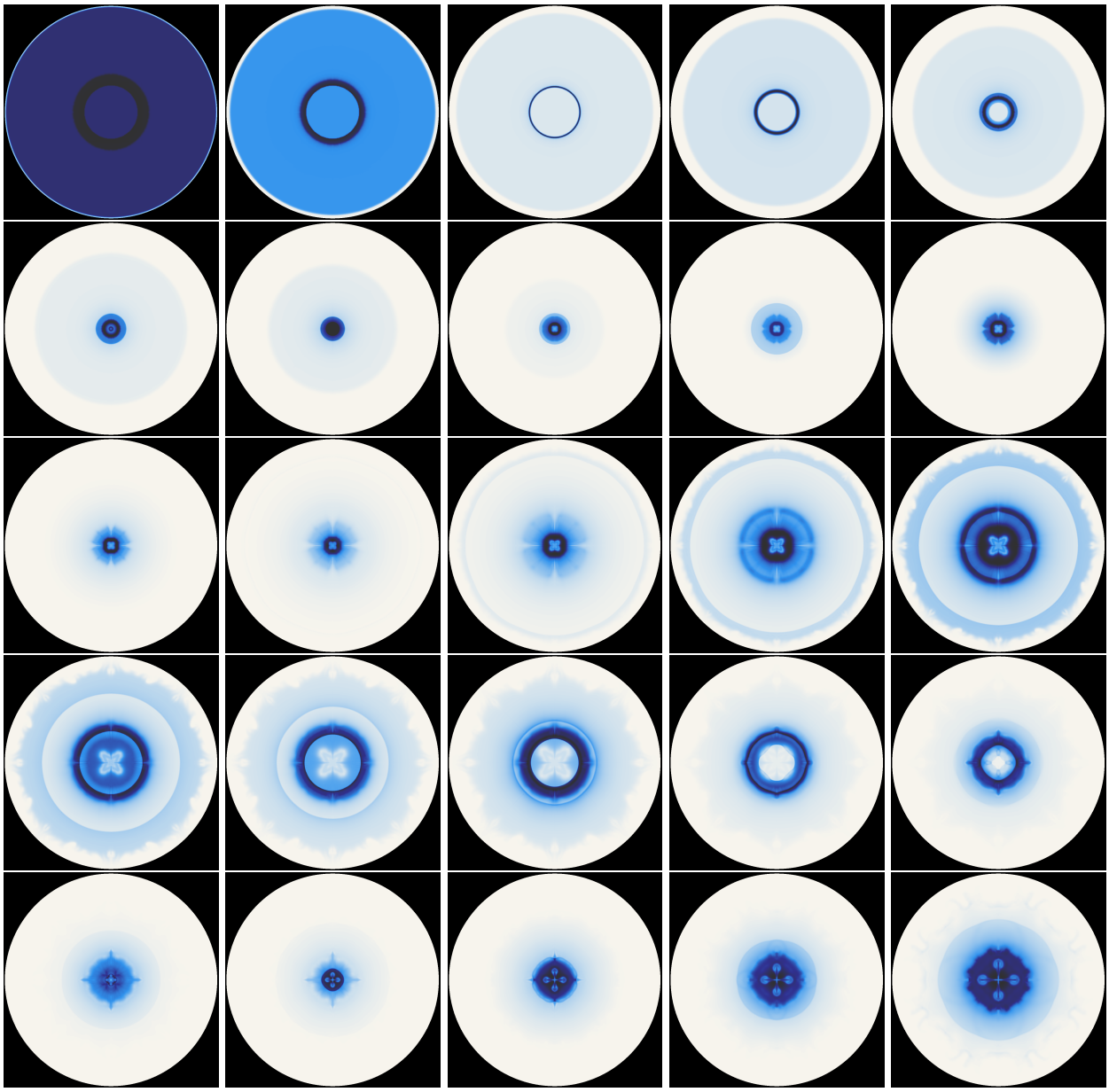

Figure 7-2 Implosion electron mass density: evolution screenshots.

This figure illustrates evolution of the density for time frames $0/1600$ to $250/1600$ at regular intervals of 10 (read from left to right and top to bottom). Contrast has been automatically adjusted for each frame in order maximize the resolution of details. Frames $150-180$ show some tearing or fingering-like instability in the outer skirts of the circle where a strong vacuum is formed.

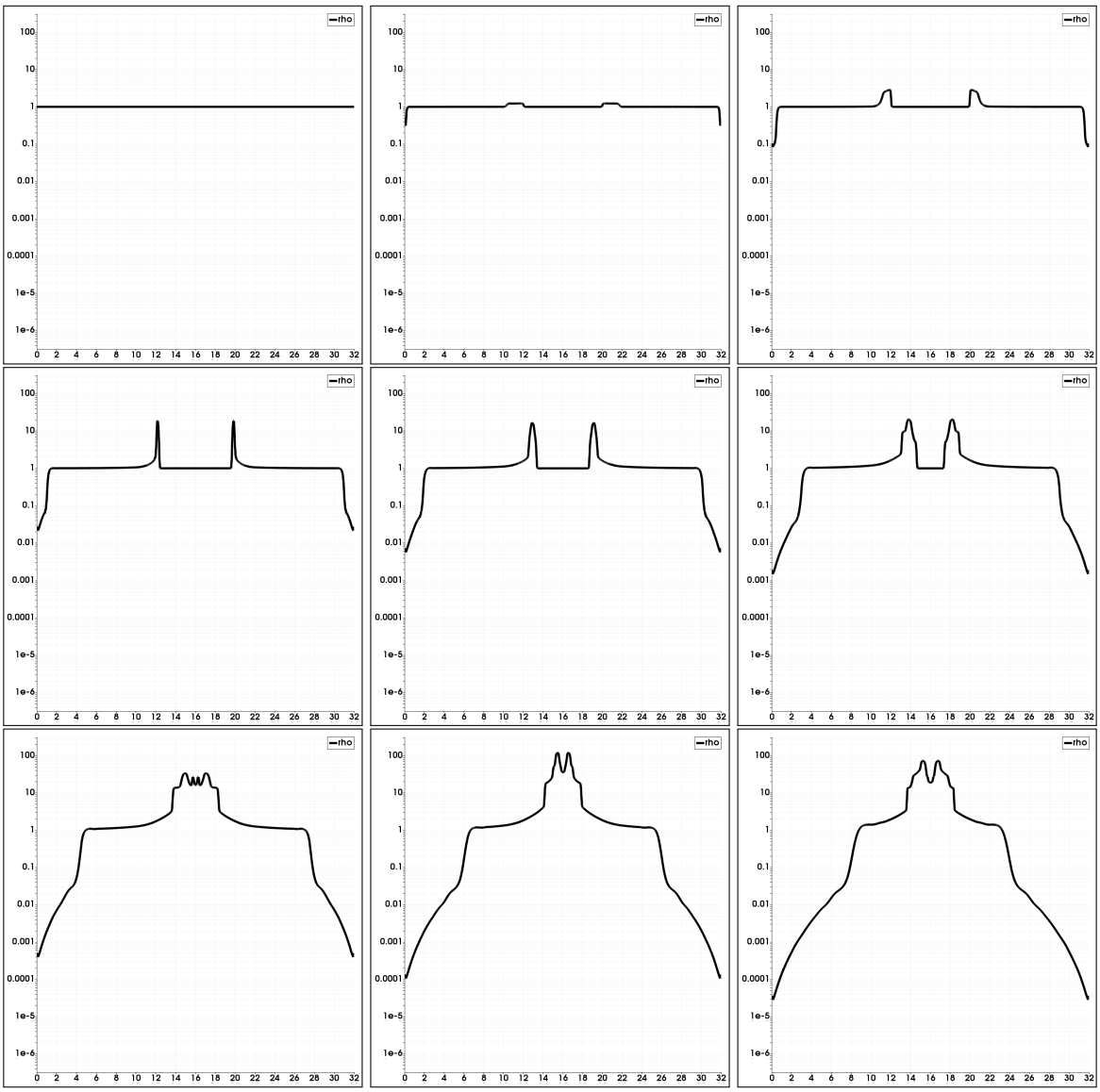

Figure 7-3 Implosion electron mass density: plot-overline.

This figure illustrates evolution of the density for time frames $0/1600$ to $80/1600$ at regular intervals of 10 (read from left to right and top to bottom). The y-axis represents density in logarithmic scale in order to fully appreciate the dynamic range of this test. The electron density on the walls drops by almost 5 orders of magnitude. Overall, the dynamic range of the entire simulation peaks at six-orders of magnitude in some of the missing frames.

Let $\omega_c = \frac{|B|q_e}{m_e}$ denote the cyclotron angular frequency. In the context of low temperature regimes, and $\omega_p << \omega_c$ (which usually entails regimes with very low electron densities combined with very large magnetic fields) model (98) formally reaches the asymptotic limit

$$\begin{aligned} \partial_t \rho_e + \operatorname{div}(\rho_e \mathbf{v}_e) &= 0\,, \\ -\varepsilon\Delta\partial_t\varphi &= -\tfrac{q_e}{m_e}\operatorname{div}(q_e\mathbf{v}_e)\,, \\ \mathbf{v}_e &:= -\frac{\nabla\varphi\times\mathbf{B}}{|\mathbf{B}|^2}\,, \end{aligned} \tag{99}$$

see for instance [86, 87, 36] for more details. In a more direct fashion, model (99) can be formally derived from (98) passing to the limits $m_e, \theta_0 \to 0^+$ which simply wipes out all inertial and pressure terms. Model (99) is known as the guiding-center drift-limit [87] and it is somewhat related to the gyro-fluid approximation [39, 38].

It is worth mentioning that (99) contains neither hydrodynamic time-scales, nor sound speed, nor electrostatic plasma oscillation, nor kinetic energy, nor electron inertial effects. Discretizing and solving model (99) is reasonably trivial. However, developing an asymptotic preserving scheme for (98) that smoothly degenerates into the model (99) does not appear to be an easy task. In fact, the schemes advanced in this manuscript were not conceived to have such properties or be efficient in such regimes.

In this regard, publication [39] is one of the few landmark papers, where the authors develop a scheme for Euler's equation with "given" electric field E and magnetic fields B that is asymptotic preserving in the magnetic-drift limit. There is still a big gap in the numerical analysis literature between single-minded methods for a single uncoupled PDE satisfying just one constraint (e.g. either minimum principle of the entropy, or asymptotic consistency, etc) and methods that preserve two or more of these constraints and compute their own electromagnetic fields in a self-consistent manner. For instance, we are not aware of the existence of any scheme for Euler-Maxwell or Euler-Poisson model that satisfies two or more of the following list of properties: (i) it is consistent in the magnetic-drift limit, (ii) computes its own electromagnetic fields (i.e. beyond "given" E and B fields), (iii) preserves the electro-kinetic energy in the source-dominated regime, (iv) it is asymptotically well-posed in the high-density regime, (v) preserves the invariant set of Euler's equation (e.g. positivity of density and minimum principle of the specific entropy), and (vi) is fully-discrete (i.e. actually implementable scheme).

The list (i)-(vi) may sound as an exaggerated collection of requirements, but many naïve tests and technical applications are multiscale in nature and make even two dimensional computations challenging regardless of the computational resources available. In this regard, the diocotron instability is an interesting example that taps exactly into the regime where the guiding-center drift-limit model (low density and high B-field) is a lot more appropriate than a full Euler-Poisson or Euler-Maxwell model. The setup of this instability is explained in the following subsection together with some preliminary numerical results.

8.2. Diocotron instability

The diocotron instability consists in an initial configuration of electrons moving with velocity $\mathbf{v}$ given by

$$\mathbf{v} := \boldsymbol{\omega}(r) \times \boldsymbol{x} \;\text{ where }\; \boldsymbol{\omega} = \omega(r)\widehat{k}\,,\;\; \boldsymbol{x} = [\boldsymbol{x}_1, \boldsymbol{x}_2, 0]^\top\,,\;\; r = |\boldsymbol{x}| \tag{100}$$

where $\omega(r)$ is an angular velocity carefully chosen in order to produce centrifugal forces that balance the pressure forces, electric force, and magnetic forces exactly, see Remark 8.1 for more details. The initial electron density profile is discontinuous, which leads to a discontinuous angular velocity $\omega(r)$. This creates shear between the layers that rotate at different speeds while also triggering specific resonant modes, see for instance [36] and Chapter 6 of [35].

We considered the following set of parameters and physical domain

$$\varepsilon = 10^{-2}\,,\; \tfrac{q_e}{m_e} = 10^{-2}\,,\; B = 50\,,\; \theta_0 = 0.001\,,\; \Omega = \{\boldsymbol{x} \in \mathbb{R}^2 \,||\boldsymbol{x}|_{\ell^2} \leq 16\} \tag{101}$$

and the following choice of initial electron and ion density profiles

$$n_e = \begin{cases} \delta^+ n_0 & \text{if } |\boldsymbol{x}|_{\ell^2} \leq 4 \\ n_0 & \text{if } 4 < |\boldsymbol{x}|_{\ell^2} \leq 8 \\ \delta^- n_0 & \text{if } |\boldsymbol{x}|_{\ell^2} > 8 \end{cases} \text{ where } n_0 = 1\,,\; \delta^+ = 0.175\,,\; \delta^- = 10^{-5}\,, \text{ while } n_i = \delta^- n_0\,. \tag{102}$$

The boundary conditions are $\mathbf{p} \cdot \mathrm{n} = 0$ and $\varphi = 0$ on the entirety of the boundary. This setup of parameters was chosen to guarantee that the inequality $\omega_p << \omega_c$ holds. The choice of electron and ion and density distributions was picked from [36] in order to trigger the 3-mode of the Diocotron instability. A computational procedure used to compute an (approximate) equilibrium initial velocity profile is detailed in Remark 8.1.

The simplest approach to incorporate the magnetic forces into either schemes (55)-(56) or (69)-(70) is by compounding operator-Splitting. Time integration of the magnetic forces using operator splitting while still preserving internal energy is relatively trivial to achieve using Crank-Nicolson scheme which preserves the kinetic energy exactly. A fully-coupled Schur-complement approach leading to non-symmetric linear algebra was also tested. Both approaches (compounded operator splitting and/or Schur complement approach) delivered nearly identical results. In both cases establishing positivity of density and internal energy is straightforward. Figure 8-1 shows some numerical results of the 3-mode of the Diocotron instability triggered by the initial choice of electron density profile detailed in (102).

While in principle it is possible to solve quite a lot important problems with such a simple minded numerical approach, and we can reproduce well-established analytical results such as the Diocotron instability, there is plenty to improve here. The results of Figure 8-1, while aesthetically beautiful and even compelling from the mathematical point of view, they exhibit a strong dependence on the parameters (101). In particular, reducing the electron specific mass m_e while increasing the value of B (simultaneously) take us to the magnetic-Drift regime. This can very quickly put some serious stress into the scheme. While catastrophic failure is unlikely to

happen, very large material velocities will lead to negligible time-step sizes due to hyperbolic cfl-constrants. In practice, this means that even simple two-dimensional non-technical cases can become extremely difficult to solve, possibly taking many days to complete, making three-dimensional technically relevant computations completely out of reach. This kind of pathological situations appears to be the signature of numerical schemes that are not asymptotically consistent with magnetic drift-limits.

These are not problems that might get solved anytime soon by a bigger more powerful computer. Similarly, blind usage of implicitness will not buy us much either (see for instance [38]). It would be quite important to revisit the literature [39, 24, 38], improve the state of affairs by formulating new methods that satisfy/preserve multiple constraints and are actually implementable in the context of modern finite element libraries/frameworks.

Remark 8.1 (Computation of the angular velocity profile)**.** The initial velocity profile $\mathbf{v}$ of the Diocotron problem satisfies the following equilibrium relationship:

$$\rho(\mathbf{v}\cdot\nabla)\mathbf{v}+\nabla p=-\tfrac{q_e}{m_e}\rho\nabla\varphi+\tfrac{q_e}{m_e}\rho\mathbf{v}\times\mathbf{B}\,. \tag{103}$$

Using (100) we can rewrite (103) as follows

$$-\rho\omega(r)^2\boldsymbol{x}+\nabla p=-\tfrac{q_e}{m_e}\rho\nabla\varphi+\tfrac{q_e}{m_e}\rho\omega(r)(\boldsymbol{x}_\perp\times\mathbf{B})\ \text{ where }\ \boldsymbol{x}_\perp:=[-\boldsymbol{x}_2,\boldsymbol{x}_1,0]^\top.$$

Taking the dot product with $\boldsymbol{x}$ we get

$$-\rho\omega(r)^2|\boldsymbol{x}|_{\ell^2}^2+\nabla p\cdot\boldsymbol{x}=-\tfrac{q_e}{m_e}\rho\nabla\varphi\cdot\boldsymbol{x}+\tfrac{q_e}{m_e}\rho\omega(r)(\boldsymbol{x}_\perp\times\mathbf{B})\cdot\boldsymbol{x}$$

which can be finally reorganized as

$$\underbrace{(\rho|\boldsymbol{x}|_{\ell^2}^2)}_{=a}\omega(r)^2+\underbrace{\big(\tfrac{q_e}{m_e}\rho(\boldsymbol{x}_\perp\times\mathbf{B})\cdot\boldsymbol{x}\big)}_{=b}\omega(r)\underbrace{-\big(\nabla p\cdot\boldsymbol{x}+\tfrac{q_e}{m_e}\rho\nabla\varphi\cdot\boldsymbol{x}\big)}_{=c}=0 \tag{104}$$

which is clearly a quadratic equation for $\omega(r)$. Therefore, the algorithm/script required to compute equilibrium profiles consists in the following steps: (i) Choose a θ-symmetric electron density and ion density profiles n_e and n_i respectively, (ii) Compute the pressure $p=\theta_0\rho=\theta_0 m_e n_e$ using the electron density profile n_e chosen in step (i), (iii) find the corresponding electrical potential by solving $-\varepsilon\Delta\varphi=q_e n_e+q_i n_i$ with proper boundary conditions, (iv) Solve the quadratic equation:

$$(\rho_i|\boldsymbol{x}_i|_{\ell^2}^2)\omega(r_i)^2+\big(\tfrac{q_e}{m_e}\rho_i(\boldsymbol{x}_{i,\perp}\times\mathbf{B})\cdot\boldsymbol{x}_i\big)\omega(r_i)-\big((\nabla p)_i\cdot\boldsymbol{x}_i+\tfrac{q_e}{m_e}\rho_i(\nabla\varphi)_i\cdot\boldsymbol{x}_i\big)=0 \tag{105}$$

for each node $i\in\mathcal{V}$. This algorithm can be encoded into any reasonable finite element library/framework and will deliver accurate equilibrium profiles without resorting to iterative solution methods.

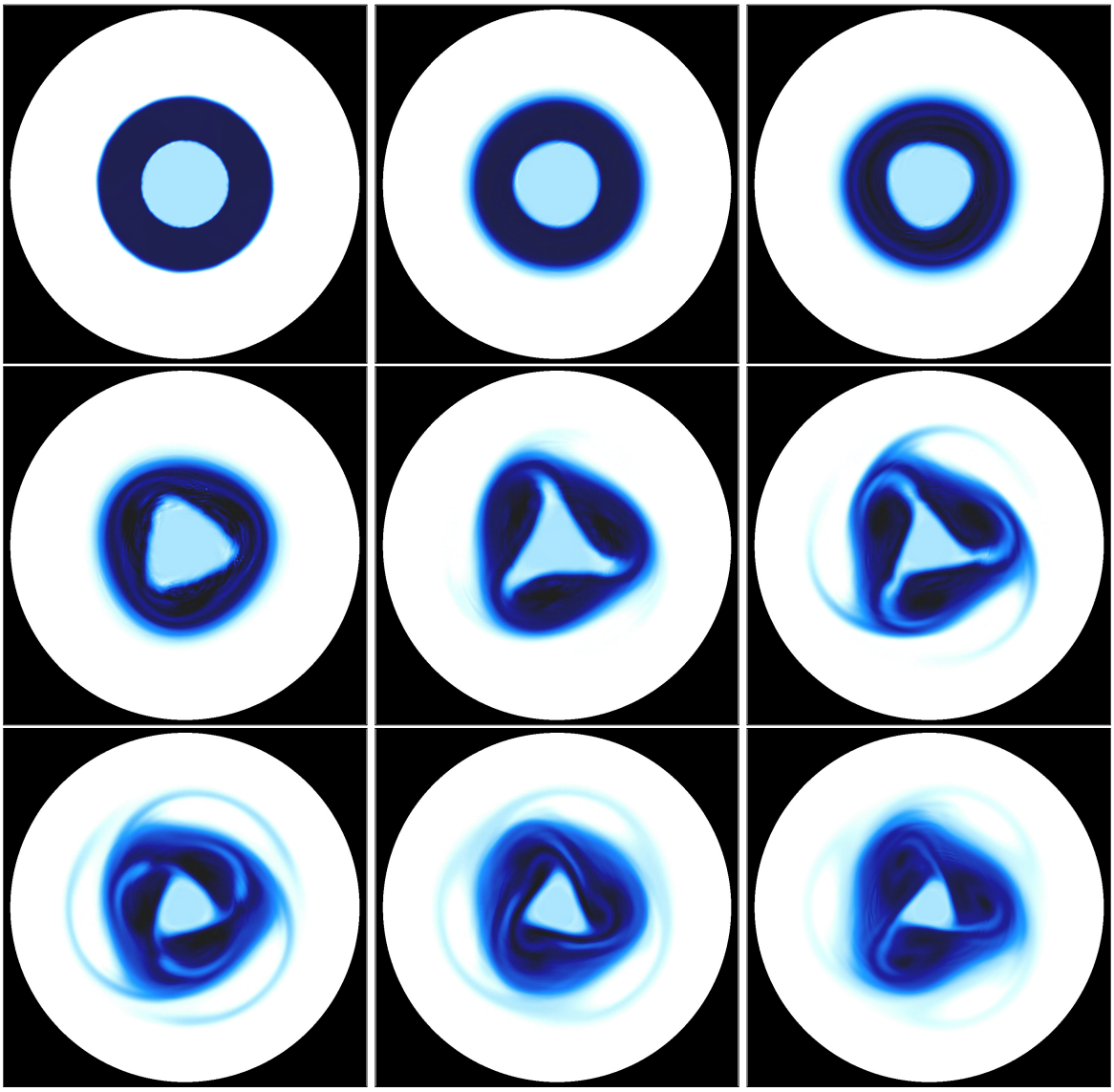

Figure 8-1 Diocotron instability: electron density.
This figure illustrates evolution of the Diocotron instability, for the 3-mode.

9. CONCLUSION

An overview of the main stability properties satisfied by Euler-Maxwell and Euler-Poisson model was presented in Section §2. These results establish the natural definitions of stability and energ-flux balance that these models are meant to preserve. All of the results in Section §2 are elementary in nature but: (i) They cannot be easily found in the scientific literature, (ii) They are the backbone of the main stability arguments used in the remainder of the manuscript. In particular, we note that the energy-flux balance arguments for Euler-Poisson's model where greatly simplified by interpreting the electrostatic problem as an evolutionary problem rather than as an elliptic constraint (electric Gauss law). We think this approach is original and much more fruitful than sticking the traditional elliptic-constraint paradigm. This fundamental change on view carried over the entire manuscript and laid the path to rigorous discrete energy-arguments in the numerical analysis context.

Serving as guideline or template of ideas, in Section §3 we presented a collection of baseline constructions for Euler-Maxwell system that preserve positivity of density, internal energy, electro-kinetic energy, and total energy of the system using purely collocated discretizations. While these mathematical results are theoretical in nature and collocated discretization are unlikely to be applicable in the context of Euler-Maxwell and Euler-Poisson's system we note that: (i) A primary layer of time-integration mathematical theory was established §3. One of the main results is a formal proof of energy-stability for Euler-Maxwell system when using operator-splitting (see Lemma 3.3) which is, to the best of our knowledge, the first of its kind. (ii) A large portion of the results of Section §3 were carried over into the context of Euler-Poisson model, in particular those results that are related to the preservation of internal energy.

In Section §4 we presented two main source-update schemes for the Euler-Poisson model: both of them preserve positivity of density, internal energy and the electro-kinetic energy. The first scheme is a somewhat traditional fully-coupled scheme leading to a Schur complement algebraic problem. The second scheme avoids the method of lines and leads directly to a fully decoupled scheme: there is no Schur complement in this second-scheme since the resulting discrete system is lower-triangular (the solution can be found by blockwise forward substitution). Only the second scheme is guaranteed to be "asymptotic preserving" or "asymptotically well-posed" in the context of large densities: in other words its linear algebra system is guaranteed to be unconditionally invertible. Full detail about the mathematical properties satisfied by each scheme is provided. The emphasis of Section §4 is not forcing the will of the reader onto taking a specific choice, but rather on providing choices while also informing about the consequences/properties associated to each one. Both schemes are highly specialized constructions that require very precise choices of finite element spaces, mesh type, and time-discretizations. However, it is worth highlighting that these schemes are not finite volume/element/difference hybrids that have to be patched together from different pieces of code as it is usually advocated/advanced in the computational-physics literature. Even though the computational implementation of these schemes require a significant amount of coding craft, they can fit under the roof of most leading finite element software frameworks (e.g. [2, 9, 3]).

In Section §4.5 we provided the basic algorithmic workflow and modifications of the scheme in order to accommodate either static or time-dependent "given" background of ions. This requires

only minor modifications to the scheme. We note that none of the schemes advanced in this manuscript is self-starting. This is related to the initial value of the electric potential which has to be pre-computed before we even start the time-integration process. In Section §5.2 we provide some of the details related to the initialization of the Scheme.

Section §2.3 is an informal discussion on the boundary conditions for Euler-Poisson. We note that the mathematical background and overall numerical analysis state-of-the-art about boundary conditions for Euler-Maxwell and Euler-Poisson is borderline non-existent. Any discussion on this topic is usually of questionable scientific value since very little can be established rigorously. At the very least some heuristic guidelines are required in order to understand what boundary conditions might either make the PDE-model unstable and/or lead to data-incompatibility. Informal analysis of the source dominated regime sheds some light into this issue. In particular, some preliminary conclusions are: (i) Homogeneous Neumann boundary conditions for the potential are data-compatible with reflecting boundary conditions for Euler's subsystem, (ii) Piecewise constant Dirichlet data for the potential should preserve the tangent component of the current, but might either draw or inject current into the walls of the domain, (iii) Non-homogeneous Neumann boundary conditions for the Euler-Poisson model without resistive/damping source terms do not seem to be mathematically and/or physically meaningful.

Section §7 presents some modest numerical results. We present two primary examples: "pure-plasma oscillation" and "electrostatic implosion". The pure-plasma oscillation is meant to illustrate the ability of the scheme preserve purely oscillatory phenomena due to the electrostatic plasma frequency and overstep the plasma period. The pure plasma-oscillation test does not intend to be brutalization test where the breakdown limits of the scheme are explored. On the other hand, the electrostatic implosion is meant to push the capabilities of the scheme much harder in order to create conditions of strong expansions, strong vacuum, strong shocks, high-densities, high-pressures, etc. We can confidently say that we are nowhere near the breakdown limit of the proposed schemes. There is plenty of purely computational work pending to be done in relationship to both: (i) Validation of the code (with convergence rates). Exact solutions for Euler-Poisson model in the repulsive case do not seem to be widely available and the method of manufactured solutions, for reasons that go beyond the scope of this manuscript, is not a technically viable solution. In this regard, the literature of attractive Euler-Poisson system appears to offer a reasonable collection of exact analytical solutions that can be used for validation purposes [108, 109]. (ii) Stronger more aggressive test have to be designed for display purposes.

Section §8 offers an outlook into problems and regimes where the schemes proposed in this manuscript indeed work but much more serious mathematical development is required. In particular, section §8 describes what is known as the "magnetic-drift limit" or "guiding center drift-limit". This is related to what is known as asymptotic preservation in the context of strong magnetic fields. The scientific state-of-the-art is, for the time being, incomplete and more investment would be needed. We also propose a numerical test that taps exactly in the magnetically-driven drift regime and show that while our methods work, there is still plenty of room for improvements. Overall, Section §8 defines a quite exiting path future research.

Finally, we mention that sections §2.4, §4.6, §5.1 are ancillary and they do not correspond with any part of the funded/proposed work. Those sections are related to the attractive

(self-gravitational) Euler-Poisson system used is cosmological simulations and galactic dynamics. Those sections were included in the report for the sake of completeness and because their inclusion required negligible time and effort. Last but not least they were included because they are of general scientific interest.

REFERENCES

[1] Remi Abgrall and Harish Kumar. Robust finite volume schemes for two-fluid plasma equations. *J. Sci. Comput.*, 60(3):584–611, 2014.

[2] Martin Alnæs, Jan Blechta, Johan Hake, August Johansson, Benjamin Kehlet, Anders Logg, Chris Richardson, Johannes Ring, Marie E Rognes, and Garth N Wells. The fenics project version 1.5. *Archive of Numerical Software*, 3(100), 2015.

[3] Robert Anderson, Julian Andrej, Andrew Barker, Jamie Bramwell, Jean-Sylvain Camier, Jakub Cerveny, Veselin Dobrev, Yohann Dudouit, Aaron Fisher, Tzanio Kolev, et al. Mfem: A modular finite element methods library. *Computers & Mathematics with Applications*, 81:42–74, 2021.

[4] D. N. Arnold and A. Logg. Periodic table of the finite elements. *SIAM News*, 47(9), 2014.

[5] Douglas N. Arnold, Richard S. Falk, and Ragnar Winther. Finite element exterior calculus, homological techniques, and applications. *Acta Numer.*, 15:1–155, 2006.

[6] Uri M. Ascher, Steven J. Ruuth, and Raymond J. Spiteri. Implicit-explicit Runge-Kutta methods for time-dependent partial differential equations. volume 25, pages 151–167. 1997. Special issue on time integration (Amsterdam, 1996).

[7] Santiago Badia and Ramon Codina. A nodal-based finite element approximation of the Maxwell problem suitable for singular solutions. *SIAM J. Numer. Anal.*, 50(2):398–417, 2012.

[8] Dinshaw S. Balsara, Takanobu Amano, Sudip Garain, and Jinho Kim. A high-order relativistic two-fluid electrodynamic scheme with consistent reconstruction of electromagnetic fields and a multidimensional Riemann solver for electromagnetism. *J. Comput. Phys.*, 318:169–200, 2016.

[9] Wolfgang Bangerth, Ralf Hartmann, and Guido Kanschat. deal. iiâĂŤa general-purpose object-oriented finite element library. *ACM Transactions on Mathematical Software (TOMS)*, 33(4):24–es, 2007.

[10] M. S. Benilov. A kinetic derivation of multifluid equations for multispecies nonequilibrium mixtures of reacting gases. *Physics of Plasmas*, 4(3):521–528, 1997.

[11] Alfredo Bermúdez, Dolores Gómez, and Pilar Salgado. *Mathematical models and numerical simulation in electromagnetism*, volume 74 of *Unitext*. Springer, Cham, 2014. La Matematica per il 3+2.

[12] Stefano Bianchini and Alberto Bressan. Vanishing viscosity solutions of nonlinear hyperbolic systems. *Ann. of Math. (2)*, 161(1):223–342, 2005.

[13] J. A. Bittencourt. *Fundamentals of plasma physics*. Pergamon Press, Oxford, 1986.

[14] Pavel Bochev and R. B. Lehoucq. On the finite element solution of the pure Neumann problem. *SIAM Rev.*, 47(1):50–66, 2005.

[15] Pavel B. Bochev and James M. Hyman. Principles of mimetic discretizations of differential operators. In *Compatible spatial discretizations*, volume 142 of *IMA Vol. Math. Appl.*, pages 89–119. Springer, New York, 2006.

[16] Daniele Boffi, Franco Brezzi, and Michel Fortin. *Mixed finite element methods and applications*, volume 44 of *Springer Series in Computational Mathematics*. Springer, Heidelberg, 2013.

[17] Andrea Bonito and Jean-Luc Guermond. Approximation of the eigenvalue problem for the time harmonic Maxwell system by continuous Lagrange finite elements. *Math. Comp.*, 80(276):1887–1910, 2011.

[18] M. Bonitz, Zh. A. Moldabekov, and T. S. Ramazanov. Quantum hydrodynamics for plasmasâĂŤquo vadis? *Physics of Plasmas*, 26(9):090601, 2019.

[19] S. Boscarino, L. Pareschi, and G. Russo. Implicit-explicit Runge-Kutta schemes for hyperbolic systems and kinetic equations in the diffusion limit. *SIAM J. Sci. Comput.*, 35(1):A22–A51, 2013.

[20] Sebastiano Boscarino and Giovanni Russo. On a class of uniformly accurate IMEX Runge-Kutta schemes and applications to hyperbolic systems with relaxation. *SIAM J. Sci. Comput.*, 31(3):1926–1945, 2009.

[21] Alain Bossavit. Discretization of electromagnetic problems: the "generalized finite differences" approach. In *Handbook of numerical analysis. Vol. XIII*, Handb. Numer. Anal., XIII, pages 105–197. North-Holland, Amsterdam, 2005.

[22] S. I. Braginskii. *Transport Processes in a Plasma*. Reviews of Plasma Physics, Ed. M. A. Leontovich, 1965.

[23] M. Brio and C. C. Wu. An upwind differencing scheme for the equations of ideal magnetohydrodynamics. *J. Comput. Phys.*, 75(2):400–422, 1988.

[24] Stéphane Brull, Pierre Degond, Fabrice Deluzet, and Alexandre Mouton. Asymptotic-preserving scheme for a bi-fluid Euler-Lorentz model. *Kinet. Relat. Models*, 4(4):991–1023, 2011.

[25] Martin Campos Pinto. Constructing exact sequences on non-conforming discrete spaces. *C. R. Math. Acad. Sci. Paris*, 354(7):691–696, 2016.

[26] Martin Campos Pinto and Eric Sonnendrücker. Gauss-compatible Galerkin schemes for time-dependent Maxwell equations. *Math. Comp.*, 85(302):2651–2685, 2016.

[27] Claudio Canuto, M. Yousuff Hussaini, Alfio Quarteroni, and Thomas A. Zang. *Spectral methods in fluid dynamics*. Springer Series in Computational Physics. Springer-Verlag, New York, 1988.

[28] F. Chen. *Introduction to Plasma Physics and Controlled Fusion*. Springer International Publishing, 2015.

[29] Huangxin Chen, Weifeng Qiu, Ke Shi, and Manuel Solano. A superconvergent HDG method for the Maxwell equations. *J. Sci. Comput.*, 70(3):1010–1029, 2017.

[30] Gary Cohen and Sébastien Pernet. *Finite element and discontinuous Galerkin methods for transient wave equations*. Scientific Computation. Springer, Dordrecht, 2017. With a foreword by Patrick Joly.

[31] Stéphane Cordier and Emmanuel Grenier. Quasineutral limit of an Euler-Poisson system arising from plasma physics. *Comm. Partial Differential Equations*, 25(5-6):1099–1113, 2000.

[32] Pierre Crispel, Pierre Degond, and Marie-Hélène Vignal. An asymptotically stable discretization for the Euler-Poisson system in the quasi-neutral limit. *C. R. Math. Acad. Sci. Paris*, 341(5):323–328, 2005.

[33] Pierre Crispel, Pierre Degond, and Marie-Hélène Vignal. Quasi-neutral fluid models for current-carrying plasmas. *J. Comput. Phys.*, 205(2):408–438, 2005.

[34] Pierre Crispel, Pierre Degond, and Marie-Hélène Vignal. An asymptotic preserving scheme for the two-fluid Euler-Poisson model in the quasineutral limit. *J. Comput. Phys.*, 223(1):208–234, 2007.

[35] Ronald C Davidson. *Physics of nonneutral plasmas*. World Scientific Publishing Company, 2001.

[36] Ronald C Davidson and Gian Marco Felice. Influence of profile shape on the diocotron instability in a non-neutral plasma column. *Physics of Plasmas*, 5(10):3497–3511, 1998.

[37] A. Dedner, F. Kemm, D. Kröner, C.-D. Munz, T. Schnitzer, and M. Wesenberg. Hyperbolic divergence cleaning for the MHD equations. *J. Comput. Phys.*, 175(2):645–673, 2002.

[38] P. Degond. Asymptotic-preserving schemes for fluid models of plasmas. In *Numerical models for fusion*, volume 39/40 of *Panor. Synthèses*, pages 1–90. Soc. Math. France, Paris, 2013.

[39] P. Degond, F. Deluzet, A. Sangam, and M.-H. Vignal. An asymptotic preserving scheme for the Euler equations in a strong magnetic field. *J. Comput. Phys.*, 228(10):3540–3558, 2009.

[40] P. Degond, H. Liu, D. Savelief, and M.-H. Vignal. Numerical approximation of the Euler-Poisson-Boltzmann model in the quasineutral limit. *J. Sci. Comput.*, 51(1):59–86, 2012.

[41] Pierre Degond. Chapter 1 - asymptotic continuum models for plasmas and disparate mass gaseous binary mixtures. In Gianfranco Capriz and Paolo Maria Mariano, editors, *Material Substructures in Complex Bodies*, pages 1 – 62. Elsevier Science Ltd, Oxford, 2007.

[42] Yinbin Deng, Tai-Ping Liu, Tong Yang, and Zheng-an Yao. Solutions of Euler-Poisson equations for gaseous stars. *Arch. Ration. Mech. Anal.*, 164(3):261–285, 2002.

[43] Stéphane Descombes, Stéphane Lanteri, and Ludovic Moya. Locally implicit time integration strategies in a discontinuous Galerkin method for Maxwell's equations. *J. Sci. Comput.*, 56(1):190–218, 2013.

[44] Daniele Antonio Di Pietro and Alexandre Ern. *Mathematical aspects of discontinuous Galerkin methods*, volume 69 of *Mathématiques & Applications (Berlin) [Mathematics & Applications]*. Springer, Heidelberg, 2012.

[45] Alexandre Ern and Jean-Luc Guermond. *Theory and practice of finite elements*, volume 159 of *Applied Mathematical Sciences*. Springer-Verlag, New York, 2004.

[46] Jeffrey P Freidberg. *Plasma physics and fusion energy*. Cambridge university press, 2008.

[47] Hermano Frid. Maps of convex sets and invariant regions for finite-difference systems of conservation laws. *Arch. Ration. Mech. Anal.*, 160(3):245–269, 2001.

[48] David Gérard-Varet, Daniel Han-Kwan, and Frédéric Rousset. Quasineutral limit of the Euler-Poisson system for ions in a domain with boundaries. *Indiana Univ. Math. J.*, 62(2):359–402, 2013.

[49] Vivette Girault and Pierre-Arnaud Raviart. *Finite element methods for Navier-Stokes equations*, volume 5 of *Springer Series in Computational Mathematics*. Springer-Verlag, Berlin, 1986. Theory and algorithms.

[50] Edwige Godlewski and Pierre-Arnaud Raviart. *Numerical approximation of hyperbolic systems of conservation laws*, volume 118 of *Applied Mathematical Sciences*. Springer-Verlag, New York, 1996.

[51] Johan P Goedbloed, Rony Keppens, and Stefaan Poedts. *Advanced magnetohydrodynamics: with applications to laboratory and astrophysical plasmas*. Cambridge University Press, 2010.

[52] Daniel Goldman and Tasso J. Kaper. *N*th-order operator splitting schemes and nonreversible systems. *SIAM J. Numer. Anal.*, 33(1):349–367, 1996.

[53] Sigal Gottlieb, David Ketcheson, and Chi-Wang Shu. *Strong stability preserving Runge-Kutta and multistep time discretizations*. World Scientific Publishing Co. Pte. Ltd., Hackensack, NJ, 2011.

[54] Jean-Luc Guermond, Matthias Maier, Bojan Popov, and Ignacio Tomas. Second-order invariant domain preserving approximation of the compressible navier–stokes equations, 2020, to appear in CMAME.

[55] Jean-Luc Guermond, Murtazo Nazarov, Bojan Popov, and Ignacio Tomas. Second-order invariant domain preserving approximation of the Euler equations using convex limiting. *SIAM J. Sci. Comput.*, 40(5):A3211–A3239, 2018.

[56] Jean-Luc Guermond and Bojan Popov. Viscous regularization of the Euler equations and entropy principles. *SIAM J. Appl. Math.*, 74(2):284–305, 2014.

[57] Jean-Luc Guermond and Bojan Popov. Invariant domains and first-order continuous finite element approximation for hyperbolic systems. *SIAM J. Numer. Anal.*, 54(4):2466–2489, 2016.

[58] Jean-Luc Guermond, Bojan Popov, and Ignacio Tomas. Invariant domain preserving discretization-independent schemes and convex limiting for hyperbolic systems. *Comput. Methods Appl. Mech. Engrg.*, 347:143–175, 2019.

[59] A. Hakim, J. Loverich, and U. Shumlak. A high resolution wave propagation scheme for ideal two-fluid plasma equations. *J. Comput. Phys.*, 219(1):418–442, 2006.

[60] Ami Harten, Peter D. Lax, C. David Levermore, and William J. Morokoff. Convex entropies and hyperbolicity for general Euler equations. *SIAM J. Numer. Anal.*, 35(6):2117–2127, 1998.

[61] Jean-Luc Guermond Sidafa Conde Roger Pawloski John Shadid Ignacio Tomas, Matthias Maier. One-fluid euler-maxwell and euler-poisson systems: numerical methods preserving the hyperbolic invariant-set and hamiltonian structures, SAND2020-14178 CTF., 2020.

[62] Shi Jin. Asymptotic preserving (AP) schemes for multiscale kinetic and hyperbolic equations: a review. *Riv. Math. Univ. Parma (N.S.)*, 3(2):177–216, 2012.

[63] Ansgar Jüngel and Hailiang Li. Quantum Euler-Poisson systems: global existence and exponential decay. *Quart. Appl. Math.*, 62(3):569–600, 2004.

[64] Ansgar Jüngel and Yue-Jun Peng. A hierarchy of hydrodynamic models for plasmas: zero-relaxation-time limits. *Comm. Partial Differential Equations*, 24(5-6):1007–1033, 1999.

[65] Ansgar Jüngel and Yue-Jun Peng. A hierarchy of hydrodynamic models for plasmas. Quasi-neutral limits in the drift-diffusion equations. *Asymptot. Anal.*, 28(1):49–73, 2001.

[66] Ohannes A. Karakashian and Frederic Pascal. A posteriori error estimates for a discontinuous Galerkin approximation of second-order elliptic problems. *SIAM J. Numer. Anal.*, 41(6):2374–2399, 2003.

[67] George Em Karniadakis and Spencer J. Sherwin. *Spectral/hp element methods for computational fluid dynamics*. Numerical Mathematics and Scientific Computation. Oxford University Press, New York, second edition, 2005.

[68] Harish Kumar and Siddhartha Mishra. Entropy stable numerical schemes for two-fluid plasma equations. *J. Sci. Comput.*, 52(2):401–425, 2012.

[69] A Alvarez Laguna, Andrea Lani, Herman Deconinck, NN Mansour, and Stefaan Poedts. A fully-implicit finite-volume method for multi-fluid reactive and collisional magnetized plasmas on unstructured meshes. *Journal of Computational Physics*, 318:252–276, 2016.

[70] Randall J. LeVeque. *Finite difference methods for ordinary and partial differential equations*. Society for Industrial and Applied Mathematics (SIAM), Philadelphia, PA, 2007. Steady-state and time-dependent problems.

[71] Chao Li, Ute Ebert, and Willem Hundsdorfer. Spatially hybrid computations for streamer discharges with generic features of pulled fronts. I. Planar fronts. *J. Comput. Phys.*, 229(1):200–220, 2010.

[72] Chao Li, Ute Ebert, and Willem Hundsdorfer. Spatially hybrid computations for streamer discharges: II. Fully 3D simulations. *J. Comput. Phys.*, 231(3):1020–1050, 2012.

[73] Hailiang Li and Peter Markowich. A review of hydrodynamical models for semiconductors: asymptotic behavior. volume 32, pages 321–342. 2001. Dedicated to Constantine Dafermos on his 60th birthday.

[74] Yeping Li. Diffusion relaxation limit of a nonisentropic hydrodynamic model for semiconductors. *Math. Methods Appl. Sci.*, 30(17):2247–2261, 2007.

[75] Michael A Lieberman and Alan J Lichtenberg. *Principles of plasma discharges and materials processing*. John Wiley & Sons, 2005.

[76] P. A. Markowich, C. A. Ringhofer, and C. Schmeiser. *Semiconductor equations*. Springer-Verlag, Vienna, 1990.

[77] E. T. Meier and U. Shumlak. A general nonlinear fluid model for reacting plasma-neutral mixtures. *Physics of Plasmas*, 19(7):072508, 2012.

[78] Ralph Menikoff and Bradley J. Plohr. The Riemann problem for fluid flow of real materials. *Rev. Modern Phys.*, 61(1):75–130, 1989.

[79] D. Michta, F. Graziani, and M. Bonitz. Quantum hydrodynamics for plasmas âĂŞ a thomas-fermi theory perspective. *Contributions to Plasma Physics*, 55(6):437–443, 2015.

[80] Dimitri Mihalas and Barbara Weibel Mihalas. *Foundations of radiation hydrodynamics*. Oxford University Press, New York, 1984.

[81] S. T. Miller, E. C. Cyr, J. N. Shadid, R. M. J. Kramer, E. G. Phillips, S. Conde, and R. P. Pawlowski. IMEX and exact sequence discretization of the multi-fluid plasma model. *J. Comput. Phys.*, 397:108806, 22, 2019.

[82] Peter Monk. *Finite element methods for Maxwell's equations*. Numerical Mathematics and Scientific Computation. Oxford University Press, New York, 2003.

[83] Masashi Ohnawa. Asymptotic stability of plasma boundary layers to the Euler-Poisson equations with fluid-boundary interaction. *SIAM J. Math. Anal.*, 47(4):2795–2831, 2015.

[84] Will Pazner. Sparse invariant domain preserving discontinuous galerkin methods with subcell convex limiting, 2020.

[85] Benoit Perthame and Chi-Wang Shu. On positivity preserving finite volume schemes for Euler equations. *Numer. Math.*, 73(1):119–130, 1996.

[86] J Pétri, J Heyvaerts, and S Bonazzola. Diocotron instability in pulsar electrospheres-i. linear analysis. *Astronomy & Astrophysics*, 387(2):520–530, 2002.

[87] Jérôme Pétri. Non-linear evolution of the diocotron instability in a pulsar electrosphere: two-dimensional particle-in-cell simulations. *Astronomy & Astrophysics*, 503(1):1–12, 2009.

[88] Edward G. Phillips, John N. Shadid, and Eric C. Cyr. Scalable preconditioners for structure preserving discretizations of Maxwell equations in first order form. *SIAM J. Sci. Comput.*, 40(3):B723–B742, 2018.

[89] Alfio Quarteroni and Alberto Valli. *Numerical approximation of partial differential equations*, volume 23 of *Springer Series in Computational Mathematics*. Springer-Verlag, Berlin, 1994.

[90] Yuri P Raizer and John E Allen. *Gas discharge physics*, volume 2. Springer Berlin, 1997.

[91] T. Ruggeri and S. Simić. Mixture of gases with multi-temperature: Maxwellian iteration. In *Asymptotic methods in nonlinear wave phenomena*, pages 186–194. World Sci. Publ., Hackensack, NJ, 2007.

[92] Tommaso Ruggeri and Srboljub Simić. On the hyperbolic system of a mixture of Eulerian fluids: a comparison between single- and multi-temperature models. *Math. Methods Appl. Sci.*, 30(7):827–849, 2007.

[93] V. Selmin. The node-centred finite volume approach: Bridge between finite differences and finite elements. *Computer Methods in Applied Mechanics and Engineering*, 102(1):107 – 138, 1993.

[94] V. Selmin and L. Formaggia. Unified construction of finite element and finite volume discretizations for compressible flows. *International Journal for Numerical Methods in Engineering*, 39(1):1–32, 1996.

[95] Rémi Sentis. *Mathematical models and methods for plasma physics. Vol. 1*. Modeling and Simulation in Science, Engineering and Technology. Birkhäuser/Springer, Cham, 2014. Fluid models.

[96] Denis Serre. *Systems of conservation laws. 2*. Cambridge University Press, Cambridge, 2000. Geometric structures, oscillations, and initial-boundary value problems, Translated from the 1996 French original by I. N. Sneddon.

[97] Sergei F Shandarin and Ya B Zeldovich. The large-scale structure of the universe: Turbulence, intermittency, structures in a self-gravitating medium. *Reviews of Modern Physics*, 61(2):185, 1989.

[98] Bhuvana Srinivasan, Ammar Hakim, and Uri Shumlak. Numerical methods for two-fluid dispersive fast MHD phenomena. *Commun. Comput. Phys.*, 10(1):183–215, 2011.

[99] Gilbert Strang. On the construction and comparison of difference schemes. *SIAM J. Numer. Anal.*, 5:506–517, 1968.

[100] Eitan Tadmor. A minimum entropy principle in the gas dynamics equations. *Appl. Numer. Math.*, 2(3-5):211–219, 1986.

[101] Samuel B. Tanenbaum. *Plasma Physics*. McGraw-Hill Physical and Quantum Electronics Series. McGraw-Hill, 1967.

[102] A. H. Taub. Relativistic rankine-hugoniot equations. *Phys. Rev.*, 74:328–334, Aug 1948.

[103] A. H. Taub. Relativistic fluid mechanics. *Annual Review of Fluid Mechanics*, 10(1):301–332, 1978.

[104] Harry F. Tiersten. *A development of the equations of electromagnetism in material continua*, volume 36 of *Springer Tracts in Natural Philosophy*. Springer-Verlag, New York, 1990.

[105] Yoshihiro Ueda, Shu Wang, and Shuichi Kawashima. Dissipative structure of the regularity-loss type and time asymptotic decay of solutions for the Euler-Maxwell system. *SIAM J. Math. Anal.*, 44(3):2002–2017, 2012.

[106] E. L. Walker and B. Samuel Tanenbaum. Transport equations for a weakly ionized electron gas. *The Physics of Fluids*, 11(9):1955–1958, 1968.

[107] J. G. Wöhlbier, S. Jin, and S. Sengele. Eulerian calculations of wave breaking and multivalued solutions in a traveling wave tube. *Physics of Plasmas*, 12(2):023106, 2005.

[108] Manwai Yuen. Analytical blowup solutions to the 2-dimensional isothermal Euler-Poisson equations of gaseous stars. *J. Math. Anal. Appl.*, 341(1):445–456, 2008.

[109] Manwai Yuen. Blowup for the Euler and Euler-Poisson equations with repulsive forces. *Nonlinear Anal.*, 74(4):1465–1470, 2011.

[110] Xiangxiong Zhang and Chi-Wang Shu. On positivity-preserving high order discontinuous Galerkin schemes for compressible Euler equations on rectangular meshes. *J. Comput. Phys.*, 229(23):8918–8934, 2010.

APPENDIX A. APPENDIX

A.1. Complete equation of state, ideal gas law, and simplifications

Definition A.1 (Complete equation of state)**.** Let the thermodynamic behaviour of the fluid/substance of interest be entirely described by a specific entropy $s = \sigma(v,e)$ where v is the specific volume and e is the specific internal energy. We assume that σ is concave with respect to v and e and that $\frac{\partial \sigma}{\partial e} > 0$. We assume that Gibb's identity (a thermodynamics axiom of equilibrium thermodynamics) holds true

$$\theta \mathrm{d}s := \mathrm{d}e + p\mathrm{d}v\,, \tag{106}$$

which encodes the first and second principles of thermodynamics. We further assume that $s = \sigma(v,e)$, the complies with the exact-differential structure of identity (106):

$$\mathrm{d}s = \tfrac{1}{\theta}\mathrm{d}e + \tfrac{p}{\theta}\mathrm{d}v \iff \mathrm{d}s = \tfrac{\partial \sigma}{\partial e}\mathrm{d}e + \tfrac{\partial \sigma}{\partial v}\mathrm{d}v \ \ (\text{with } \mathrm{d}v = -\tfrac{1}{\rho^2}\mathrm{d}\rho)\,,$$

which implies the following standard relationships (cf.[78, 56])

$$\tfrac{\partial \sigma}{\partial e} := \theta^{-1} \ \text{ and } \ \tfrac{p}{\theta} := \tfrac{\partial \sigma}{\partial v} \implies p := -\rho^2 \left[\tfrac{\partial \sigma}{\partial \rho}\right]\left[\tfrac{\partial \sigma}{\partial e}\right]^{-1}. \tag{107}$$

Formulas (106)-(107) are a minimal description of the framework of complete equations of state: all observables (e.g. temperature, pressure, soundspeed, etc) are computed from the specific entropy describing thermodynamic behaviour of a substance of interest in a way that is consistent with the first and second principles of thermodynamics.

Remark A.1 (Ideal gas law closure and simplifications)**.** For the case of ideal gas law, extensively used for the thermodynamic description of electrons and ions, we have that the specific entropy is given by

$$\sigma(e,\rho) = \log(e^{\frac{1}{\gamma-1}}\rho^{-1})\,, \tag{108}$$

using the general formulas (107) we obtain the following expressions for the temperature and pressure

$$\theta := (\gamma-1)e\ , \ \ p := (\gamma-1)\rho e\ , \tag{109}$$

Note that the pressure formula is quite often written as $p = \theta\rho$ in the plasma literature, which is consistent with (109). We can consider the specific isoentropic and isothermal closures which further simplify the ideal-gas law (108)-(109):

- Isothermal closure: $p := \theta_0\rho$ where $\theta_0 = const$ is the plasma temperature.
- Isoentropic closure: $p := \kappa\rho^\gamma$ where $\kappa := (\gamma-1)e^{(\gamma-1)s_0}$, $s_0 = const$ is the constant entropy of the fluid, and $\gamma = 5/3$. This closure is derived from the assumption $\log(e^{\frac{1}{\gamma-1}}\rho^{-1}) = s_0$.

In both of these simplified cases, isoentropic and isothermal, the evolution for the total mechanical energy $\mathcal{E}$ becomes redundant since the specific internal energy e can be easily recovered with no computational cost. For the isothermal case $e := \frac{\theta_0}{\gamma-1}$, while $e := (\rho e^{s_0})^{\gamma-1}$ for the isoentropic case. Both isothermal and isoentropic closures are quite popular in the semiconductor modeling literature.

DISTRIBUTION

Hardcopy—External

Number of Copies	Name(s)	Company Name and Company Mailing Address

Hardcopy—Internal

Number of Copies	Name	Org.	Mailstop

Email—External [redacted]

Name	Company Email Address	Company Name

Email—Internal [redacted]

Name	Org.	Sandia Email Address
Technical Library	1911	sanddocs@sandia.gov

Sandia National Laboratories

Sandia National Laboratories is a multimission laboratory managed and operated by National Technology & Engineering Solutions of Sandia LLC, a wholly owned subsidiary of Honeywell International Inc., for the U.S. Department of Energy's National Nuclear Security Administration under contract DE-NA0003525.